Unravelling the mechanisms causing astrocytic death during early epileptogenesis

Inaugural-Dissertation

zur Erlangung des Doktorgrades

der Hohen Medizinischen Fakultät

der Rheinischen Friedrich-Wilhelms-Universität

Bonn

Zhou Wu

aus Hubei/China

2020

Angefertigt mit der Genehmigung
der Medizinischen Fakultät der Universität Bonn

1. Gutachter: Prof. Dr. Christian Steinhäuser
2. Gutachter: Prof. Dr. Karl Schilling

Tag der Mündlichen Prüfung: 12.12.2019

Aus dem Institut für Zelluläre Neurowissenschaften
Direktor: Prof. Dr. Christian Steinhäuser

Meinen Familien

Table of Contents

List of abbreviations

ACD	accidental cell death
BCL2	B cell lymphoma 2
CA	Cornu Ammonis
CASP	cysteine-aspartic acid protease
DG	dentate gyrus
DTT	dithiothreitol
dsRNA	double-stranded RNA
ER	endoplasmic reticulum
ESCRT	endosomal sorting complex required for transport
GFAP	glial fibrillary acidic protein
GLT	glutamate transporter
GPX4	glutathione peroxidase 4
IFN	type I interferon
i.p.	intraperitoneally
ICAD	inhibitor of caspase-activated DNase
IL-1β	interleukin 1β
IL-6	interleukin 6
KCNJ10	Kir4.1 encoding gene
LC3	light chain 3
LCD	lysosomal cell death
LMP	lysosomal membrane permeabilization
MLKL	mixed lineage kinase domain like pseudo-kinase
MOMP	mitochondrial outer membrane permeabilization
NDS	normal Donkey Serum
Nec-1	necrostatin-1
NF-κB	nuclear factor kappa-light-chain-enhancer of activated B-cells X
NGS	normal Goat Serum
NLPR	NACHT, LRR and PYD domains-containing protein
NTRK3	neurotrophic receptor tyrosine kinase 3
PE	phosphatidyl-ethanolamine

PI	propidium iodide
PI(3)P	phosphatidyl-inositol 3-phosphate
PRRs	pathogen recognition receptors
RCD	regulated cell death
RHIM	RIPK homotypic interaction motif
RIPK3	receptor interacting kinase 3
ROS	reactive oxygen species
RT-PCR	real-time polymerase chain reaction
SE	status epilepticus
SGZ	subgranular zone
SLM	stratum lacunosum moleculare
SMAC	second mitochondria-derived activator of caspases
SO	stratum oriens
SP	stratum pyramidale
SR	stratum radiatum
TNF-α	tumor necrosis factor α
TNFR1	tumor necrosis factor receptor 1
TLE	temporal lobe epilepsy
TLR	toll-like receptor
TRPM7	transient receptor potential cation channel subfamily M member 7
TUNEL	terminal deoxynucleotidyl transferase dUTP nick end labeling
XIAP	X-linked inhibitor of apoptosis protein

1. Introduction

1.1 Astrocytes

Astrocytes, presenting typical stellate morphology, have a ramified structure with fine processes (Fig. 1). The main component of intermediate filaments of all astrocytes is the glial fibrillary acidic protein (GFAP), which is expressed in adult astrocytes (Brenner et al., 1994). A distinction is made between the protoplasmic astrocytes, especially in the gray matter and the fibrous astrocytes, which are found mainly in the white matter. The fibrous astrocytes have an elongated shape and are often aligned parallel to the axons. However, the protoplasmic astrocytes are characterized by a more compact form, which is caused by a very dense network of lateral branches that arise from the thicker primary projections. With the help of different staining methods, it has been found that protoplasmic astrocytes are organized into domains (Bushong et al., 2002; Ogata and Kosaka, 2002). In this case, a cell occupies a polyhedral shaped space, so that all synapses and blood vessels in this area are in contact with one astrocyte. Therefore, an astrocyte can contact several thousand of synapses (Clarke and Barres 2013). The domains of adjacent cells slightly overlap only at the outer borders. This phenomenon was observed in both murine and human astrocytes in the cortex and hippocampus (Oberheim et al. 2006). However, there is also evidence that the size of astrocytes and their degree of overlap are not constant, but can change during the course of life (Grosche et al. 2013). Astrocytes make up around 80 % of all types of cells in human brain (Kettenmann and Ransom, 1995).

Astrocytes communicate intercellularly via gap junction coupling (GJC) which allows molecules with less than 1 kDa weight and 1.5 nm diameter pass through (Giaume et al., 2010). GJC is formed by two adjacently docked connexons, each of which consists of six connexin oligomers (Bosco, Haefliger, and Meda 2011). Connexin (Cx) 43 and 30 are two major connexins expressed in astrocytes, whose expressions varies throughout different cerebral regions (Gosejacob et al., 2011; Griemsmann et al., 2015). Physiologically, many molecules, e.g. K^+, cyclic adenosine monophosphate (cAMP), inositol triphosphate (IP3), Ca^{2+}, glucose, glutamate etc., can be transported across astrocytic networks via GJCs. K^+ spatial buffering is one of the important

functions of GJCs. Astrocytic GJCs accelerate K_+ clearance and limit K_+ accumulation during synchronized neuronal firing. Genetic deletion of astrocyte gap junctions leads to impaired K_+ buffering, spontaneous epileptiform activity and a decreased threshold for eliciting seizure activity (Wallraff et al. 2006). Besides, astrocytic coupling networks regulate neuronal function, energy supply, blood flow control and neurovascular signaling to capillary pericytes, etc. (Giaume et al. 2010; Mishra et al. 2016). Nevertheless, astroglial networks also contribute to brain dysfunction. In epileptic conditions, an increase in Cx43 expression and gap junctional communication was reported in hippocampal organotypic cultures (Samoilova et al. 2003). Interestingly, application of Cx43-mimetic peptides could attenuate epileptiform activity, indicating that enhanced coupling in astroglial networks might support or trigger epileptic activity (Samoilova et al. 2008). More importantly, the astroglial coupling in vivo was impaired during epileptogenesis and disappeared during chronic phase of epilepsy (Bedner et al. 2015).

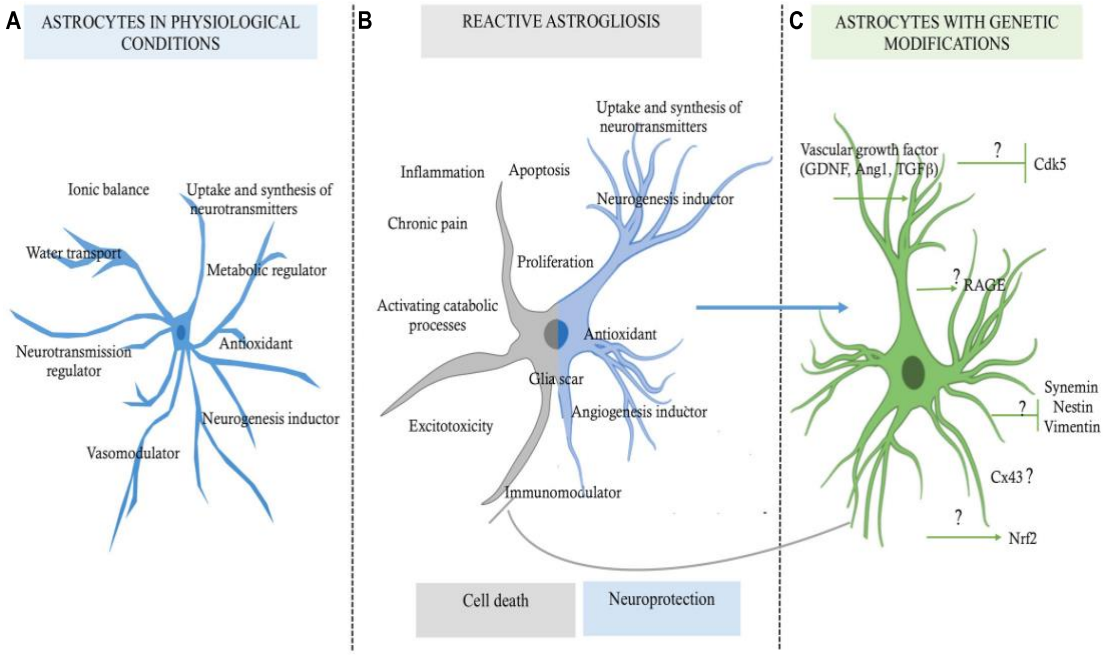

Fig. 1: Role of astrocytes in a micro-environment dependent-mode. **(A)** Functions of the astrocytes in physiological conditions. **(B)** Reactive astrocytosis, which has a double function which is highly discussed, one for inducing cell death and one for being neuroprotection probably in a context dependent-mode. **(C)** Astrocytes with genetic modifications. (Becerra-Calixto and Cardona-Gomez 2017)

1.2 Microglia

Microglia represents the innate immune system of the brain (Kreutzberg, 1996). Interestingly, the morphology and density of microglia varies a lot as a function of their localization in the brain (Lawson et al., 1990). The hippocampus contains the highest density of microglia in the brain (Jinno et al., 2007). Microglial morphology is traditionally classified as ramified, bushy, or reactive, corresponding to a spectrum within which cells range from passively monitoring to actively modifying brain structure and function (Fig. 2) (Karperien, Jelinek, and Buchan 2008). As evident in the general trends shown in Fig. 2, in normal adult human brain and spinal cord, small- bodied cells with long, finely branched processes are presumed to be "resting". In the resting state, the microglia have a ramified morphology, a small cell soma with fine extensions, whereas in pathological CNS, “reactive” cells, which have begun to swell in their processes, or may have completely lost them, are assumed to be "active" (Streit, Walter, and Pennell 1999; Hanisch and Kettenmann 2007; Karperien, Ahammer, and Jelinek 2013; Kettenmann et al. 2011). A characteristic feature of microglia is its activation at a very early stage after an injury or infection (Cherry et al., 2014; Rock et al., 2004). Microglia detect pathological changes in the tissue, and become activated. Microglia activation is characterized by the increased proliferation, morphological transformation, the release of various types of proinflammatory cytokines such as tumor necrosis factor α (TNF-α), interleukin 1β (IL-1β), interleukin 6 (IL-6) and / or chemokines (Banati et al., 1993; Smith et al., 2012; Vezzani et al., 2008). Microglia can play both neuroprotective as well as neurotoxic roles depending on the situation (Ransohoff and Perry, 2009). Activated microglia have been observed in both animal models of epilepsy (Avignone et al., 2008; Eyo et al., 2014) and brain tissue resected from patient with TLE (Beach et al., 1995).

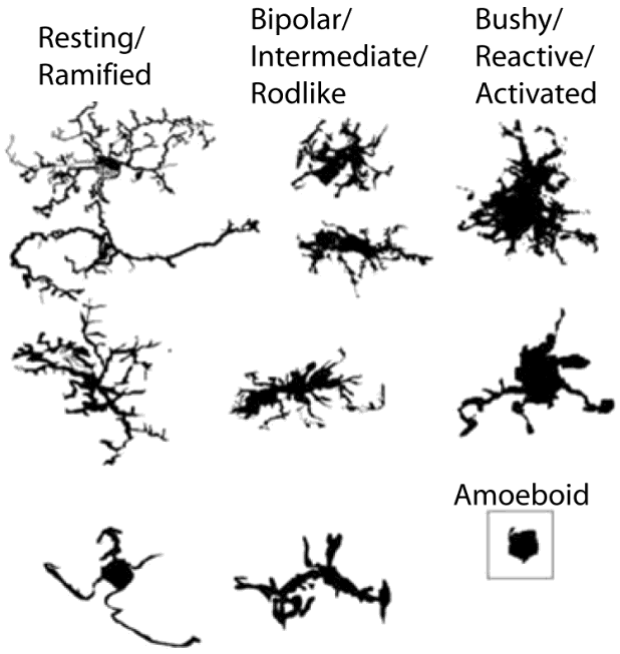

Fig. 2: Morphological characteristics of microglia. Microglial morphology is traditionally classified as ramified, bushy, or reactive, corresponding to a spectrum within which cells range from passively monitoring to actively modifying brain structure and function. In normal adult human brain and spinal cord, small- bodied cells with long, finely branched processes are presumed to be “resting”, whereas in pathological CNS, “reactive” cells, which have begun to swell in their processes, or may have completely lost them, are assumed to be “active. From (Karperien, Jelinek, and Buchan 2008).

1.3 Hippocampus

The hippocampus is located in the medial temporal lobe and it is the part of the cortex. It contains several regions: cornu ammonis (CA) 1 to CA3 and the dentate gyrus (DG). The CA region consists of several layers: stratum pyramidale (SP), stratum oriens (SO), stratum radiatum (SR) and stratum lacunosum moleculare (SLM). The SP layer contains the somata of excitatory pyramidal neurons, which stretch their axons into the SO and on the other side of the SP, the dendrites of these neurons extend into the SR. The other layers contain inhibitory interneurons and several types of glial cells. The dentate gyrus contains the neuronal granular cell layer. The inside of this layer is called hilus and the outer layer is called stratum molecular (Amaral and Witter, 1989). The subgranular zone (SGZ) is the innermost part of the granule cell layer, which contains neural stem cells which can differentiate into new neurons (Seri et al., 2001). The neuronal circuit in the hippocampus is a trisynaptic excitatory pathway as shown in Fig.

3. TLE is the most common form of adult localization-related epilepsy. Hippocampal onset accounts for at least 80 % of all temporal lobe seizures (hence called mesial temporal lobe epilepsy (MTLE) or mesial temporal seizures (MTS)) (Tatum, 2012).

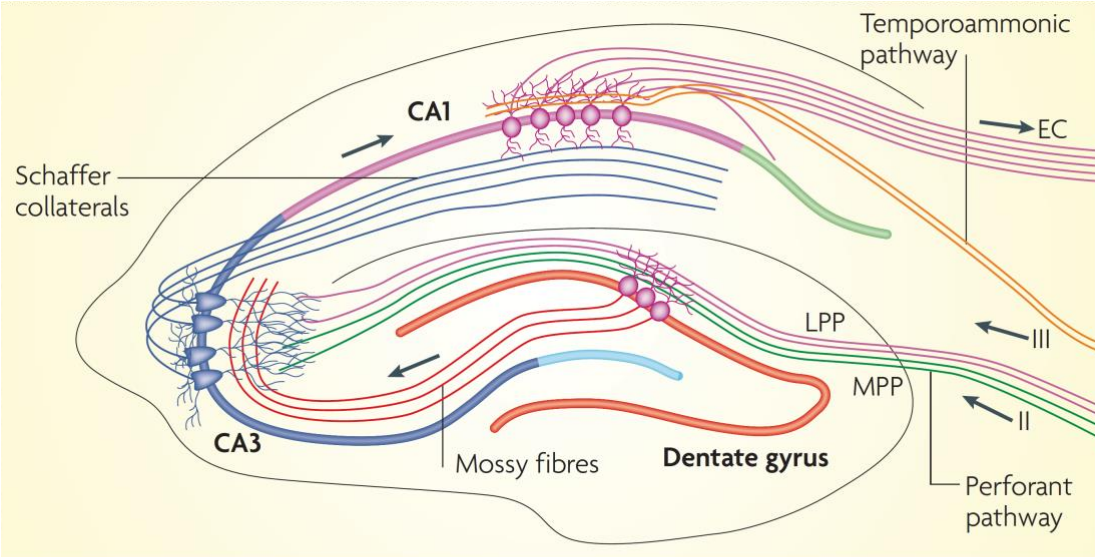

Fig. 3: Neuronal circuit of the hippocampus. The synaptic input from the entorhinal cortex reaches at DG; from DG it is sent via mossy fibers to the CA3 pyramidal neurons, from CA3 it is transferred by Schaffer collaterals to the CA1 neurons, CA1 neurons signal back to the entorhinal cortex. LPP, lateral perforant pathway; MPP, medial perforant pathway. From (Deng, Aimone, and Gage 2010).

1.4 Cell death

Physiologically, cell death is a highly regulated and crucial homeostatic mechanism required to maintain the size and functions of tissues and organs. A large amount of experimental evidence accumulating over the past years has revealed and characterized a set of genetically encoded mechanisms for targeted elimination of superfluous, irreversibly damaged, and/or potentially harmful cells (Weinlich et al. 2017; Fuchs and Steller 2015; Pasparakis and Vandenabeele 2015). Intriguingly, regulated cell death (RCD) is not unique to multicellular life forms. This is a condition in which RCD has an obvious advantage for organismal homeostasis in both physiological and pathological settings (Galluzzi, Bravo-San Pedro, et al. 2016; Fuchs and Steller 2011; Galluzzi, Lopez-Soto, et al. 2016). In striking contrast with RCD, accidental cell death (ACD) is defined as the instantaneous and catastrophic demise of cells exposed to severe insults of physical, chemical, or mechanical nature.

Cell death in mammalian cells is morphologically classified into three types (Fig. 4): 1) Apoptosis (Type 1 cell death); 2) Autophagy-associated cell death (Type 2 cell death); 3) Necrosis (Type 3 cell death). (Of note, other type-3 subtypes exist, see below Table 1 & 2).

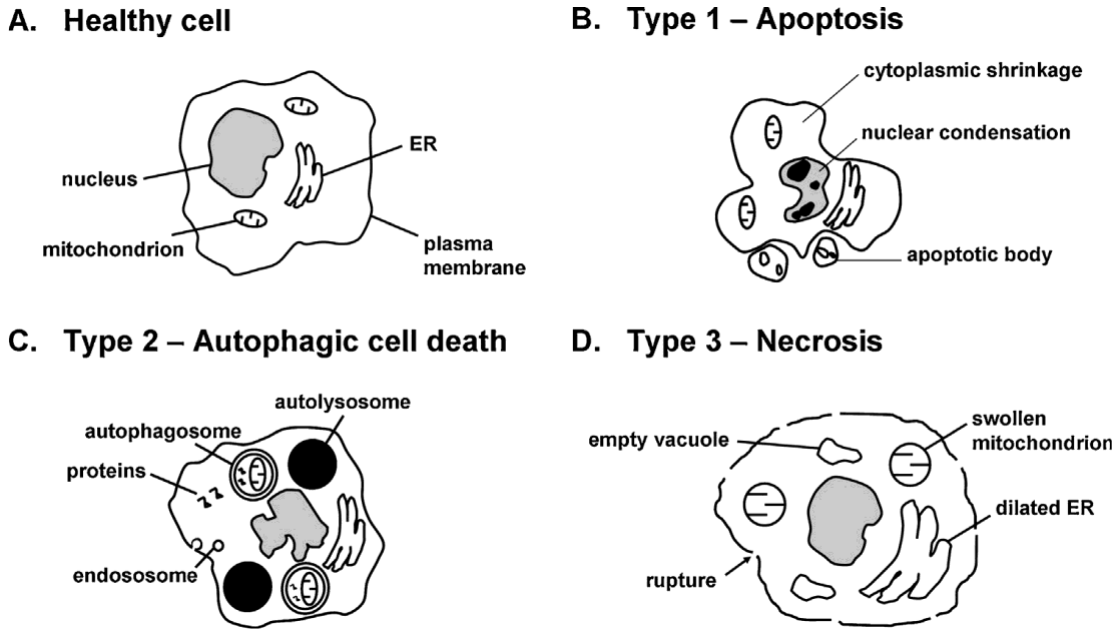

Fig. 4: Schematic description of the three main types of cell death. (A) Healthy cell. (B) Type 1 – Apoptosis: Nucleus: shrinkage, chromatin condensation, pyknosis, fragmentation. Plasma membrane: convolution, budding, formation of apoptotic bodies. Cytoplasm: shrinkage, organelles appear almost normal, but loss of ribosomes from the rough endoplasmic reticulum (ER) and polysomes. **(C) Type 2 – Autophagic cell death:** Nucleus: sometimes shrinkage and moderate pyknosis. Plasma membrane: often intense endocytosis. Cytoplasm: numerous autophagosomes and autolysosomes, Golgi often enlarged. **(D) Type 3 – Necrosis:** Nucleus: little change, but swelling. Plasma membrane: swelling and rounding up of cell, sometimes with rupture of plasma membrane. Cytoplasm: dilation of organelles, vacuolization. From (Puyal, Ginet, and Clarke 2013).

1.4.1 Apoptosis

1.4.1.1 Intrinsic apoptosis

Intrinsic apoptosis (shown in Fig. 5) is a form of RCD initiated by a variety of microenvironmental perturbations including (but not limited to) growth factor withdrawal, DNA damage, ER stress, reactive oxygen species (ROS) overload, replication stress, microtubular alterations or mitotic defects (Czabotar et al. 2014; Roos, Thomas, and Kaina 2016; Nunez et al. 1990). Apoptotic cells retain plasma membrane integrity and metabolic activity (to some degree) as the process proceeds

to completion. The critical step for intrinsic apoptosis is irreversible and widespread mitochondrial outer membrane permeabilization (MOMP) (Tait and Green 2010; Galluzzi, Kepp, and Kroemer 2016), which is controlled by pro-apoptotic and anti-apoptotic members of the B cell lymphoma 2 (BCL2) (Moldoveanu et al. 2014; Shamas-Din et al. 2013).

1.4.1.2 Extrinsic apoptosis

Extrinsic apoptosis (shown in Fig. 5) is an RCD modality initiated by perturbations of the extracellular microenvironment (Flusberg and Sorger 2015; Gibert and Mehlen 2015b). Extrinsic apoptosis is mostly driven by either of two types of plasma membrane receptors: (1) death receptors, and (2) dependence receptors (Gibert and Mehlen 2015b; Aggarwal, Gupta, and Kim 2012; Wajant 2002; Mehlen and Bredesen 2011). Death receptors include: Fas cell surface death receptor (FAS), and TNF receptor 1A (TNFR1), 10a (TRAILR1 or DR4), and 10b (TRAILR2 or DR5) (Aggarwal, Gupta, and Kim 2012; Wajant 2002; von Karstedt, Montinaro, and Walczak 2017). The execution of extrinsic apoptosis driven by death receptors follows two distinct pathways: 1) type 1, the cysteine-aspartic acid protease (CASP) 8-dependent proteolytic maturation of executioner CASP3 and CASP7 suffices to drive RCD, which cannot be inhibited by the transgene-driven overexpression of anti-apoptotic BCL2 proteins, the co-deletion of Bax and Bak1, or the loss of BID (a pro-apoptotic member of the Bcl-2 family); 2) type 2, CASP3 and CASP7 activation is restrained by X-linked inhibitor of apoptosis protein (XIAP) (Jost et al. 2009). Extrinsic apoptosis requires the proteolytic cleavage of BID by CASP8 (Yin et al. 1999; Li and Yuan 1998; Luo et al. 1998). Dependence receptors consists of: (1) the netrin 1 (NTN1) receptors, unc-5 netrin receptor A (UNC5A), UNC5B, UNC5C, and UNC5D; (2) the neurotrophic receptor tyrosine kinase 3 (NTRK3); and (3) the sonic hedgehog (SHH) receptor patched 1 (PTCH1) (Gibert and Mehlen 2015a; Mehlen and Tauszig-Delamasure 2014). Intriguingly, in physiological conditions dependence receptors promote cell survival, proliferation and differentiation, but activate distinct lethal signaling cascades once ligand availability falls below a specific threshold level (Mehlen and Tauszig-Delamasure 2014).

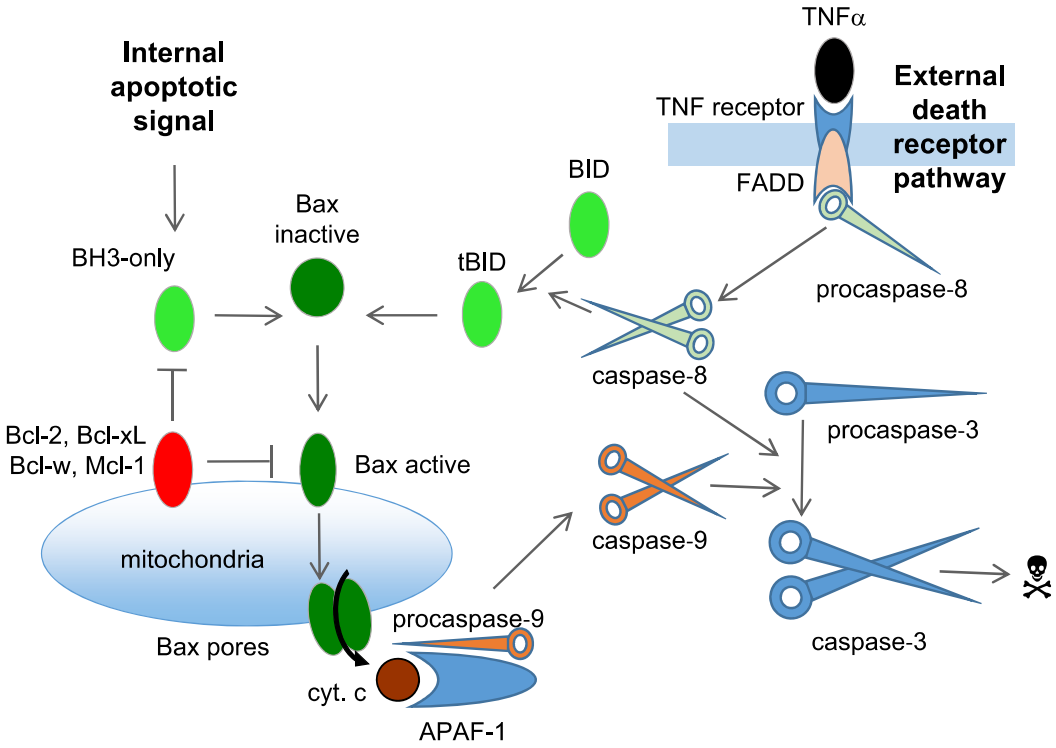

Fig. 5: Mechanisms of apoptosis. Overview of apoptosis. The internal (mitochondrial) pathway of apoptosis is triggered within the cell, causing expression or activation of BH3-only proteins that activate Bax (and/or Bak in some cells) to form pores in the outer mitochondrial membrane, releasing cytochrome *c* to bind APAF-1, activating caspase-9 to cleave and activate downstream caspases, which degrades cellular proteins. The external (death receptor) pathway starts outside the cell with death ligands activating death receptors to activate caspase-8, which either cleaves downstream caspases or cleaves and activates the BH3-only protein Bid. Anti-apoptotic proteins, such as Bcl-2, hold inactive Bax or BH3-ony proteins. From (Fricker et al. 2018b)**.**

1.4.2 Autophagic cell death

Autophagy is defined as a process of cell "self-eating" whereby intracellular constituents are transported to the lysosome for digestion and recycling (Galluzzi, Baehrecke, et al. 2017). Normally, autophagy acts as an important way to prevent cell death, but it can cause cell death under overloaded condition. Autophagic cell death can be defined as a form of RCD that depends on the autophagic machinery — under conditions of a regulated process. Both the process of autophagy and its machinery are conserved from yeast to mammals (Wen and Klionsky 2016; Bento et al. 2016). In mammals, different types of autophagy, such as macroautophagy, microautophagy, chaperone-mediated autophagy, RNautophagy and others, have been described

(Shah et al. 2015; Galluzzi, Baehrecke, et al. 2017). Macroautophagy is the variant of autophagy best described so far, in part due to its morphological changes — the formation of double-membraned autophagosome, via which the transport of cellular reservoirs to lysosome occurs (Galluzzi, Baehrecke, et al. 2017). Macroautophagy initiation (shown in Fig. 6) in mammals is associated with an ER subdomain enriched for the lipid phosphatidylinositol 3-phosphate (PI(3)P) (Axe et al. 2008). The phagophore (the precursor of the autophagosome) elongates into a cup-shaped structure and begins to engulf cellular material. The membrane supply for phagophore growth can apparently be sourced to a variety of cellular reservoirs (Lamb, Yoshimori, and Tooze 2013). The conserved machinery for autophagosome formation (Suzuki et al. 2017; Mizushima, Yoshimori, and Ohsumi 2011) contains two major initiation complexes: the unc-51-like autophagy activating kinase 1 (ULK1) complex and the class III PI 3-kinase complex I (PI3KC3–C1). Beclin 1 protein is also a central regulator of autophagosome formation (Cao and Klionsky 2007). Light chain 3 (LC3), a mammalian homologue of autophagy-related 8 (Atg8), has been identified on the autophagosomal inner membrane (Kabeya et al. 2000), which is considered to be a hallmark for macroautophagy. The modification of LC3 by the phospholipid phosphatidyl-ethanolamine (PE) (Ichimura et al. 2000) is an essential process for the formation of the autophagosome (Fig. 6). LC3 is cleaved by cysteine protease Atg4 and then conjugated with PE by Atg7 and Atg3. This lipidated LC3-II then associates with newly forming autophagosome membranes. LC3-II remains on mature autophagosome until its fusion with lysosomes (Burman and Ktistakis, 2010). The conversion of LC3 to LC3-II is a marker of autophagy-induction.

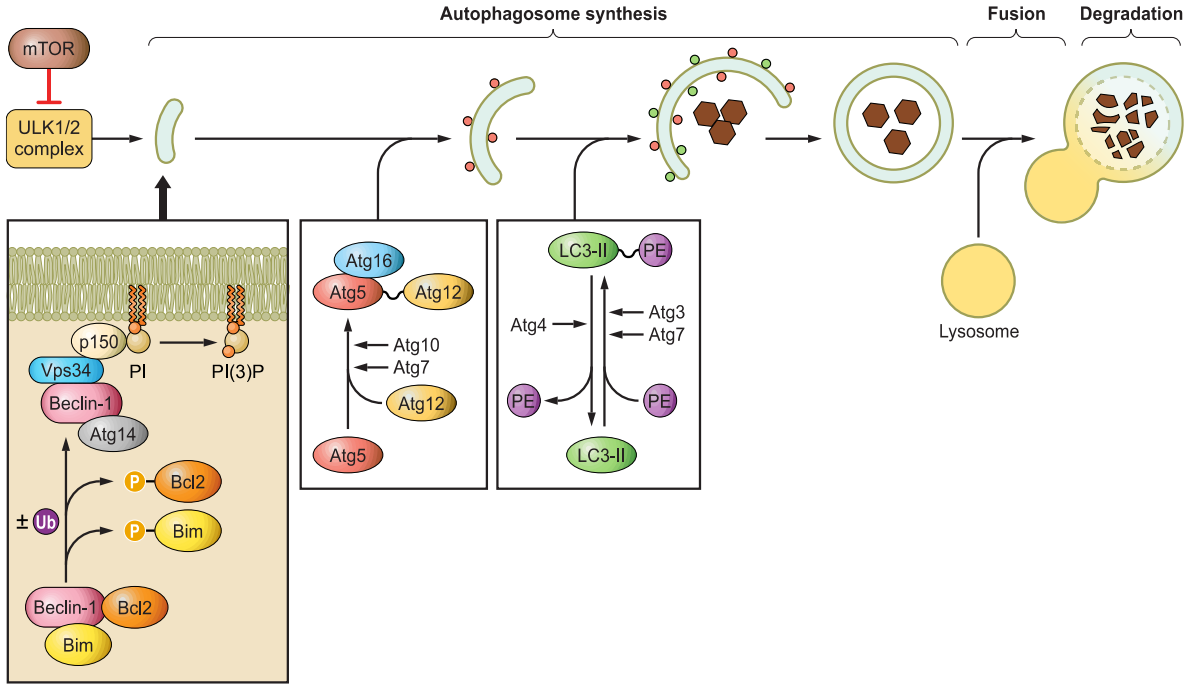

Fig. 6: Macroautophagy. Autophagy normally promotes survival during starvation or growth factor withdrawal, but, if excessive, can cause autophagic cell death, characterized by the accumulation of autophagic vacuoles. Note the cross talk between autophagy and apoptosis as Beclin-1 is held via its BH3 motif in an inactive state by binding to anti-apoptotic Bcl2 family members or to Bim when it is tethered on microtubules. From (Fricker et al. 2018a).

1.4.3 Necrosis

Recently, it has become more clear that many distinct mechanisms are involved in necrosis — so called regulated necrosis. Regulated (or programmed) necrosis is distinguished from unregulated necrosis, which is based on the fact that regulated necrosis is genetically controlled and engages active cellular processes, the blockade of which is principally feasible, whereas unregulated necrosis engages passive processes the blockade of which is difficult or impossible (Vanden Berghe et al. 2014).

1.4.3.1 Necroptosis

Necroptosis, the best-described form of regulated necrosis, is a form of RCD initiated by perturbations of the extracellular or intracellular microenvironment detected by specific death receptors, including FAS and TNFR1 (Vercammen et al. 1997; Vercammen et al. 1998; Degterev et al. 2005b; Galluzzi et al. 2014; Degterev et al. 2008), or pathogen recognition receptors (PRRs), including TLR3, TLR4, and Z-DNA

binding protein 1 (known as DAI), etc. (Kaiser et al. 2013; Upton, Kaiser, and Mocarski 2012, 2010) (shown in Fig. 7).

Necroptosis critically depends on the sequentially activated kinase activity of receptor interacting kinase (RIPK) 3 and mixed lineage kinase domain like pseudo-kinase (MLKL) (Linkermann and Green 2014b; Murphy et al. 2013). Upon necroptosis initiation by TNFR1, RIPK3 is activated by RIPK1 (provided that CASP8 is inactive) through a mechanism involving the physical interaction between their respective RIPK homotypic interaction motif (RHIM) domains and RIPK1 catalytic activity (Vandenabeele et al. 2010; Li et al. 2012; Cho et al. 2009b). Accordingly, pharmacological inhibitors of RIPK1 including necrostatin-1 (Nec-1) and Nec-1s (Nec-1 derivatives) robustly inhibit TNFR1-driven necroptosis, both in vitro and in vivo (Degterev et al. 2005a; Degterev et al. 2008). Alternatively, RIPK3 can be directly activated following the RHIM-dependent interaction with: (1) TRIF upon either TLR3 activation by double-stranded RNA (dsRNA) within endosomes, or TLR4 activation by lipopolysaccharide (LPS) or various DAMPs at the plasma membrane (Kaiser et al. 2013); (2) ZBP1, which operates as a sensor for cytosolic DNA-promoting type I interferon (IFN) synthesis and nuclear factor kappa-light-chain-enhancer of activated B-cells (NF-κB) activation (Maelfait et al. 2017; Lin et al. 2016; Newton et al. 2016).

The TNFR1 pathway is an important and best described trigger for RIPK3 activation. In particular, the activation of RIPK3 down-stream of TNFR1 ligation relies on the formation of a RIPK1-containing and RIPK3-containing amyloid-like signaling complex commonly known as necrosome (Vandenabeele et al. 2010; Grootjans, Vanden Berghe, and Vandenabeele 2017), wherein first RIPK1 and then RIPK3 undergo a series of (auto)phosphorylation events that are required for MLKL recruitment and necroptosis activation and execution (Li et al. 2012; Cho et al. 2009a; Sun et al. 2012a). MLKL is a specific substrate for RIPK3 kinase activity (Zhao et al. 2012; Sun et al. 2012b; Murphy et al. 2013) and appears to execute the process of necroptosis by targeting the plasma membrane (Chen et al. 2014b; Wang et al. 2014; Cai et al. 2014). Activated RIPK3 recruits and phosphorylates MLKL, resulting in the formation of MLKL oligomers (most likely trimers or detramers) (Huang et al. 2017; Cai et al. 2014; Liu et al. 2017) that translocate to the plasma membrane, where they bind specific

phosphatidylinositol phosphate species by a roll-over mechanism and hence induce plasma membrane permeabilization (Wang et al. 2014; Chen et al. 2014a; Hildebrand et al. 2014a). The phosphorylation of MLKL by RIPK3 has been proposed to promote necroptosis by inducing essential steps, allowing the formation of oligomers, migration to plasma membrane and binding to phosphatidylinositol lipids to directly disrupt membrane integrity (Chen et al. 2014b; Wang et al. 2014; Cai et al. 2014; Hildebrand et al. 2014b). Among the residues Ser345, Ser347 and Thr349 within the murine MLKL activation loop (Murphy et al. 2013), phosphorylation of Ser345 is a key event in the activation of MLKL by RIPK3 (Rodriguez et al. 2016). MLKL must be phosphorylated at Ser345 by RIPK3 to translocate to the plasma membrane and execute necroptosis (Rodriguez et al. 2016). Eventual necrotic cell death is induced by the translocation of MLKL to plasma membrane (Chen et al. 2014b; Hildebrand et al. 2014a). Of note, phosphorylated MLKL also appears to translocate to the nucleus preceded by necroptosis execution, which might facilitate the necroptosis process (Yoon et al. 2016).

Moreover, it has also been reported that MLKL oligomerization promotes a cascade of intracellular events involving (1) phosphorylated MLKL mediated Ca^{2+}-influx, targeting transient receptor potential cation channel subfamily M member (TRPM) 7 (Cai et al. 2014); and (2) phosphorylated MLKL mediated PS-exposure, forming PS-exposing plasma membrane bubbles whose breakdown and release is negatively regulated by the antagonistic activity of the endosomal sorting complex required for transport (ESCRT)-III machinery , by which MLKL activation is limited (Gong et al. 2017). Once localized at the plasma membrane, MLKL reportedly activates cell-surface proteases of the ADAM family, which can promote the shedding of plasma membrane-associated proteins (Cai et al. 2016), or form Mg^{2+} permeant channels (Xia and Gao 2017; Gunther et al. 2016a). Of note, a few RCD involving MLKL (but not RIPK3) (Gunther et al. 2016a) or RIPK3 (but not MLKL) (Zhang, Zhang, et al. 2016) have also been described as necroptosis.

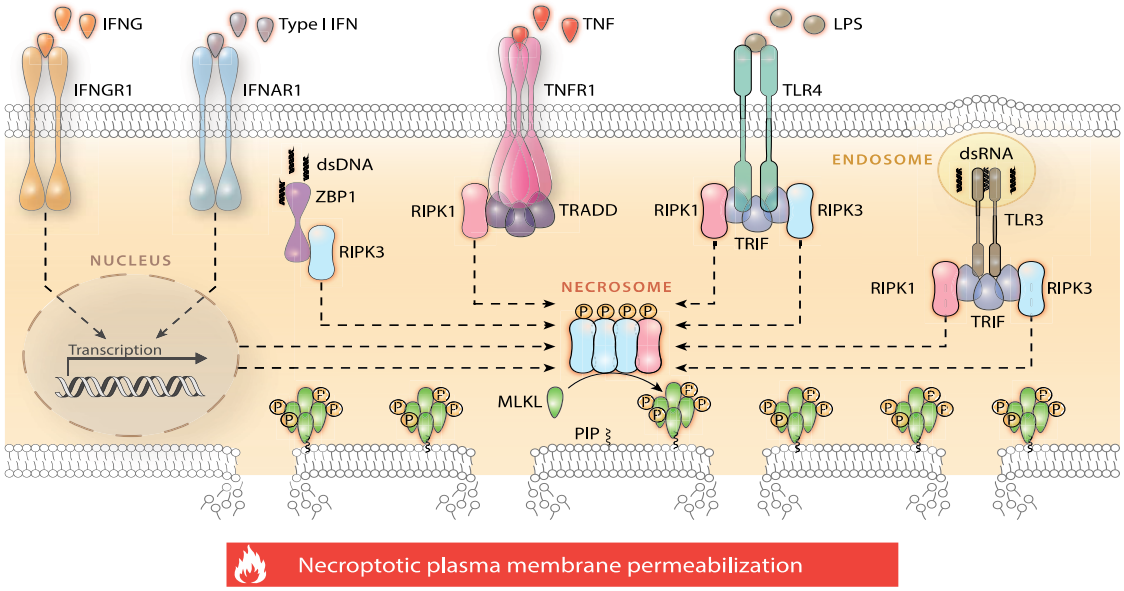

Fig. 7: Molecular mechanisms of necroptosis. Necroptosis critically depends on the RIPK3 – mediated phosphorylation of MLKL, resulting in MLKL oligomerization, translocation to the inner leaflet of the plasma membrane, and cell death. The formation of the RIPK3- and MLKL-containing complex that precipitates necroptosis, the so-called necrosome, can be elicited by extracellular signals (such as the ligation of death receptors) as well as by intracellular cues (such as the presence of viral nucleic acids) and is regulated by a complex network of physical and functional protein-to-protein interactions. The best characterized signal transduction cascade resulting in necroptotic cell death is initiated by TNFR1 ligation in the presence of caspase inhibitors and/or SMAC mimetics and critically depends on the phosphorylation of RIPK3 by RIPK1. In several other circumstances, however, RIPK1 is dispensable for necroptotic responses or even inhibits them in an active manner. This applies to various other TNFR1 interactors that participate in necroptotic signaling, most of which also regulate CASP8-dependent apoptosis and proinflammatory NF-κB activation. Please note that several physical or functional interactions have been omitted for the sake of simplicity. From (Galluzzi, Kepp, et al. 2017a).

Recent studies reveal that heat shock protein 90 kDa (HSP90) regulates the stability and function of RIPK3 and MLKL (Zhao et al. 2016; Jacobsen et al. 2016a) (shown in Fig. 8). HSP90 has been characterized as a molecular chaperon that modulates both the structure and function of associated proteins referred to as clients. Inhibition of HSP90 function disrupted the association between HSP90 and RIPK1, and resulted in the degradation of RIPK1 (Lewis et al. 2000). HSP90 and CDC37 acted as RIP3-associated proteins and dissected the essential role of the HSP90-CDC37 complex in RIP3 activation. 17AAG, a HSP90 specific inhibitor, disrupted the association of RIPK3 with MLKL (Li et al. 2015). Moreover, recent observations from both Jacobsen et al.

(Jacobsen et al. 2016b) and Zhao et al. (Zhao et al. 2016) recovered that HSP90 modulates MLKL stability and function in the necroptosis pathway. HSP90 is also able to regulate necroptosis by directly modulating the functions of RIPK1, RIPK3 and MLKL.

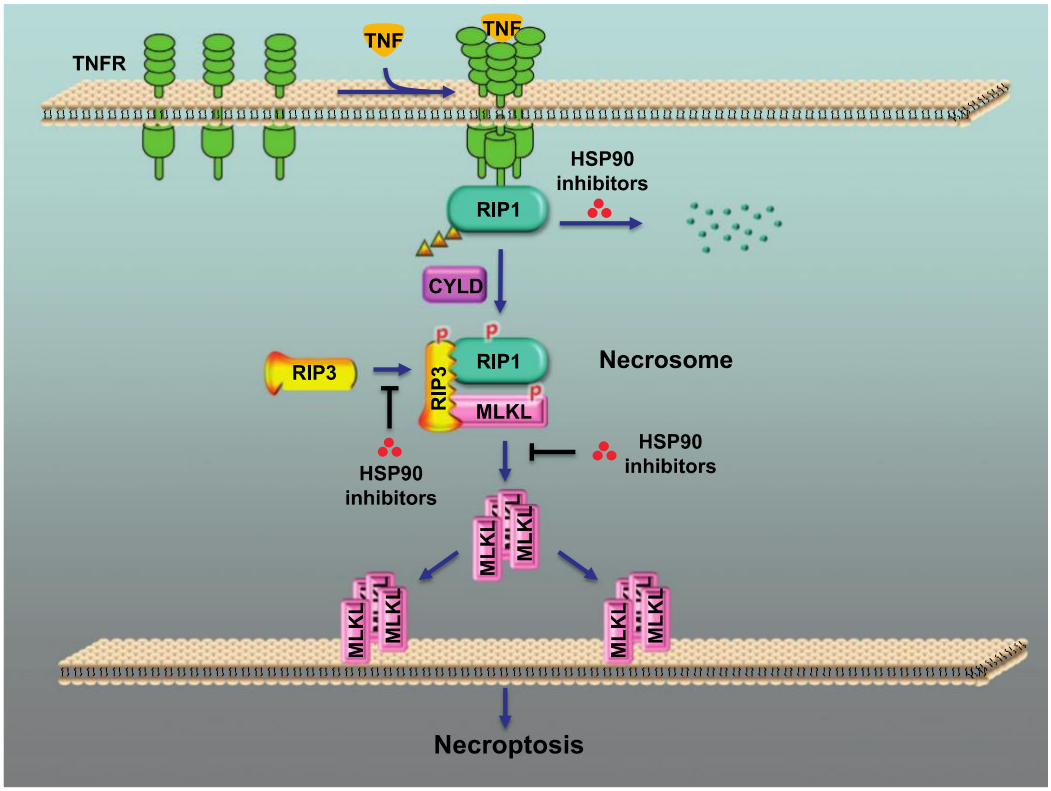

Fig. 8: The role of HSP90 in the regulation of necroptosis. In TNF-induced necroptosis, RIPK1 binds to RIPK3 to form a necrosome, leading to the activation of RIPK3. Subsequently, activated RIPK3 phosphorylates MLKL. Phosphorylated MLKL forms oligomers and translocates to the plasma membrane, inducing necroptosis. Inhibition of HSP90 function blocks necroptosis by directly disrupting the following steps: (i) RIPK1 stability, (ii) RIPK3 activation, and (iii) MLKL oligomerization and translocation to the membrane. From (Yang and He 2016).

1.4.3.2 Pyroptosis

Pyroptosis is a form of regulated necrosis mediated by caspase-1 (also a form of RCD), triggered by perturbations of extracellular or intracellular homeostasis related to innate immunity manifesting with specific morphological features (Jorgensen and Miao 2015). Pyroptosis is mechanistically distinct from other forms of cell death, e.g. necroptosis, apoptosis and autophagy. Active caspase 1 is a defining feature of pyroptosis, and is the key enzyme that mediates the process of this type of cell death (Fig. 9). Caspase 1 is not involved in apoptosis, and caspase 1-deficient mice have no defects in apoptosis and develop normally (Li et al. 1995; Kuida et al. 1995). The apoptotic

caspases, including caspase 3, caspase 6 and caspase 8, are not involved in pyroptosis (Brennan and Cookson 2000; Bergsbaken and Cookson 2007b; Sun et al. 2005), and substrates of apoptotic caspases, including poly (ADP-ribose) polymerase and inhibitor of caspase-activated DNase (ICAD), do not undergo proteolysis during pyroptosis (Brennan and Cookson 2000; Fink and Cookson 2006a; Bergsbaken and Cookson 2007a). Pyroptosis features rapid plasma-membrane rupture and release of proinflammatory intracellular contents. Caspase 1-dependent plasma-membrane pores breakdowns cellular ionic gradients, producing a net increased osmotic pressure, water influx, cell swelling and, eventually, osmotic lysis and release of inflammatory intracellular contents (Fink and Cookson 2006b). Pyroptosis requires cleavage of pro-caspase-1 to active caspase-1 within the inflammasome, a cytosolic protein complex normally consisting of one of several sensor proteins: NACHT, LRR and PYD domains-containing protein (NLPR) 1, NLPR3, NLPR4 (Fig. 10). Gasdermin D (the executor of pyroptosis) is cleaved at Asp276 by active caspase-1 or caspase-11, forming pores that directly permeabilize the plasma membrane (and possibly other mem- branes) causing necrotic cell death (Kayagaki et al. 2015; He et al. 2015; Shi et al. 2015).

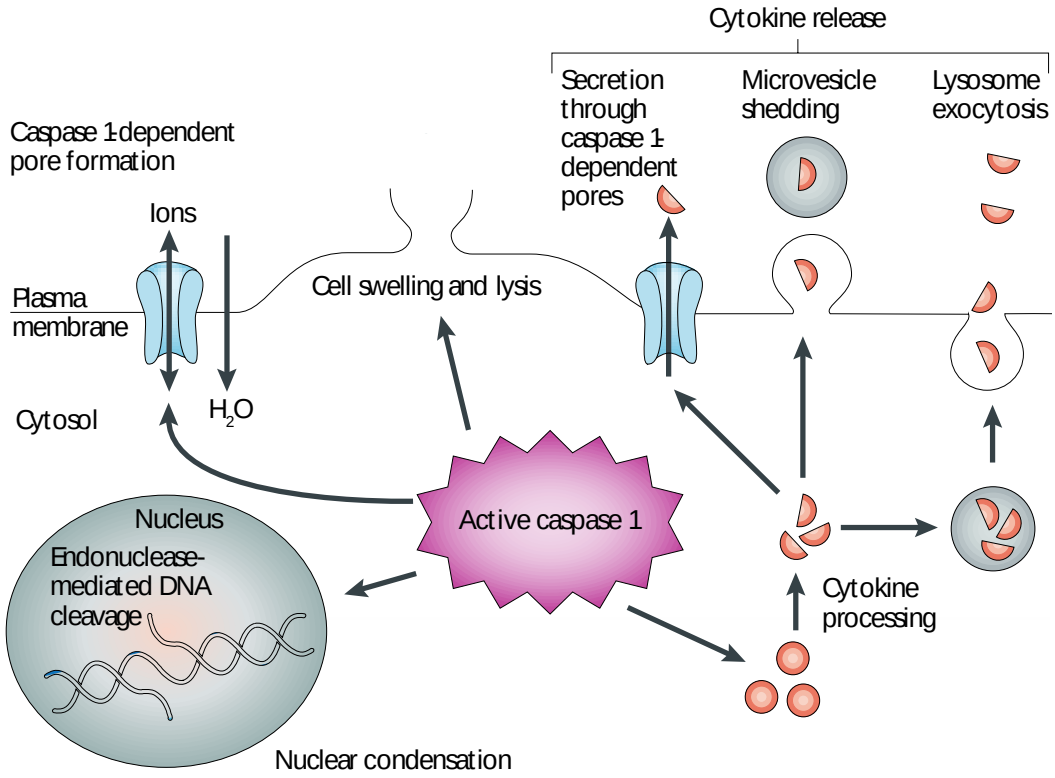

Fig. 9: Mechanisms of pyroptosis. Pyroptosis means that caspase 1, cleaved and activated in response to multiple stimuli, results in a conserved program of cell death.

Caspase 1 activation also leads to rapid formation of plasma-membrane pores with a diameter of 1.1–2.4 nm, which dissipate cellular ionic gradients. From (Bergsbaken, Fink, and Cookson 2009).

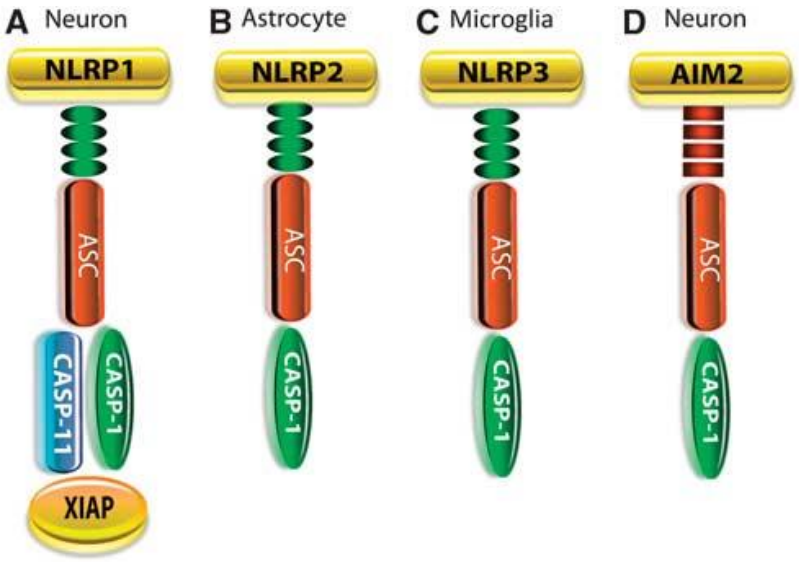

Fig. 10: Inflammasome structure. The sensory component of NLRs or absent in melanoma-2 (AIM2)-like receptors interacts with the caspase-activating recruitment domain protein (ASC) and caspase-1. (A,D) In neurons, the NLRP1 inflammasome contains XIAP and caspase-11 and the AIM2 inflammasome comprises caspase-1, ASC, and AIM2. (B) In astrocytes, the NLRP2 inflammasome is present and comprises caspase-1, ASC, and NLRP2. (C) In microglia, the NLRP3 inflammasome comprises NLRP3, ASC, and caspase-1. From (de Rivero Vaccari, Dietrich, and Keane 2014).

1.4.3.3 Ferroptosis

Ferroptosis is an iron-dependent and lipid-peroxidation-driven form of regulated necrotic cell death (also a form of RCD) (Fig. 11). This type of cell death was recently identified (Dixon et al. 2012) using a pharmacological approach — erastin (Dolma et al. 2003) and RSL3 (Yang and Stockwell 2008). The mechanisms of ferroptosis resulting in necrosis downstream of lipid peroxidation may involve AIF release from mitochondria and nuclear translocation (Pallast et al. 2010; Seiler et al. 2008; Yang et al. 2016), which may share late-stage mechanisms with parthanatos. Glutathione peroxidase 4 (GPX4) plays a critical role in preventing excessive lipid peroxidation in a glutathione-dependent manner, and inhibitors of GPX4 can trigger ferroptosis (Yang et al. 2014).

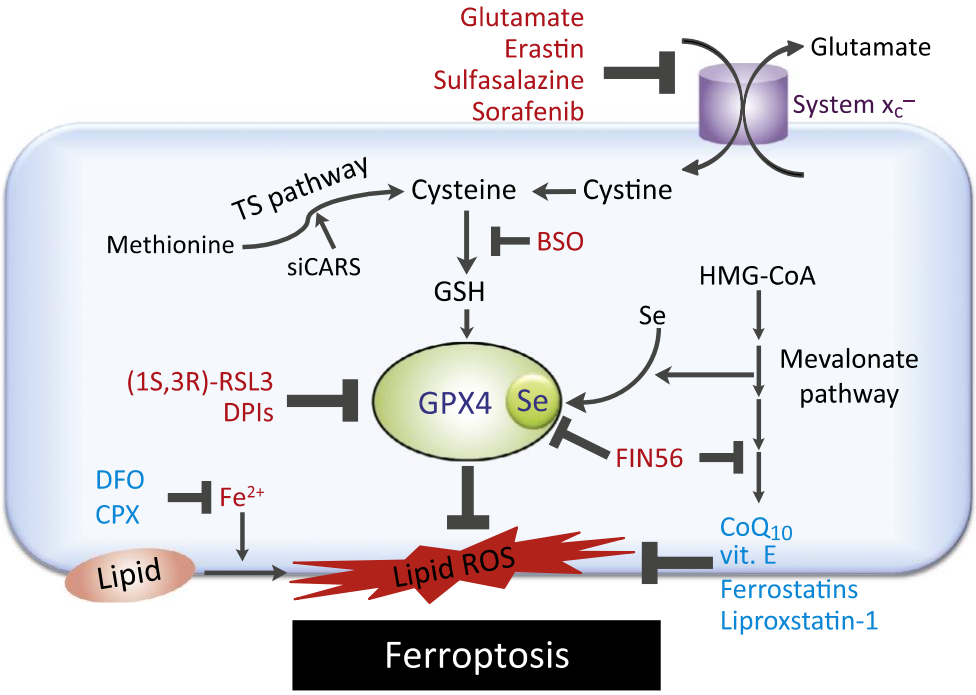

Fig. 11: Molecular pathways of ferroptosis regulation. Small-molecule inducers of ferroptosis are colored red; small-molecule inhibitors of ferroptosis are colored blue. Abbreviations: TS pathway, transsulfuration pathway; Se, selenocysteine; DFO, deferoxamine; CPX, ciclopirox olamine; CoQ10, coenzyme Q10. From (Stockwell 2018).

1.4.3.4 Parthanatos

Parthanatos, a type of regulated necrosis or RCD, is dependent on the activity of poly (ADP-ribose) polymerases (PARP) (Fatokun, Dawson, and Dawson 2014) (Fig. 12). PARP-dependent death requires AIF translocation from the mitochondria to the nucleus and subsequent chromatin degradation (Yu et al. 2002; Cheung et al. 2006). PAR, the product of PARP activity, induces AIF nuclear translocation and also causes bioenergetic collapse through inhibition of the glycolytic enzyme hexokinase, resulting in necrosis (Andrabi et al. 2006; Alano et al. 2010). Cytotoxic effects are mediated by PARP1 hyperactivation, including: (1) NAD_+ and ATP depletion, which ultimately results in a bioenergetic and redox collapse, and (2) the accumulation of poly (ADP-ribose) polymers and proteins at mitochondria, ultimately causing MOMP. Currently, considerable evidences support a role of parthanatos in various neurodegenerative disorders. Blockade of PARP-1 and (in some cases) PARP-2 reduces AIF nuclear translocation and neuroprotection in models of stroke (Eliasson et al. 1998; Bhattacharyya 2015; Culmsee et al. 2005), Parkinson's disease (Mandir et al. 1999;

Kim et al. 2013), Alzheimer's disease (Yu et al. 2010) and traumatic brain injury (Stoica et al. 2014).

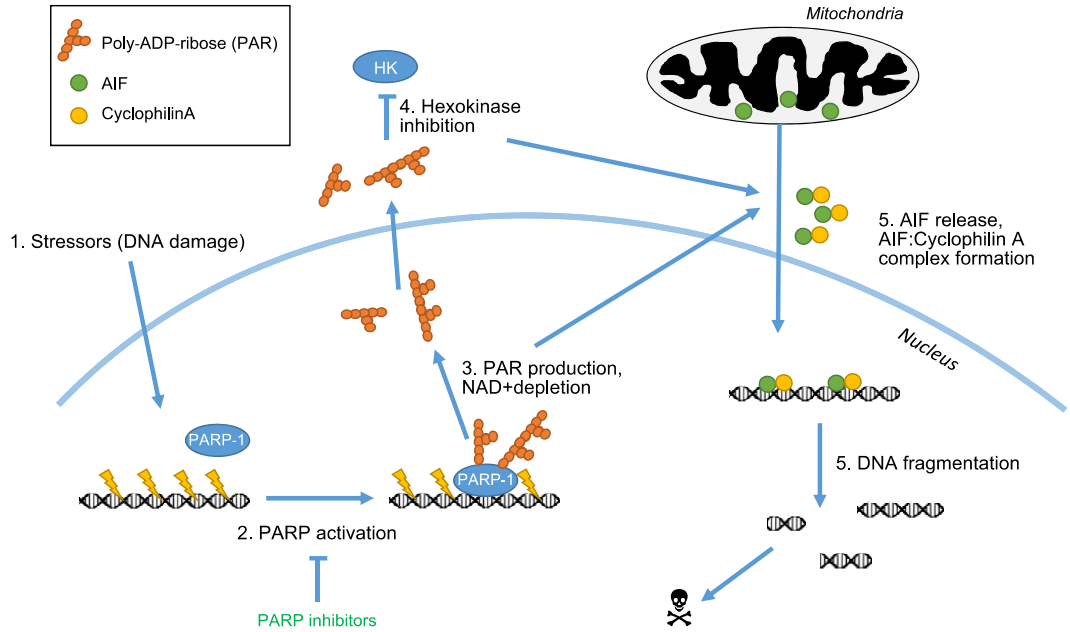

Fig. 12: Molecular Pathways of Parthanatos Regulation. PARP-dependent death requires AIF translocation from the mitochondria to the nucleus and subsequent chromatin degradation. The product of PARP activity, PAR, induces AIF nuclear translocation and also causes bioenergetic collapse through inhibition of the glycolytic enzyme hexokinase, resulting in necrosis. From (Fricker et al. 2018b)

1.4.4 Other types of necrosis

Apart from the forms of regulated necrosis described above, some other forms of regulated necrosis have been identified, e.g. oncosis, lysosomal cell death and cell death by mitochondrial permeability. Oncosis, a form of unregulated necrosis, is mediated by ATP depletion and cell swelling. The trigger of oncosis can be ischemia and mitochondrial dysfunction and/or excessive ATP consumption. Ischemia deprives cells of energy substrates, leading to ATP depletion, followed by failure of the Na^+-K^+ pump, leading to swelling of the cell that may eventually rupture the plasma membrane and plasma membrane depolarization that can open voltage-gated Na^+ and Ca^+ channels. ATP depletion could also causes failure of the Ca^+ pumps, elevating cytosolic calcium, which can induce necrosis via activation of proteases, phospholipases and mitochondrial permeability transition. Lysosomal cell death (LCD) is defined as cell death resulting from lysosomal membrane permeabilization (LMP). LCD is executed mainly by proteases released from lysosomes into the cytosol.

Release of DNase II can also cause nuclear degradation (Thompson, Graham, and Webster 2012). Mitochondria permeability transition is another distinct mechanism causing cell death, which is defined as a largely increased permeability of mitochondria inner membrane related to uncoupling of oxidative phosphorylation, intercellular energy depletion and necrotic cell death. Mitochondria permeability makes the inner membrane freely permeable to protons, ions and all small molecules (< 10 kDa).

Tab. 1: Comparison of different types of cell death

Type of cell death	Initiators	Mediators	Inhibitors	Outcome	DNA Break	Pores
Extrinsic apoptosis	TNF-α, FasL	Caspase 8,3,6,7	Bcl-2	Phagocytosis	Yes	No
Intrinsic apoptosis	Multipe	Caspase 9,3,6,7	Bcl-2, IAPs	Phagocytosis	Yes	Mitochondria outer
Necroptosis	TNF, IAP	RIPK1/3, MLKL	Caspase8	Necrosis via MLKL	No	Plasma membrane
Autophagic	Stress	Beclin, autophagy	Bcl-2	Various	No	No
Ferroptosis	Iron, glutamate	Fe^{2+}, ROS	GTH, GPX4	Necrosis via ROS	No	No
Pyroptosis	Inflammation	Caspase1, gasdermin		Necrosis inflammation	Yes	Plasma membrane
Parthanatos	DNA damage	PARP1, PAR, AIF	Caspase3	Necrosis via ATP↓	Yes	No
Oncosis	Ischemia	Calpain 1, ATP		Necrosis via ATP↓	No	No
Lysosomal	Ca^{+}, ROS	LMP, cathepsin↓	HSP	Necrosis inflammation	Yes	Lysosome
Phagocytic	Inflammatio, stress	PS, CRT, opsonins	CD47	Phagocytosis	No	No
MitoPore	Ca^{+}, ROS	Cyclophilin, ANT	ATP	Necrosis via ATP↓	No	Mitochondria inner

Table revised from (Fricker et al. 2018a; Minchew and Didenko 2017).

Tab. 2: Biomarkers of different types of cell death

Type of cell death	Biomarkers	Note
Apoptosis	Cleaved Caspase 3	RCD
Necroptosis	Phospho-RIPK3/MLKL, Necrosome, (translocation to membrane)	RCD/ Regulated necrosis
Autophagic	Beclin, LC3, Autophagosome	RCD
Ferroptosis	Lacking distinct marker (Excessive lipid peroxidation with necrotic feature)	RCD/ Regulated necrosis
Pyroptosis	Cleaved gasdermin-D, Cleaved Caspase 1	RCD/ Regulated necrosis
Parthanatos	PARP, PAR, AIF	RCD/ Regulated necrosis
Oncosis	/	ACD/ Unregulated necrosis
Lysosomal	Lysosome membrane permeabilization, cathepsin, DNase II	RCD/ Regulated necrosis
Phagocytic	Engulfed cells/orgenelle within phagocytes	RCD
MitoPore	Mitochondrial swelling and rupture	RCD/ Regulated necrosis

From (Fricker et al. 2018a).

1.4.5 Other types of cell death

Currently multiple other forms of cell death, distinguished from the apoptosis, autophagic cell death and necrosis, are discovered and defined either by the stimulus that induces death or the mechanism that executes cell death. Entosis is defined as

engulfment of living cells by other cells, which induces an atypical cell death process (Martins et al. 2017). The key morphological feature of entosis is the cell-in-cell structure. Engulfed cells are eliminated through lysosomal degradation by the host cell. So far no specific biochemical markers for entosis have been described. Apart from entosis, recently other cell death types based on different mechanisms have been introduced, for example, emperipolesis, cannibalism, emperitosis and phagoptosis, and so on (Martins et al. 2017).

1.5 Epilepsy

Epilepsy is a brain state that supports repeated, unprovoked seizures which are unusual, paroxysmal changes in the electrical activity of the brain (Goldberg and Coulter 2013). At any given time, it is estimated that ~50 million individuals worldwide have a diagnosis of epilepsy posing an immense socioeconomic challenge (Birbeck 2010). Seizures can be classified into two clinically useful categories: partial and generalized. The classification of epilepsies has been based on whether or not a focal brain abnormality could be identified (localization related vs. generalized epilepsies) and whether or not a cause could be identified (symptomatic vs. idiopathic) (Shorvon 2011). Temporal lobe epilepsy (TLE) is the most common form of adult localization-related epilepsy. Hippocampal onset accounts for at least 80 % of all temporal lobe seizures (hence called mesial temporal lobe epilepsy (MTLE) or mesial temporal seizures (MTS)) (Tatum 2012). In MTLE syndrome, ~56 % of the cases present a condition termed hippocampal sclerosis (MTLE-HS) (Thom 2014). Although increasingly being understood at the molecular level, epileptogenesis is extremely complex process posing a challenge for the effective pharmacotherapy. Indeed, ~75 % of the total epilepsy cases are pharmacoresistant warranting a resective surgery (Schmidt and Loscher 2005).

1.5.1 MTLE-HS

Anatomically, the hippocampus is a medial temporal lobe structure that runs along a dorsal (septal)-to ventral (temporal) axis in rodents, corresponding to a posterior-to-anterior axis in humans (Strange et al., 2014). The Cornu Ammonis (CA) is divided into four subregions (CA1–CA4; Fig. 13). The human CA1 is represented by a large layer of pyramidal neurons which is in continuity with the subiculum (presubiculum); the CA2

consists of a more compact and narrow layer; the CA3 corresponds to the curve of the CA3 band; and the CA4 lies within the hilus of the dentate gyrus (also referred to as end folium).

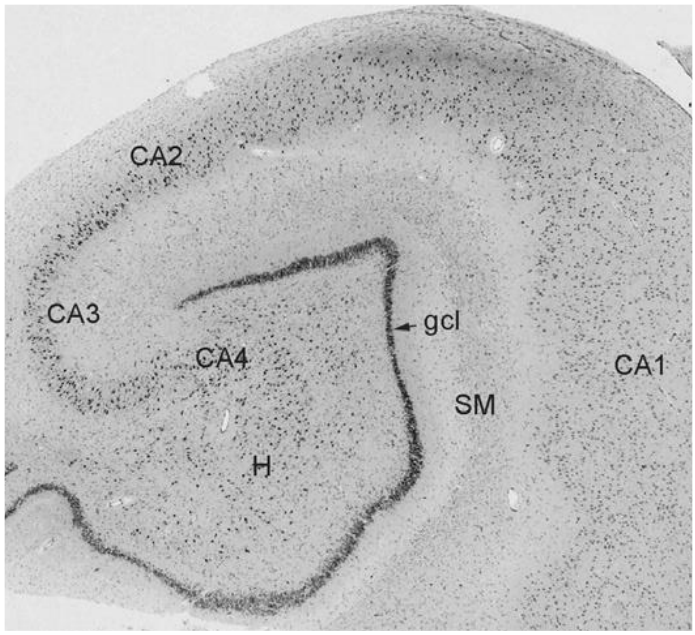

Fig. 13: Hippocampus structure. CA, cornu Ammonis subregions; gcl, granular cell layer of the dentate gyrus; SM, stratum moleculare (molecular layer of the dentate gyrus); H, hilus of the dentate gyrus. From (Ozkara and Aronica 2012).

Gliosis is a major feature of HS (Wieser and Hane 2004) and can be confirmed by immunostaining for GFAP, showing dense astrogliosis in the hilar region of the dentate gyrus as well as in CA subfields where prominent neuronal loss is observed (CA3 and CA1), often including fibrillary gliosis, which supports the chronicity of the atrophic process. A role for astroglial cells in epilepsy (including epilepsy associated with HS) indicates that astroglia can display different morphologies and functional phenotypes within the epileptic focus, potentially contributing to seizure development. The classification of MTLE (Blumcke et al. 2007) is based on the measurements of neuronal cell numbers within the hippocampal subfields CA1–CA4 and in the granule cell layer, using NeuN-stained sections and cluster analysis to identify the different subtypes of neuropathological patterns (Table 3; Fig. 14).

Tab. 3: Classification of mesial temporal lobe epilepsy.

Subtype	Main features
No MTS	Neuronal cell density no different from age-matched autopsy controls
MTS type la (classic hippocampal sclerosis)	Severe cell loss in CA1 and moderate loss in other subfields, excluding CA2
MTS type lb (severe hippocampal sclerosis)	Severe cell loss in all hippocampal subfields
MTS type 2 ("atypical" hippocampal sclerosis)	Severe neuronal loss restricted to CA1
MTS type 3 ("atypical" hippocampal sclerosis)	Severe neuronal loss restricted to the hilar region

MTS, mesial temporal sclerosis.

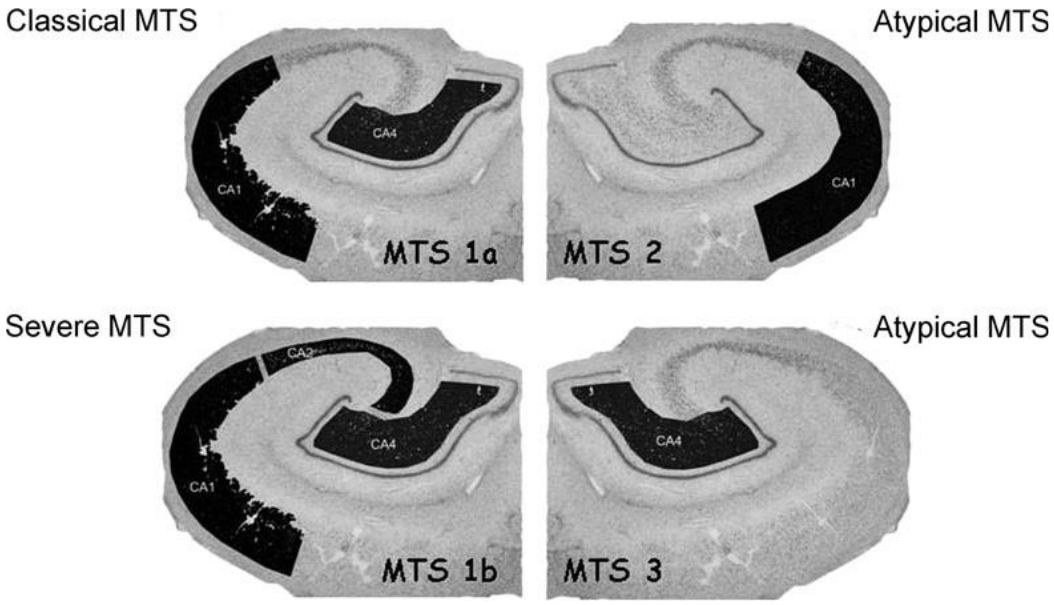

Fig. 14: Classification of mesial temporal sclerosis patterns. MTS 1a: severe cell loss in CA1 and moderate loss in other subfields, excluding CA2; MTS 1b: severe cell loss in all hippocampal subfields; MTS 2: severe neuronal loss restricted to CA1; MTS 3: severe neuronal loss restricted to hilar region. From (Ozkara and Aronica 2012).

1.5.2 Role of astrocytes in epilepsy

The contribution of astrocytes to epileptogenesis can be envisaged from the physiological functions played by them. Astrocyte-mediated metabolic supply sustaining neuronal firing is viewed as pro-epileptic function (Rouach et al., 2002). On the other hand, astrocytic contribution to ion, water and neurotransmitter homeostasis is perceived as being anti-epileptic. Remarkably, this homeostatic function of astrocytes is perturbed in epilepsy. Seizure activity leads to an upsurge in extracellular K_+ which in MTLE-HS is ineffectively regulated partly because of the downregulation of astrocyte Kir4.1 channels and reduction in extracellular space volume (Heuser et al., 2012). This downregulation of Kir4.1 channels is reflected in reduced inward rectifying currents (Hinterkeuser et al., 2000). The resultant accumulation of extracellular K_+ is

expected to exacerbate seizures (Walz, 2000). Interestingly, mutations in the Kir4.1 encoding gene (*KCNJ10*) along with mutations in the aquaporin 4 gene have been linked with MTLE (Heuser et al., 2010). Aquaporins facilitate water movement across the membrane along the osmotic gradients. Aquaporin 4, a predominant water channel expressed by astrocytes in the brain is dislocalized from its position in perivascular end feet due to dystrophin down regulation in MTLE-HS (Eid et al., 2005). Its total expression is however increased (Lee et al., 2004). These alterations in aquaporin expression pattern are expected to disturb not only water but also K_+ homeostasis owing to the fact that the uptake of K_+ drives water flux into the cell. In experimental epilepsy, the perivascular dislocalization of aquaporin takes place even before the chronic phase indicating that it is not mere a consequence but rather can be a contributing factor to the process of epileptogenesis (Alvestad et al., 2013). Furthermore, impairment of gap junction coupling (GJC) function and connexin (Cx) 43 (a main component of GJC) of astrocytes play a crucial effect during epileptogenesis (Deshpande et al. 2017; Bedner et al. 2015).

1.6 Aim of study

Previous unpublished data from our laboratory ((Deshpande 2017)) revealed that there is a significant and transient reduction in the number of GFAP-positive astrocytes in the SR of the ipsilateral hippocampus at 4 h following kainate injection (i.e. during the acute phase). The number of Hoechst-positive nuclei was also reduced, indicating that the astrocytes might die during epileptogenesis. Only a few studies have reported so far that the astrocytes die after epilepsy induction in the hippocampus. A decreased GFAP occupied area and apoptotic astrocytes were discovered in DG region (Kang et al. 2006; Kim et al. 2010; Kim et al. 2011; Kim et al. 2014; Borges et al. 2006), and autophagic astrocytes were discovered in the CA1 region (Ryu, Kim, Yeo, Kim, et al. 2011), whose checkpoints range from days to weeks. However, whether astrocytic death in the CA1 area occur immediately after epilepsy induction, i.e. kainate injection, is remaining unclear so far. Our recent research showed that early astrocytic dysfunction might be a cause of epilepsy development (Bedner et al. 2015). Thus, the goal of this project was to investigate whether and how astrocytes might die immediately after SE, which might contribute to the initiation of epileptogenesis. Using

the established intracortical kainate model of epilepsy, we will address following questions:

Which mechanism(s) is/are responsible for the loss of astroglial cells in epileptic tissue during the early and late phase of epileptogenesis?

Which signal(s) or process(es) trigger this/these mechanism(s)?

2. Materials and Methods

2.1 Animals

Maintenance and handling of animals was according to the local government regulations. Experiments were approved by the LANUV (AZ 84-02.04.2015. A393). Mice were kept under standard housing conditions (12 h/12 h dark-light cycle, food and water ad libitum). Wild-type mice (FVB background) of 90-120 d age were used. The MTLE animal model was established by unilateral intra-cortical kainate injection as described before (Bedner et al., 2015). All kainate injections were performed by Dr. P. Bedner, Institute of Cellular Neurosciences, Bonn. Briefly, the mice were anesthetized (medetomidine (0.3 mg/kg, i.p.) and ketamine (40 mg/kg, i.p.)) and placed in a stereotaxic frame equipped with a manual microinjection unit (TSE Systems GmbH, Bad Homburg, Germany). 70 nl of a 20 mM solution of kainate (Tocris, Bristol, UK) in 0.9 % sterile NaCl were stereotactically injected into the neocortex just above the right dorsal hippocampus. The stereotactic coordinates were 1.9 mm posterior to bregma, 1.5 mm from midline and 1.7 mm from the skull surface. Control mice were given injections of 70 nl saline under the same conditions. After injection the scalp incision was sutured and anesthesia stopped with atipamezol (300 mg/kg, i.p.). Brains from these mice were perfusion fixed with 4 % PFA at 4 h after kainate injection.

2.2 Materials

2.2.1 Chemicals, solutions and reagents

Product	Company
Acetic acid	Sigma Aldrich, Munich, Germany
Acrylamide solution (Rotiphorese Gel 30 (37, 5:1)	Carl Roth, Karlsruhe, Germany
Albumin fraction V	AppliChem, Darmstadt, Germany
Dithiothreitol (DTT)	Carl Roth, Karlsruhe, Germany
Ethanol	Carl Roth, Karlsruhe, Germany
Gel code blue safe protein stain	Pierce (Now Thermo Scientific Waltham, MA, USA)
Hoechst 33258	Sigma Aldrich, Munich, Germany

Isopropanol	Carl Roth, Karlsruhe, Germany
Ketamine 10 %	Bela Pharma, Vechta, Germany
Methanol	Carl Roth, Karlsruhe, Germany
Normal Goat Serum (NGS)	Chemicon (Now Merck Millipore, Darmstadt, Germany)
Normal Donkey Serum (NDS)	Carl Roth, Karlsruhe, Germany
PageRuler	Thermo Scientific Waltham, MA, USA
Paraformaldehyde	Sigma Aldrich, Munich, Germany
Permafluor mounting medium	Thermo Scientific Waltham, MA, USA
Propidium iodide	Sigma Aldrich, Munich, Germany
Phosphate Buffered Saline (PBS)	Gibco (Now Thermo Scientific Waltham, MA, USA)
Protease and phosphatase inhibitor cocktail	Pierce (Now Thermo Scientific Waltham, MA, USA)
Protein A beads	Invitrogen (Now Thermo Scientific Waltham, MA, USA)
Roti-Load buffer (Laemli buffer 4x)	Carl Roth, Karlsruhe, Germany
TritonX-100	Sigma Aldrich, Munich, Germany
Tween-20	AppliChem, Darmstadt, Germany
Tetramethylethylenediamine (TEMED)	Carl Roth, Karlsruhe, Germany
Xylazine	Ceva, Dusseldorf, Germany

2.2.2 Kits

Product	Company
BCA assay kit	Thermo Scientific
Click-iT® TUNEL Alexa Fluor® Imaging Assay	Thermo Scientific
WesternBright® Sirius HRP substrate	Advansta

2.2.3 General materials

Material	Company
Gloves	Ansell ltd, Staffordshire, UK

Mice surgery equipment	Fine Science Tools (F.S.T), Germany
Microscopic slides	Advansta
Pasteur pippetts	Carl-Roth, Karlsruhe, Germany
Pipette tips	Greiner GmbH, Frickenhausen, Germany
PVDF membrane	Millipore, Schwalbach, Germany
Sterile filters	Millipore, Schwalbach, Germany

2.2.4 Software

Product	Company
Gene Tools	Thermo Scientific
ImageJ	Advansta

2.2.5 Instruments

Instrument	Company
Centrifuge 5424	Eppendorf, Hamburg, Germany
DynaMag magnet	Thermo Scientific Waltham, USA
Gene Gnome Imaging system	Synaptics ltd. Cambridge, England
Heat block	VWR, Darmstadt, Germany
SP8® Laser Scanning Microscope	Leica Microsystems, Wetzlar, Germany
Mini-Protean 3 Cell	Bio-Rad, Munich, Germany
Mini-Trans blot Cell	Bio-Rad, Munich, Germany
pH meter	Mettler Toledo, Giessen, Germany
Rotator PTR-30	Grant-Bio, UK
SDS gel electrophoresis power supply	Bio-Rad, Munich, Germany
Shaker	Grant-Bio, UK
Vibratome VT1200S	Leica, Nussloch, Germany
Vortexer	VWR, Darmstadt, Germany
Weighing balance	Acculab, Sartorius group, Germany
Western Blotting power supply	Bio-Rad, Munich, Germany
4℃ Refrigerator	Liebherr, Biberach, Germany

-20℃ Freezer	Liebherr, Biberach, Germany
-80℃ Freezer	Thermo Scientific, Bonn, Germany

2.2.6 Primary antibodies

Antigen	Species	Dilution	Company
RIPK1	rabbit	IF 1:200	Abcam
RIPK3	rabbit	IF 1:200	Abcam
MLKL	rabbit	IF 1:100	LSBio
pMLKL (Ser345)	mouse	IF 1:200	Millipore
GFAP	mouse	IF 1:500	Millipore
GFAP	goat	IF 1:500	Abcam
Iba1	goat	IF 1:300	Abcam
Cadherin	rabbit	IF 1:200	Abcam
LC3B	rabbit	IF 1:200	NovusBio
Cleaved-caspase 3	rabbit	IF 1:200	Cell Signaling Technology

2.2.7 Secondary antibodies

Product	Species	Dilution	Company
Anti-mouse HRP	sheep	IB 1:5000	GE Healthcare
Anti-mouse HRP	donkey	IB 1:5000	GE Healthcare
Alexa Fluor 488	goat-anti mouse	IF 1:500	Invitrogen
Alexa Fluor 488	donkey-anti mouse	IF 1:500	Invitrogen
Alexa Fluor 594	goat-anti rabbit	IF 1:500	Invitrogen
Alexa Fluor 594	donkey-anti goat	IF 1:500	Invitrogen
Alexa Fluor 555	donkey-anti goat	IF 1:500	Invitrogen
Alexa Fluor 647	goat-anti rabbit	IF 1:500	Invitrogen
Alexa Fluor 647	donkey-anti rabbit	IF 1:500	Invitrogen

2.3 Methods

2.3.1 Fixation and sectioning of brains

Mice were perfusion fixed as follows. They were first anesthetized with intraperitoneal injection (100 µl each) of Xylazine and Ketamine (in the ratio 3:2). Using small scissors, the ribcage was opened up and the pericardium was exposed. A 25-G needle connected with PBS and PFA sources was inserted into the left ventricle. An incision was made into the right ventricle in order to make an exit for the blood flow. 20 ml PBS (pH 7.4) was slowly injected into the left ventricle to remove blood, followed by further pumping of 20 ml 4 % PFA for fixation. After perfusion, the brains were isolated by opening up the skull and then were fixed again in 4 % PFA overnight at 4 °C. The next day, brains were transferred in vials containing PBS and stored until further use. They were cut into 40 um thick coronal sections with the help of a vibratome. The sections were stored in PBS containing 0.01 % sodium azide.

2.3.2 Immunohistochemistry

Brain slices prepared as described in 2.3.1 were washed 3 times (5 min each time) with PBS to remove the sodium azide and residual PFA. After permeabilization and blocking (2 h, room temperature) with 0.5 % Triton X-100 and 10 % normal goat serum (NGS) (or 10 % normal donkey serum, NDS) in PBS, the sections were incubated overnight (4°C) in 5 % NGS (or NDS) in PBS containing 0.1 % Triton X-100 and primary antibodies (listed in Table 3.2.6). After washing three times with PBS (5 min each time), the sections were incubated with secondary antibodies conjugated with Alexa Fluor® 488, Alexa Fluor® 594 or Alexa Fluor ®647 (Invitrogen, dilution 1:500 each) in PBS with 2.5 % NGS (or 2.5 % NDS) and 0.1 % Triton X-100 for 1.5 h at room temperature.

2.3.3 TUNEL assay for detection of apoptotic cells

Terminal deoxynucleotidyl transferase dUTP nick end labeling (TUNEL) was performed with the Click-iT® TUNEL Alexa Fluor Imaging Assay (Invitrogen) according to the manufacturer's instructions. Briefly, brain sections were permeabilized with 0.5 % Triton X-100 in PBS. A positive control was prepared by incubating some of the sections with DNAse I for 30 min at room temperature. TdT reaction cocktail was prepared by mixing the following components:

TdT reaction buffer (Component A): 94 µl

EdUTP (Component B): 2 µl

TdT (Component C): 4 µl

The reaction was allowed to take place for 1 h at 37 °C after which it was terminated by removing the reaction cocktail and washing the sections twice with 3 % BSA in PBS for 2 min each time. Click-iT® reaction cocktail, in which the sections were incubated for 30 min at room temperature, was prepared as follows:

Click-iT reaction buffer (Component D): 97.5 µl

Click-iT reaction buffer additive (Component E): 2.5 µl

The reaction was terminated by removing the reaction cocktail and washing the sections 3 times with 3 % BSA in PBS for 2 min each time. For GFAP staining, sections were blocked with 10 % NGS, 0.5 % TritonX-100 in 1x PBS (pH 7.4) for 2 h at room temperature and incubated with mouse GFAP antibody (1:400) in 5 % NGS, 0.25 % TritonX-100 in 1x PBS (pH 7.4) for 1 h at room temperature. The sections were washed three times for 5 min each with 1x PBS followed by incubation with goat anti mouse Alexa Fluor 488 (1:500) secondary antibody in 2.5 % NGS, 0.1 % TritonX-100 in 1x PBS (pH 7.4) for 1 h at room temperature. Sections were washed three times with 1x PBS for 5 min each, followed by staining for nuclei with Hoechst (1:1000, Biostatus ltd, Leicestershire, UK) in 1x PBS for 10 min at room temperature followed by two short washes, drying of the sections and mounting using Permafluor® mounting medium.

2.3.4 Administration of propidium iodide (PI)

We used PI for *in vivo* staining. PI (Sigma, Germany) was diluted in 0.9 % NaCl and filtered. 20 mg/kg of PI was intraperitoneally (i.p.) administered to mice 1 h before sacrifice as previously described (Fan et al. 2016; Oerlemans et al. 2012).

2.3.5 Reverse transcription and real-Time polymerase chain reaction (RT-PCR)

2.3.5.1 Preparation of brain tissue and isolation of mRNA from hippocampal slices for RT-sqPCR

Tissue samples of SR and SLM of the CA1 region were isolated from 200 µM thick coronal slices from 100 days old male FVB mice 4 h after kainate or NACl injection into the cortex (Bedner et al., 2015). By using a stereomicroscope, the CA1 region was isolated using a small scalpel, by removing SP and SO.

Total RNA from tissue samples were treated with Trizol (Invitrogen) under trituration with pipettes and strong shaking until their dissolution and homogenization. 50 µl Trizol was applied to each sample. After different centrifugation and washing steps, the RNA pellet was then dissolved in 10 µl of DEPC-treated water, and stored at -20°C.

The isolated total RNA can still contain DNA fragments, which can be amplified during PCR reaction. Therefore, genomic DNA was removed by DNaseI treatment before reverse transcription and real-time PCR. The reaction mix contained PCR buffer, 2.5 mM $MgCl_2$, 10 mM DTT (final concentration, all from Invitrogen), 40 U RNase inhibitor (Promega) and 20 U DNaseI (Roche). The final volume of each sample was 20 µl and the reaction mix was incubated at 37°C for 30 min. Subsequently, mRNA was isolated from total RNA using magnetic oligo (dT)25 linked DynabeadsTM (Invitrogen). After incubation of total RNA (20 µl) with 20 µl Dynabeads under continuous shaking for 5 min, 3 times washing, the beads with adherent mRNA were suspended in 20 µl DEPC-treated water and stored at -20°C.

2.3.5.2 RT-PCR process

First, cDNA was synthetized from the isolated mRNA (20 µl). The RT mastermix contained first strand buffer, 10 mM DTT (both from Invitrogen), 4 x 250 µM dNTPs (Applied Biosystems), 50 µM random hexamer primers (Roche), 20 U RNase inhibitor (Promega) and 100 SuperscriptIII reverse transcriptase (Invitrogen). The reaction mix (final volume 42 µl) was incubated at 37°C for 1 h.

The reaction volume for real-time PCR contained Taqman mastermix (Takyon, Eurogentec), primers (900 nM each), Taqman probe (100 nM), 1 µl cDNA, final volume 12.5 µl. The reaction mix without template served as a negative control. Samples were incubated at 50°C for 2 min, 10 min denaturated at 95°C, followed by 50 cycles of PCR (denaturation at 95°C for 15 s; primer annealing and extension at 60°C for 1 min). Fluorescence intensity was read out during each annealing/extension step (CFX384 PCR System, Biorad). For amplification of gene transcripts of the necroptosis and autophagy pathways as well as β-actin as housekeeping gene was gene expression assays containing the primer pair and the Taqman probe used (20x; Applied

Biosystems). The probes were labeled on their 5’ end with FAM (6-carboxyfluorescein) and on their 3’ end with a non-fluorescent minor groove binder (MGB):

Reagent type	Designation	Reference	Identifier	Additional information
Taqman gene expression assay	Ripk1	NCBI Reference Sequence NM_009068.3	Mm00436354_m1	1:20
	Ripk3	NM_001164107.1	Mm00444947_m1	1:20
	Mlkl	NM_029005.2	Mm01244222_m1	1:20
	Map1lc3a	NM_025735.3	Mm00458724_m1	1:20
	Map1lc3b	NM_026160.4	Mm00782868_sH	1:20
	Lamp2	NM_001017959.2	Mm00495267_m1	1:20
	Becn1	NM_019584.4	Mm01265461_m1	1:20
	Actβ	AK075973.1	Mm02619580_g1	1:20

2.3.5.3 Data Analysis

The expression ratio target gene/ β-actin was determined by comparing C_T values of the target genes with those of the reference gene, b-actin. The quantification of different genes was determined according to the following equation:

$Y = X * E_{CT}$ or, in the logarithmic form $\log Y = \log X + C_T * \log E$, (XX)

where Y is the amount of PCR product, X is the input copy number, E is the efficiency of amplification, and CT the is the cycle number at threshold (Seifert et al. 2009). According to equation XX, the fluorescence intensity R_n read-out from the real-time PCR is proportional to the amount of PCR product Y, and was determined at each PCR cycle. Threshold cycle C_T was determined for each gene at the same R_n, and the ratio in input copy number was calculated according to equation YY (C_T-method):

$X_{\text{target gene}}/X_{\beta\text{-actin}} = E_{\beta\text{-actin } CT\beta\text{-actin}}/E_{\text{target gene } CT\text{target gene}}$. (YY)

The amplification efficiency E was determined using RT qPCR by serial dilution of mouse brain mRNA, and was 1.93 for LC3b, 2.02 for Lamp2, 2.03 for Becn1, 1.10 for Ripk1, 1.94 for Ripk3, 2.16 for Mlkl, and 2.06 for Actβ.

2.3.6 Image acquisition and cell counting

All images were acquired at a resolution of *x* = 1,024, *y* = 1,024, using a confocal laser scanning microscope (Leica TCS SP8, Germany), with 63x, 40x or 20x lenses. When using 63x lenses, 30 optical sections of images with 1 µm thickness were quantified. In each mouse, 3 representative adjacent and non-overlapping fields of the areas of interest were captured using rectangular frames (each frame, 184.5 um x 184.5 um for 63x lenses, astrocytes, microglia counting; total area of each field: 34,040 um_2 for astrocytes and microglia), and digitized using a Leica SP8 laser scanning confocal microscope. In the CA1 region, the 3 counting fields of interest were located in the CA1 SR and they were positioned side-by-side, as shown in Fig. 15. Data obtained in each of the 3 frames of interest were averaged, thus providing a single value for each subfield in the hippocampi. Values of each mouse were averaged and this value was used for statistical analysis of data. The occurrence of any bias in counting cells should similarly affect control (saline-injected) and kainate-injected and mice since all hippocampi underwent the same procedure in parallel.

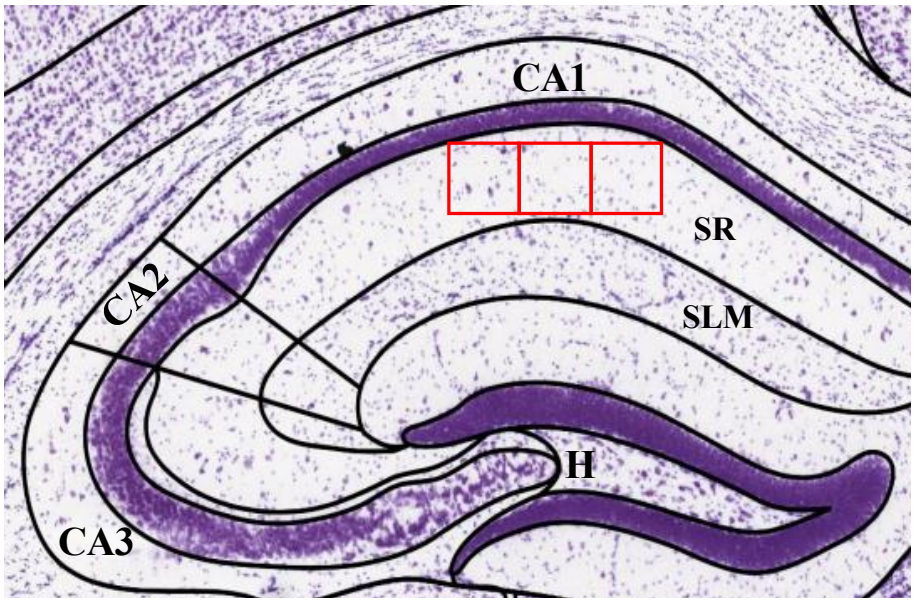

Fig. 15: Counting boxes located in the hippocampus. 3 counting boxes (red color) are located in CA1 SR. From http://atlas.brain-map.org.

2.3.7 Colocalization analysis

Colocalization analysis of all images was quantified by Z-stack using Fiji software. Composited images were converted into 8-bit format and split into single channel, and the background was subtracted. An automatic thresholding method ("Li" algorithm)

was used and kept constant for all images analyzed, without any pretreatment of the images.

2.3.8 Statistics

Data are given as mean ± standard deviation (SD). All error bars represent SD. The difference between groups was tested for significance using the Students’t-test or one way ANOVA, with Tukey post-hoc test. The level of significance was set at $P < 0.05$.

3. Results

3.1 Decreased number of astrocytes and increased proliferation of GFAP positive astrocytes during early epileptogenesis

Quantification of GFAP positive astrocytes co-localizing with the nuclear marker Hoechst were performed in 184.52 x 184.52 x 30 μm^3 counting boxes in the SR region (Fig. 16 A, B). There was a reduction of 19.28 % in the total number of astrocytes (16.29 ± 0.60 in control mice vs. 13.15 ± 1.26 in kainate-injected mice, 4 h post kainate injection). A 10.28 % decrease in the number of nuclei in the same region was also found (45.82 ± 1.46 control mice vs. 41.11 ± 3.15 in kainate-injected mice, 4 h post kainate injection). However, the number of non-GFAP positive cells did not alter significantly (29.53 ± 1.52 in control mice vs. 27.96 ± 2.32 in kainate-injected mice, 4 h post kainate-injection). The *gfap* expression showed unaltered between kainate-injected and control mice (Fig.16E). Moreover, skeleton analysis of astrocytes showed morphological alteration of astrocytes, 4 h post kainate-injection.

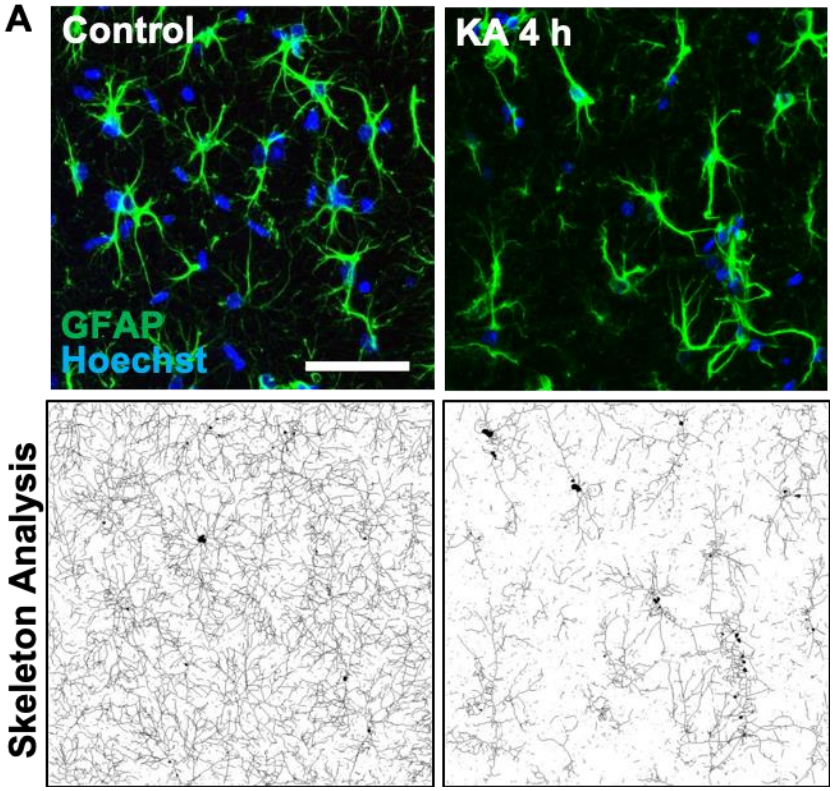

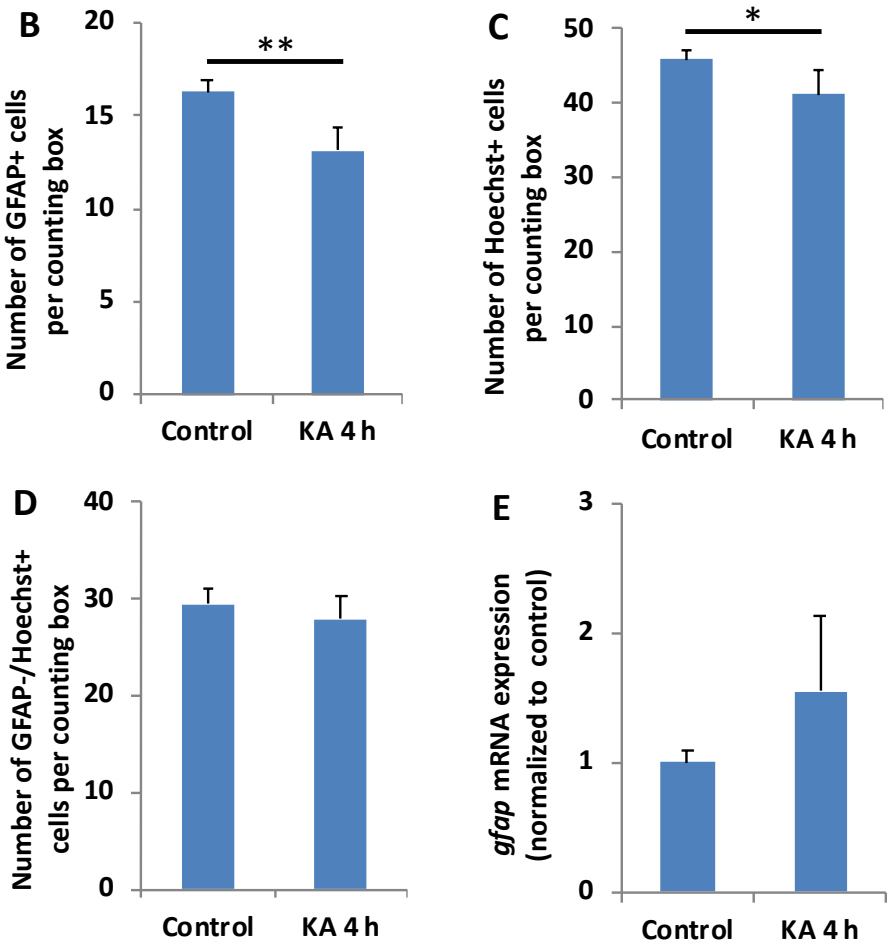

Fig. 16: Quantification of astrocyte number in the CA1 SR of hippocampi of kainate-injected mice during early epileptogenesis. (A) Representative microphotographs of GFAP immunostaining and skeleton analysis in the CA1 SR region (ipsilateral side) from control and kainate-injected (4 h post injection) mice. Scale bar = 50 µm. **(B,C,D)** Quantitative analyses of GFAP+, Hoechst+ and GFAP-/Hoechst+ cells. ** $P < 0.01$, * $P < 0.05$, n = 5 mice in control and 6 mice in KA 4 h group). **(E)** Quantitative analyses of *gfap* expression. n = 3 mice per group.

We analyzed the time course of changing astrocyte numbers post SE induction (Fig. 17A: 16.29 ± 0.60 in control, 13.15 ± 1.26 at KA 4 h, 14.33 ± 0.72 at KA 1 d and 20.15 ± 2.75 at KA 3 d). The number of astrocytes transiently decreased at 4 h post kainate-injection and subsequently repopulated by 3 d post kainate-injection. Enhanced proliferation of astrocytes happens followed by astrocytic degeneration after seizures induction (Kang et al. 2006; Borges et al. 2006). Thus proliferation of astrocytes was investigated by using a combination of GFAP, Vimentin and Ki67 staining. Fig. 17 B1,2 shows an increase of Ki67 positive astrocytes in kainate-injected mice, 3 d post injection. Additionally, a considerable amount of vimentin+ and Ki67+ cells was also

detected in kainate-injected mice, 3 d post injection, but not in control mice, indicating the presence of immature proliferating astrocytes.

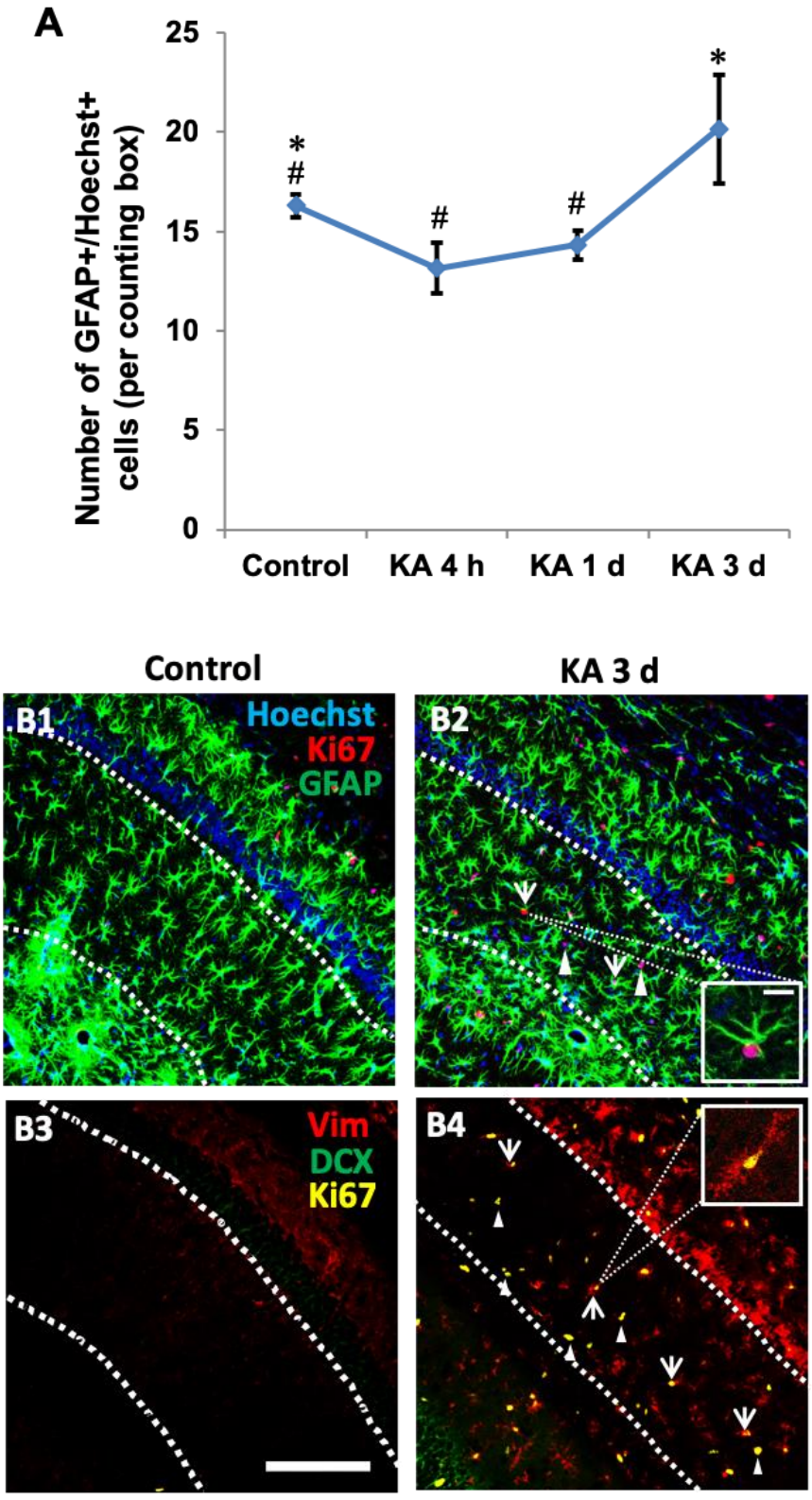

Fig. 17: Repopulation and proliferation of astrocytes in the CA1 SR of hippocampi of kainate-injected mice. **(A)** Quantitative analysis of GFAP+ cells at different time points

after SE induction. n = 5 mice in control group, 6 mice in the KA 4 h group, 3 mice in the KA 1 d group and 3 mice in the KA 3 d group). * P < 0.05 compared to KA 4 h group. # P < 0.05 compared to KA 3 d group. **(B)** Representative microphotographs of immunostaining in the CA1 SR region (ipsilateral side) from control and kainate-injected (3 d post injection) mice with the indicated antibodies. Scale Bar = 50 μm. Double staining of Ki67 and GFAP in the control group (B1) and the KA 3 d group (B2). Triple staining of Vimentin, DCX and Ki67 in the control group (B3) and the KA 3 d group (B4). Scale bar = 100 μm. Inset panel in B2 and B4, scale bar = 15 μm.

3.2 Detection of autophagic astrocytes during early epileptogenesis

Energy shortage is an important feature during SE after kainate injection, which also is a potential trigger of autophagy (Dikic and Elazar 2018). HMGB1 release from nuclei during early epileptogenesis also could induce autophagy (Maroso et al. 2010a; Tang et al. 2010a). Thus, we investigated whether there are autophagic protein-positive astrocytes in CA1 SR. An antibody to LC3B, a widely used biomarker of autophagosome, was applied to check autophagy in our study. We found an ipsilateral increase of LC3B positive astrocytes in the CA1 SR in kainate-injected mice (0.075 ± 0.035) while no LC3B positive astrocytes were found in control mice (Fig. 18A,B). This change was correlated with an upregulation of *lc3* expression (relative increase ratio: 1.36 ± 0.23 vs. 1.0 ± 0.10, for the ipsilateral CA1 SR in kainate-injected and control mice, respectively) (Fig. 18C).

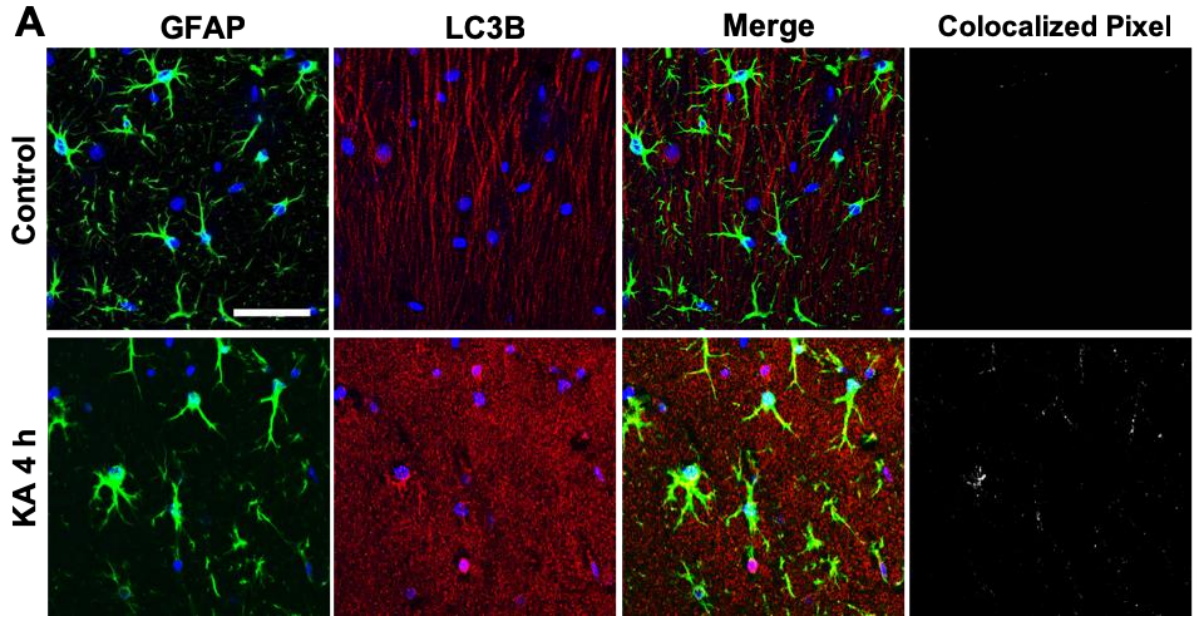

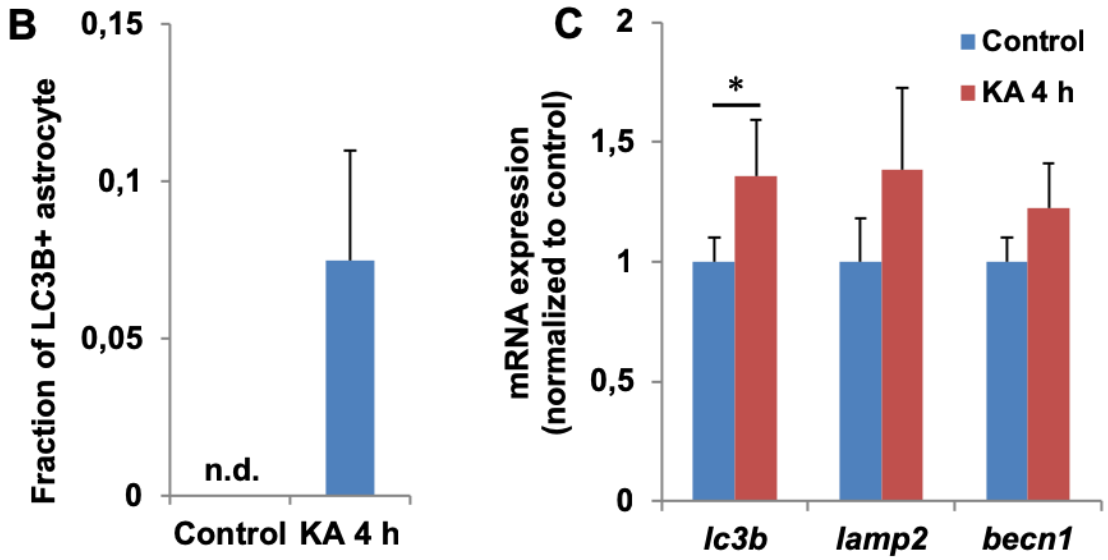

Fig. 18: Upregulation of autophagic protein (LC3) and transcript in the CA1 SR of hippocampi of kainate-injected mice. (A) Representative microphotographs of the CA1 SR (ipsilateral side) from control and kainate-injected (4 h post injection) mice with the indicated antibodies. Scale bar = 50 µm. **(B)** Quantitative analyses showed a significant increase of LC3B+ astrocytes (GFAP positive) in kainate-injected mice compared with control mice. n = 3 mice per group. **(C)** Quantitative analyses of autophagy-related genes expression. *lc3b* but not *lamp2* and *becn1* expression showed a significant increase in CA1 SR of kainate-injected mice compared with control mice. n = 5 mice per group. * $P < 0.05$. n.d.: not detected.

3.3 Detection of apoptotic and necrotic astrocytes during early epileptogenesis

We used a combination of cleaved-caspase 3 (CC3) staining and the TUNEL method (Fig. 19A,B) for detecting apoptosis, which indicate early and late apoptosis respectively. As a result, no CC3 and TUNEL positive astrocytes were detected in the CA1 SR in the ipsilateral side after kainate-injection. Subsequently, we performed PI-*in vivo* injection for detecting necrotic astrocytes in the CA1 SR. PI, a membrane impermeable dye, labels cells with damaged membranes, indicating necrotic cell death. An increase of PI positive astrocyte numbers was found in the CA1 SR in kainate-injected mice.

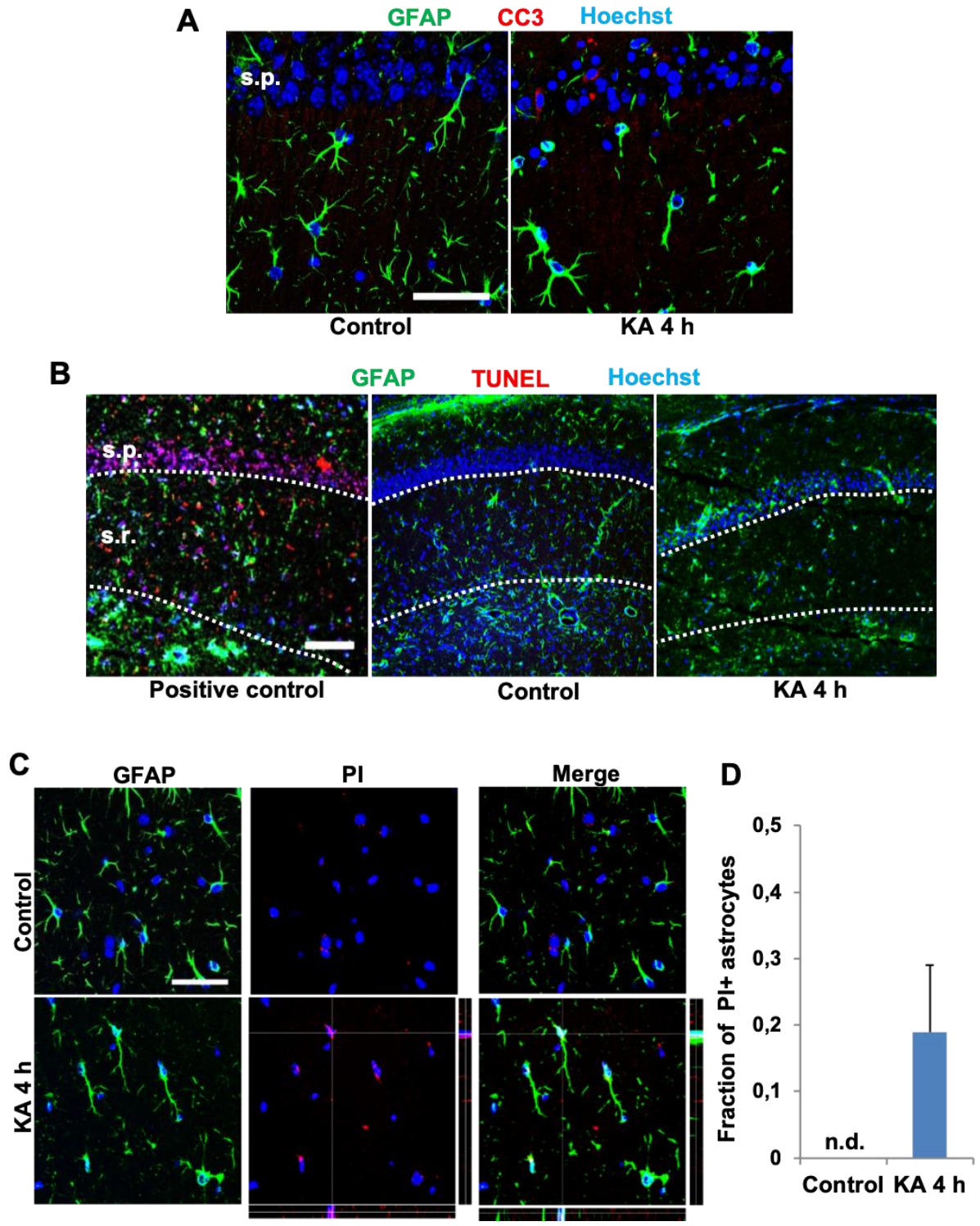

Fig. 19: Detection of apoptotic and necrotic astrocytes in the CA1 SR of hippocampi of kainate-injected mice. (A,B) Co-staining of cleaved caspase-3 (CC3)/TUNEL, GFAP and Hoechst to detect apoptotic astrocytes. No CC3+ astrocytes but a few CC3 positive pyramidal neurons were detected. DNase I treated brain sections were used as a positive control. Confocal images from the CA1 SR revealed apoptotic cells in the positive control. No TUNEL positive cells were detected in the CA1 SR, 4 h post kainate-injection. Scale bar = 100 µm. From (Deshpande 2017). **(C)** Combination of in vivo PI-labeling and GFAP immunofluoresence of the CA1 SR

(ipsilateral side) from control and kainate-injected mice (4 h post injection). Scale bar = 50 µm. **(D)** Quantification of PI+ astrocytes (GFAP positive). n.d.: not detected.n = 3 mice per group.

3.4 Necrotptoic proteins are upregulated in hippocampal astrocytes during early epileptogenesis

Since we found necrotic astrocytes in the CA1 SR, necroptosis, a frequently regulated form of necrosis, was checked in astrocytes during early epileptogensis. At 4 h after the onset of seizures, astrocytic RIPK1 immunoreactivity was found in astrocytes in the CA1 SR in both control and kainate-injected mice (Fig. 20) ipsilaterally. Subsequently, other key necroptotic proteins were checked. We found a significant increase of RIPK3 and MLKL positive astrocytes in CA1 SR (Fig. 21A-D) of kainate-injected mice (RIPK3+: 0.36 ± 0.11, MLKL+: 0.36 ± 0.07) compared to control mice (RIPK3+: 0.07 ± 0.02, MLKL+: 0.05 ± 0.03). An increase of RIPK3 and MLKL positive astrocytes was also observed in CA1 SLM, CA3 and hilus subregions of the hippocampus in kainate-injected mice (Fig. 22A,B). Taken together, these data indicate that both RIPK3 and MLKL, which are crucially engaged in necroptosis, are increased in astrocytes in all subfields of the hippoampus during early epileptogenesis. MLKL activation by phosphorylation is one of the most important step for cellular membrane disruption and death. In the next step, we therefore investigated whether and through which mechanisms MLKL in astrocytes was phosphorylated.

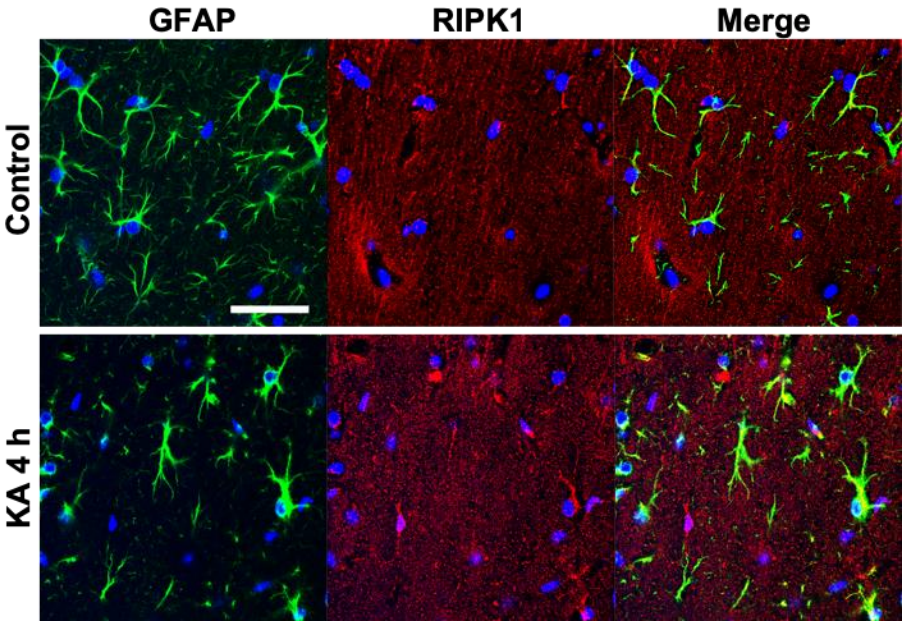

Fig. 20: Astrocytic immunoreactivity on RIPK1 in the CA1 SR hippocampi of kainate-injected mice. Representative microphotographs of the CA1 SR (ipsilateral side) from control and kainate-injected (4 h post injection) mice with the indicated antibodies. Scale bar = 50 µm.

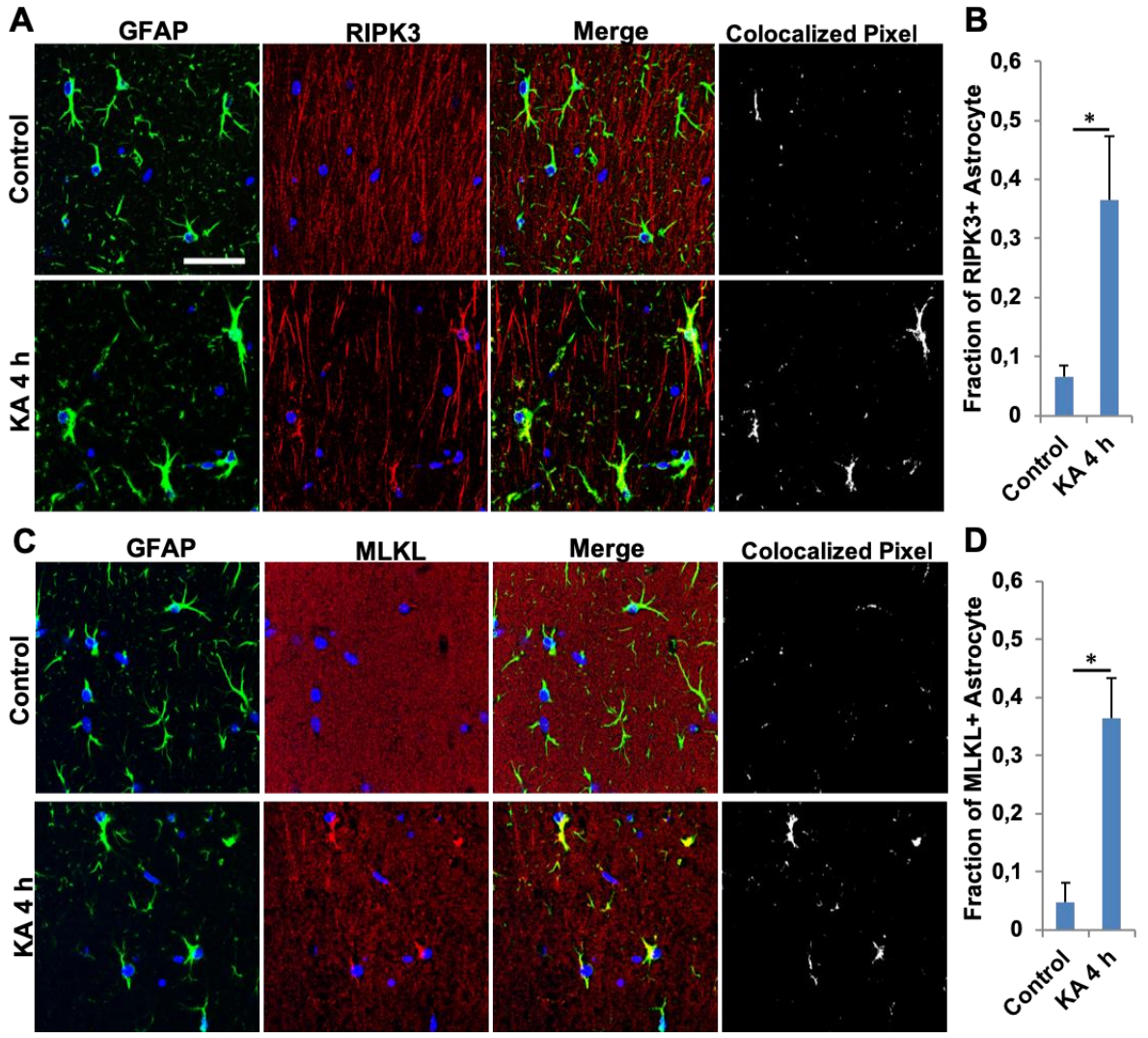

Fig. 21: Quantification of RIPK3 and MLKL positive astrocytes during early epileptogenesis. (A, C) Representative microphotographs of the CA1 SR region (ipsilateral side) from control and kainate-injected mice (4 h post injection) with the indicated antibodies. Scale bar = 50 µm. **(B, D)** Quantitative analyses showed a significant increase of RIPK3+ and MLKL+ astrocytes (GFAP positive) in kainate-injected mice compared with control mice. n = 3 mice per group. $*P < 0.05$.

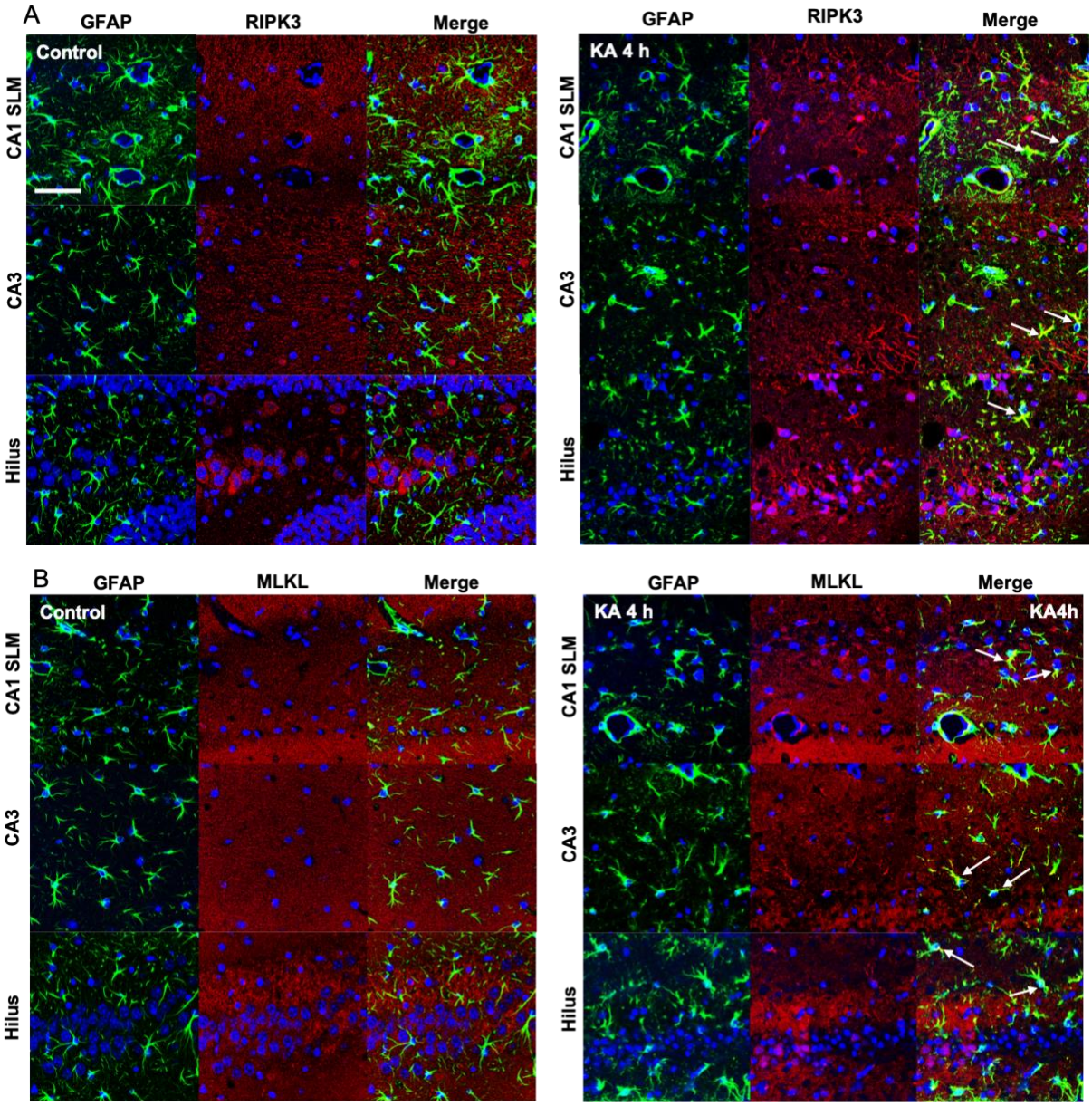

Fig. 22: Astrocytic immunoreactivity of RIPK3 and MLKL in CA1 SLM, CA3 and hilus of hippocampi of kainate-injected mice. (A, B) Representative microphotographs of CA1 SLM, CA3 and hilus (ipsilateral side) from control and kainate-injected mice (4 h post injection) with the indicated antibodies. Scale bar = 50 µm. Arrows indicate RIPK3 or MLKL positive astrocytes.

3.5 Necroptosis-related genes are upregulated in CA1 SR during epileptogenesis

We performed RT-PCR on several important genes involved in celluar necroptosis (*ripk1, ripk3 and mlkl*). As shown in Fig. 23, *ripk3* and *mlkl* but not *ripk1* were ipsilaterally up-regulated in kainate-injected mice (relative increase ratio: *ripk1*: 1.35 ± 0.30, *ripk3*: 4.10 ± 1.94, *mlkl* : 2.74 ± 0.99) compared with control mice. Thus, the

changes of *ripk3* and *mlkl* expression resemble the up-regulations of RIPK3 and MLKL protein in astrocytes of the CA1 SR.

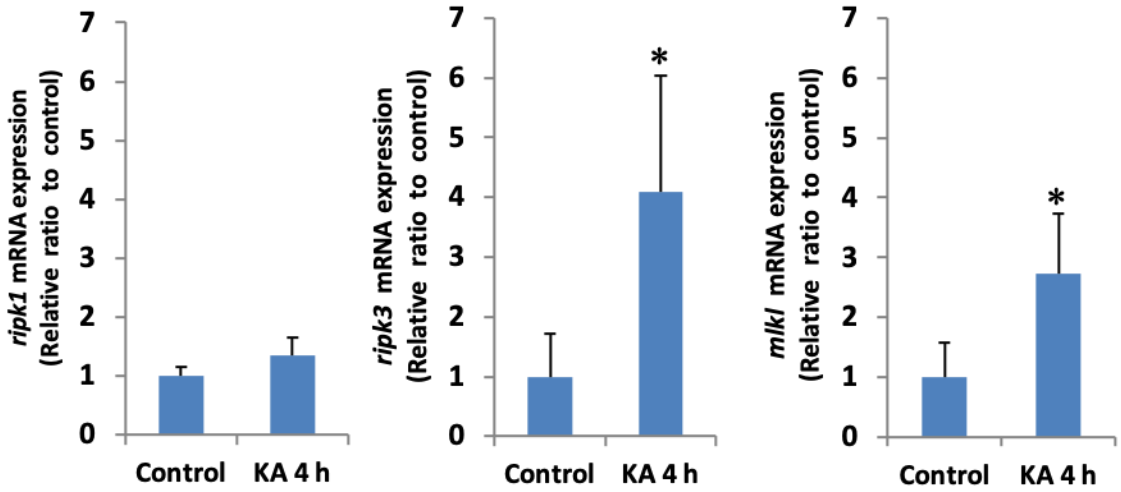

Fig. 23: Upregulation of necroptosis-realated gene expression in the CA1 SR of hippocampi of kainate-injected mice. (A-C) Quantitative analyses of necroptosis-related gene expression. *ripk3* and *mlkl* but not *ripk1* expression showed significant increases in kainate-injected mice compared with control mice (4 h post injection). n = 5 mice per group. ∗P < 0.05.

3.6 Necrosome is formed in astrocyte during epileptogenesis

During necroptosis, RIPK3 is activated by phosphorylation and binds to and phosphorylates MLKL at serine 345. Necrosome composed of RIK3 and MLKL is the executive factor that causes membrane disruption and thus cell death. To determine whether these events occur during epileptogenesis, we used an antibody specifically targeting phosphorylated serine 345 of MLKL (pMLKL). As shown in Fig. 24A,B, an increase of pMLKL positive astocytes was detected in the CA1 SR in kainate-injected mice. Subsequently, we co-labeled the CA1 SR in sections from kainate- and control mice with RIPK3 and MLKL antibodies. We found that RIPK3 and MLKL colocalized with pMLKL in astrocytes (Fig. 25A-C) in kainate-injected but not in the control SR. We found pMLKL not only in nucleus but also in the cytoplasma (Fig. 25B-D). Specially, the nuclear distribution area of pMLKL seemed to be higher than that of RIPK3 and MLKL (Fig. 25B-C). As reported before, translocation of pMLKL into the nucleus is an important sign followed by necroptosis. An subsequently performed colocalization analysis of pMLKL and hoechst (Fig. 25E) found an increase of colocalization in the kainate-injected SR while no colocalization found in control SR. Moreover, we found

that pMLKL translocated to the plasma membrane as indicated by cadherin labelling (Fig. 26).

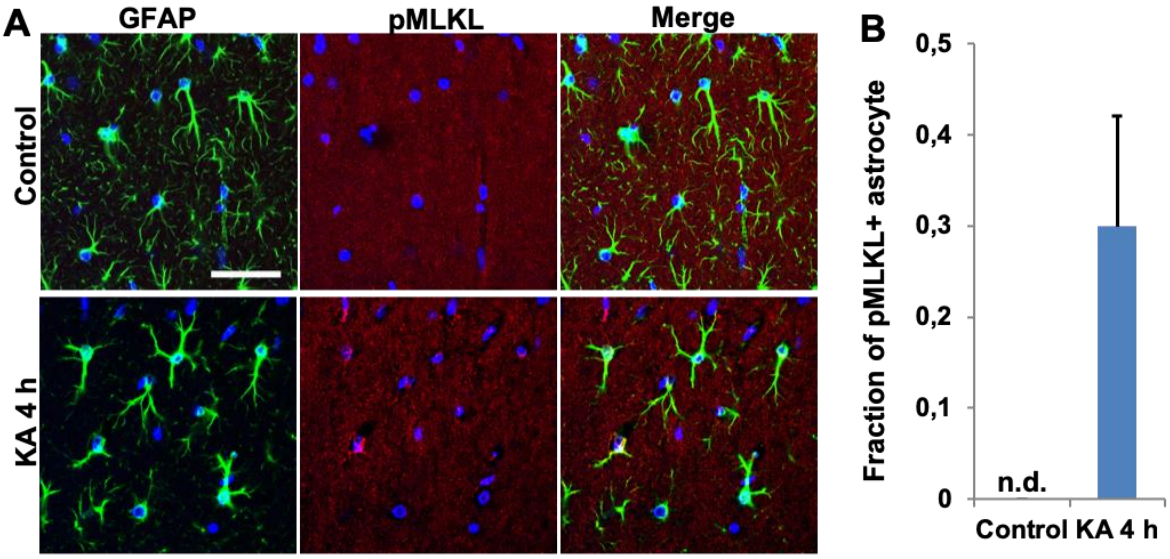

Fig. 24: Phosphorylation of MLKL in astrocytes in the CA1 SR of hippocampi of kainate-injected mice. (A) Representative microphotographs of the CA1 SR (ipsilateral side) from kainate-injected and control mice (4 h post injection) with the indicated antibodies. Scale bar = 50 µm. **(B)** Quantitative analyses showed a significant increase of pMLKL+ astrocytes (GFAP positive) in kainate-injected mice (0.29 ± 0.12) compared with control mice (not detected). n = 3 mice per group. n.d.: not detected.

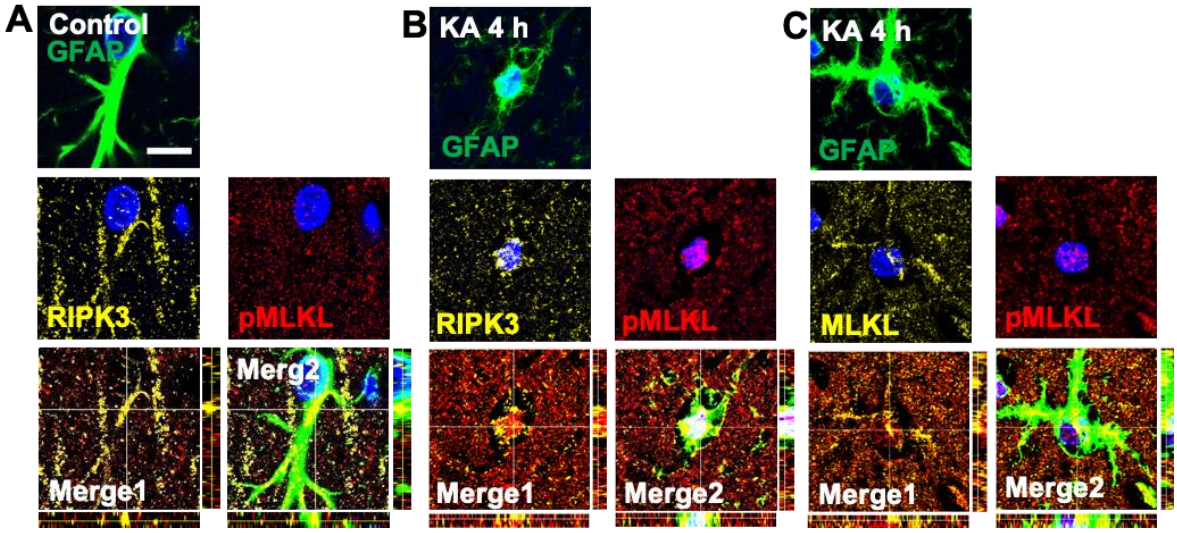

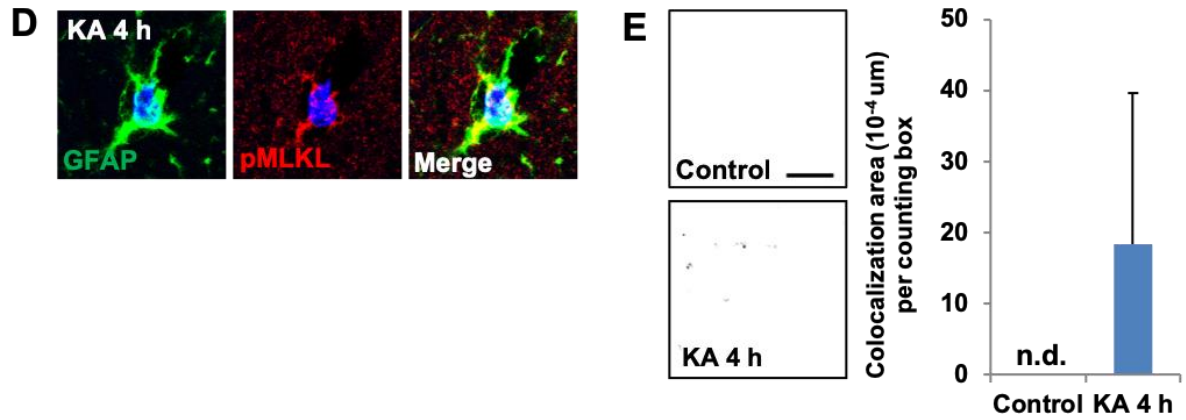

Fig. 25: Astrocytic necrosome formation in the CA1 SR of hippocampi of kainate-injected mice. (A-D) Representative microphotographs of the CA1 SR (ipsilateral side) from kainate-injected (4 h post injection) mice with the indicated antibodies. pMLKL colocalized with RIPK3 **(B)** and was present in both cytoplasm **(D)** and nucleus **(B,C)** in astrocytes while most MLKL was found in the cytoplasm **(C)**. Scale bar = 20 µm. Merge 1: pMLKL & RIPK3/MLKL. Merge 2: pMLKL, RIPK3/MLKL, GFAP & Hoechst. **(E)** Colocalization analysis of pMLKL and nuclei (Hoechst staining) in counting boxes. Scale bar = 50 µm. n.d.: not detected.

Taken together, these data provide evidence of necrosome formation in asrocytes during early epileptogenesis. MLKL phosphorylation, necrosome formation and its translocation to the plasma membrane might be sufficient and necessary for cell death (Linkermann and Green 2014b).

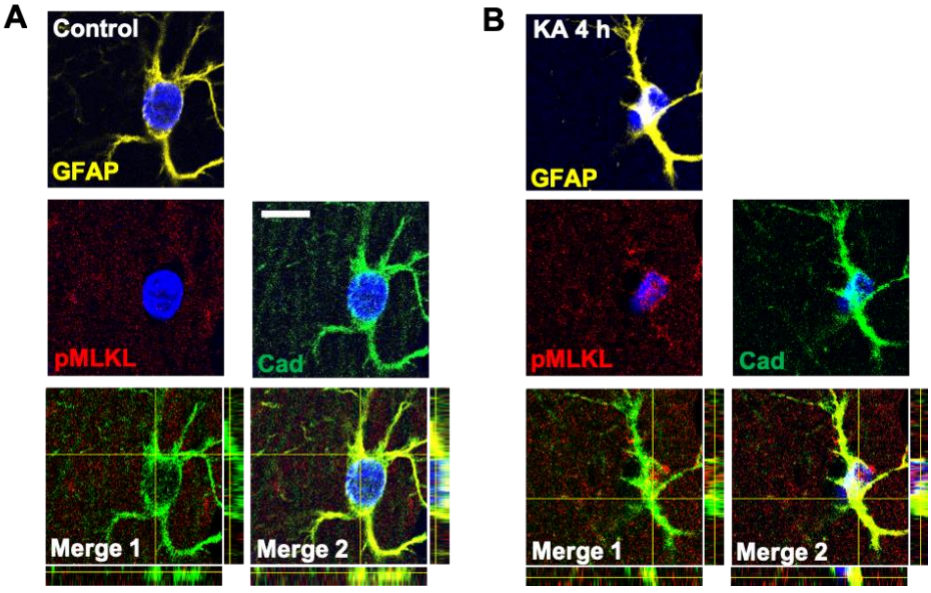

Fig. 26: Translocation of pMLKL to the plasma membrane. (A,B) Representative microphotographs of the CA1 SR (ipsilateral side) from control and kainate-injected (4 h post injection) mice with the indicated antibodies. After kainate injection, pMLKL

colocalized with the plasma membrane labelled by cadherin. Cad: cadherin. Scale bar = 20 μm. Merge 1: pMLKL & Cad. Merge 2: pMLKL, Cad, GFAP & Hoechst.

3.7 Necroptosis is detected in microglia during epileptogenesis

Microglia is activated in epileptogenesis. Whether microglia undergoes necrotptosis in our model is uncertain. We performed immunostaining by using brain sections from normal, control and kainate-injected mice (Fig. 27A). We found no pMLKL immunoreactivity in microglia in normal hippocampus as expected and strong immunoreactivity in microglia in kainate-injected mice. Interestingly, we also detected weak pMLKL immunoreactivity in microglia in control mice. In order to figure out the role of weak pMLKL expression in microglia in control condition, we made a co-staining of RIPK1, RIPK3 and pMLKL (Fig. 27B-D). RIPK1 or RIPK3 did not colocalize with pMLKL in microglia in control condition. The weak pMLKL immunoreactivity in microglia in control mice might be due to the sham surgery. As expected, RIPK1 colocalized with pMLKL in microglia in kainate-injected mice. Another difference between control and kainate-mice is the distribution of pMLKL. pMLKL translocated into nucleus in the kainate condition while pMLKL was distributed inside the cytoplasm in the control conditon. In kainate-injected mice, RIPK3 was weakly expressed. Some reasons might explain this phenomenon. First, it is RIPK3 phosphorylation which concatenates RIPK1 and MLKL and causes phosphorylation of the latter one. Second, MLKL could mediate necroptosis independently of RIPK3 (Gunther et al. 2016a), therefore quantification of both RIPK1 and pMLKL positive microglia may indicate active necroptosis.

Interestingly, we found that some morphologically changed (ameboid shape) microglia only appeared in kainate-injected mice (Fiugre 28), according to the morphological classification (Kettenmann et al. 2011; Hanisch and Kettenmann 2007). A relatively high ratio among these morphologically altered microglia was pMLKL positive microglia (with pMLKL translocation to nucleus).

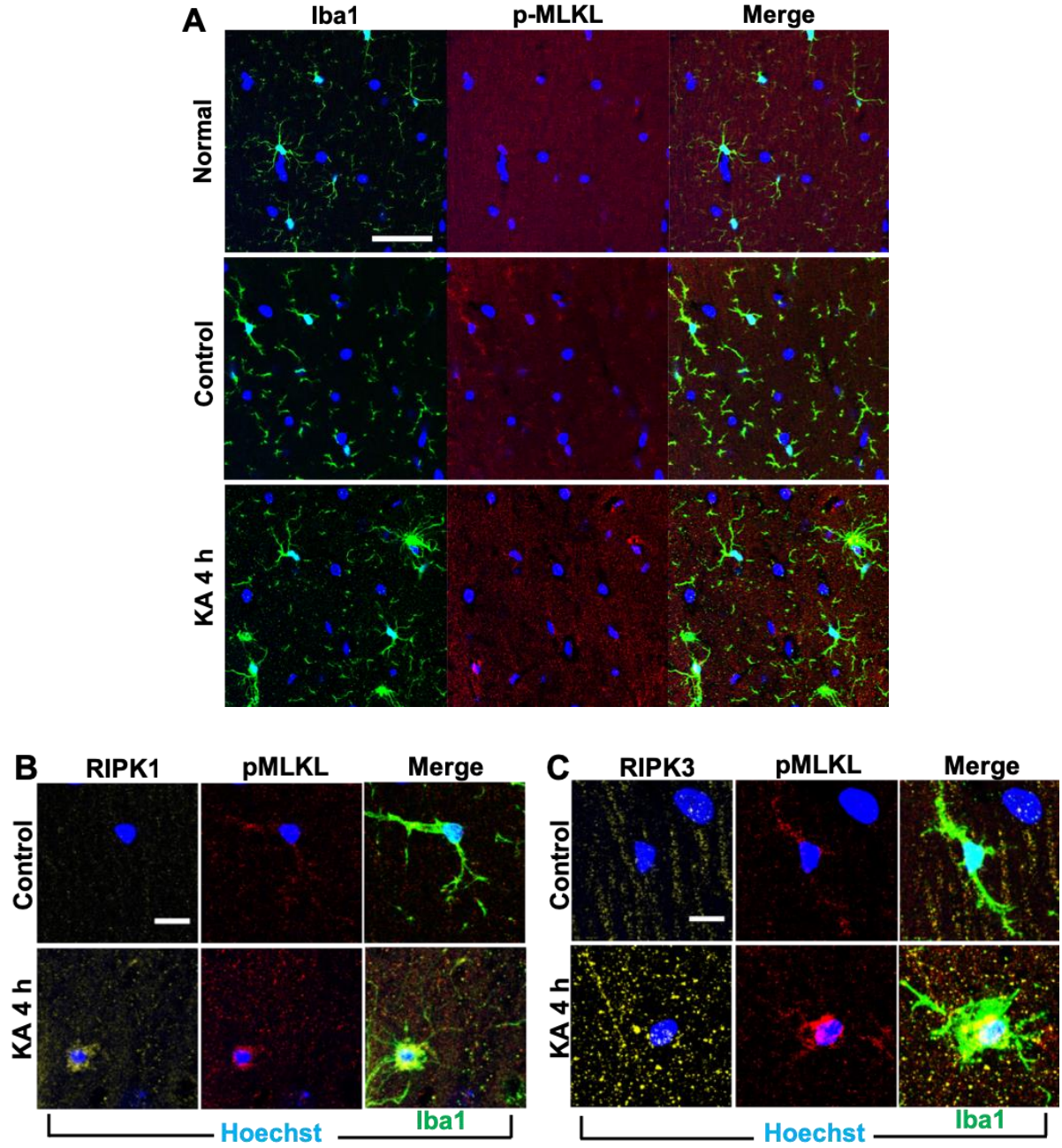

Fig. 27: Detection of necroptotic microglia in the CA1 SR of hippocampi of kainate-injected mice. (A) Representative microphotographs of the CA1 SR (ipsilateral side) from kainate-injected (4 h post injection), control and normal mice with the indicated antibodies. Scale bar = 50 µm. **(B,C)** Representative microphotographs of the CA1 SR (ipsilateral side) from control and kainate-injected mice (4 h post injection) with the indicated antibodies. Scale bar = 10 µm. pMLKL colocalized with RIPK1 in microglia of kainate-injected mice. Notice the weak immunoreactivity of microglial pMLKL, which did not colocalize with RIPK1 or RIPK3 in control mice.

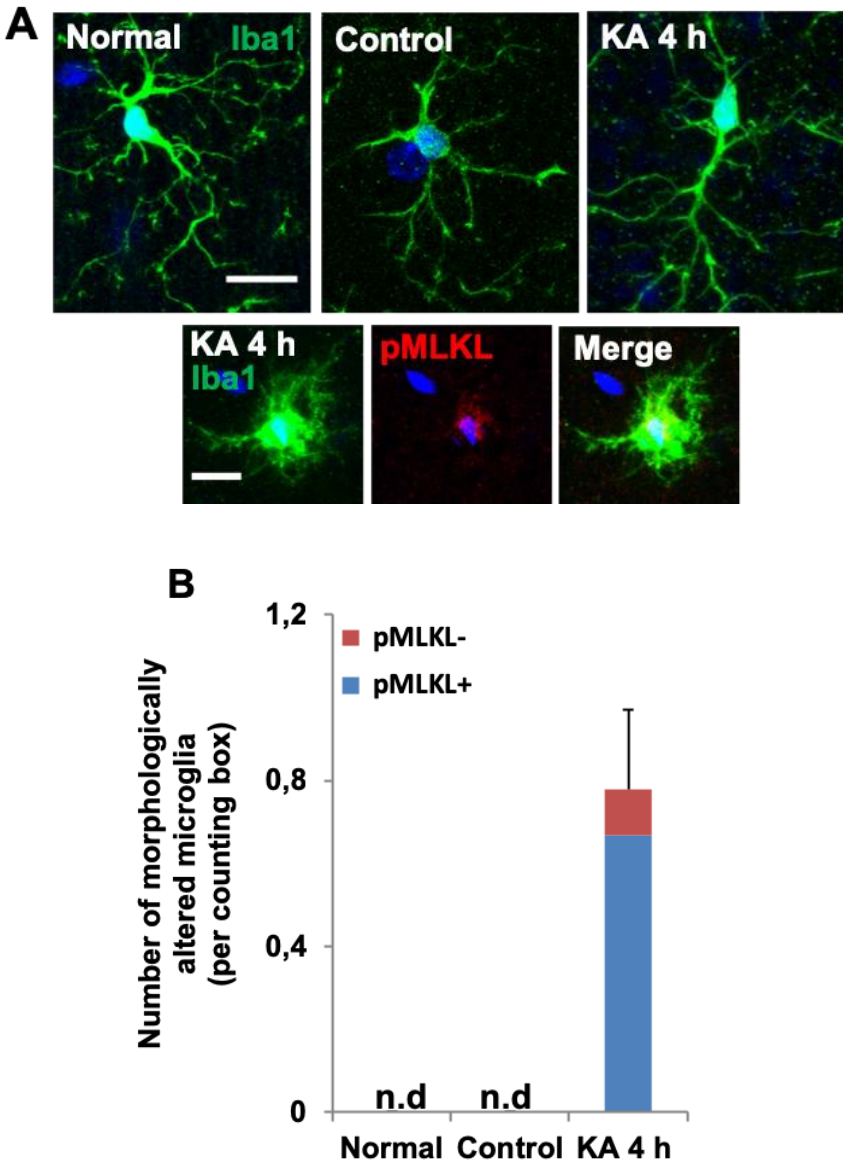

Fig. 28: Altered morphology of microglia during early epileptogenesis. (A) Representative microphotographs of the CA1 SR (ipsilateral side) from control and kainate-injected (4 h post injection) and normal mice with the indicated antibodies. **(A)** upper lane: Scale bar = 15 µm. **(A)** lower lane: Scale bar = 10 um. **(B)** Quantitative analysis of morphology altered microglia. n.d.: not detected.

3.8 Necroptosis is detected in pyramidal neurons during epileptogenesis

Whether necroptosis occurs in pyramidal neurons in our model is unknown. Double staining of RIPK1 and pMLKL, RIPK3 and pMLKL, MLKL and pMLKL can indicate necroptotic neurons. Therefore, combined immunostaining of RIPK1/RIPK3/MLKL and pMLKL was performed in CA1 pyramidal neurons (Fig. 29). As a result, we found that

a few necroptotic neurons were detected during early epileptogenesis in our mouse model of TLE.

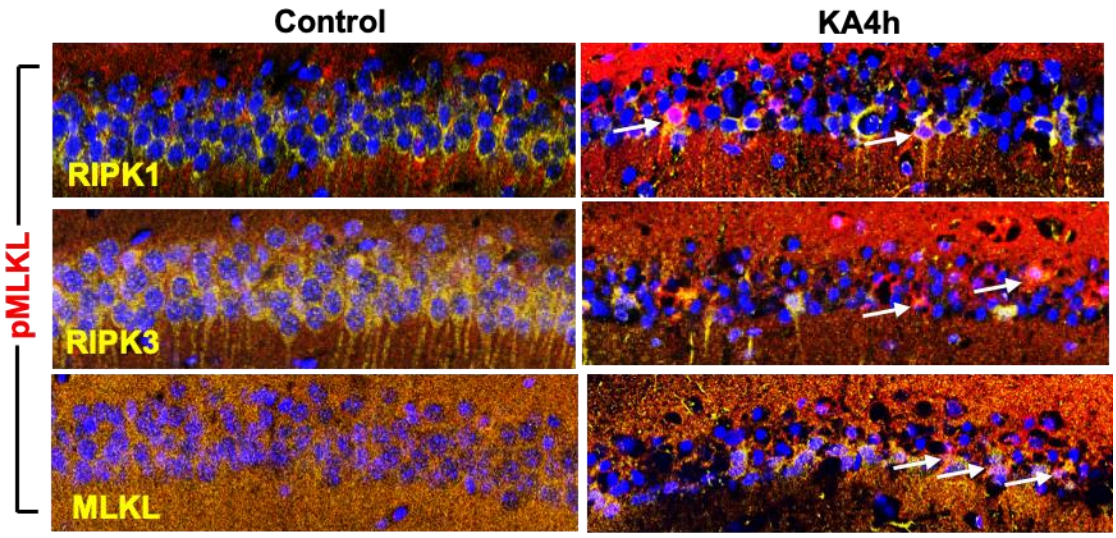

Fig. 29: Detection of necroptosis in the CA1 pyramidal layer of hippocampi of kainate–injected mice. Representative microphotographs of the CA1 pyramidal layer (ipsilateral side) from control and kainate-injected mice (4 h post injection) with the indicated antibodies. Arrows show the colocalization of pMLKL and RIPK1, RIPK3 and MLKL. Scale bar = 50 µm.

4. Discussion

Astrocytes are crucial for maintaining brain physiology (Verkhratsky and Nedergaard 2018). Aberrant functions or pathological changes of astrocytes might exacerbate the development of disease, for example, astrocyte uncoupling can cause epilepsy (Bedner et al. 2015). Astrocytes have drawn attentions from neuroscientists because of their preventive role in the development of epilepsy (Seifert, Carmignoto, and Steinhauser 2010; Steinhauser 2009; Steinhauser, Dupper, and Bedner 2013; Steinhauser and Seifert 2010; Steinhauser, Seifert, and Bedner 2012; Boison and Steinhauser 2018; Rubio-Villena et al. 2018; Hinterkeuser et al. 2000; Seifert, Schilling, and Steinhauser 2006).

Impaired K_+ clearance and increased seizure susceptibility in MTLE- HS have been shown as a result of the reduced expression of Kir4.1 channels (Das et al. 2012; Heuser et al. 2012). Furthermore, mice with glia-specific deletion of Kir4.1 (Kir4.1$^{-/-}$ mice) developed epilepsy (Chever et al. 2010; Haj-Yasein et al. 2011). Astrocytes are connected to each other via GJCs (see section 1.1), allowing the intercellular exchange of ions, second messengers, metabolites, and amino acids, etc.. The astrocytic network is expected to possess antiepileptic function because a reduction of astrocytic coupling would result in the accumulation of extracellular K_+, neuronal depolarization, and a lowered threshold for seizure generation (Crunelli, Carmignoto, and Steinhauser 2015). Our more recent research indicated that early astrocyte uncoupling might cause human MTLE-HS (Bedner et al. 2015). Disturbance of glutamate metabolism seems to be crucially engaged in the pathophysiology of epilepsy (Coulter and Eid 2012). Accordingly, glutamate cause seizures and neuronal loss in experimental epilepsy (Fremeau et al. 2002). Increased extracellular glutamate levels were also found in the hippocampi of patients with MTLE (Cavus et al. 2005). Depletion of GLT1 in mice displayed enhanced seizure susceptibility (Tanaka et al. 1997) and its inhibition reduced the threshold for evoking epileptiform activity (Campbell and Hablitz 2004; Demarque et al. 2004). Pharmacological inhibition of HSP90 dramatically suppressed spontaneous recurrent epilepsy via preventing GLT1 degradation in astrocytes (Sha et al. 2017).

All these findings indicate the tight connection between dysfunctional astrocytes and epilepsy. The pathological changes of astrocytes may contribute to epileptogenesis. The impact of astrocytic cell death in human diseases is increasingly revealed (Ofengeim et al. 2015; Fan et al. 2016; Re et al. 2014; Ito et al. 2016; Caccamo et al. 2017). Whether and how astrocytes die during early epileptogenesis is still uncertain. This important question has been addressed in the present study.

4.1 Astrocyte alteration at 4 h and 3 d post kainate injection

GFAP and S100β are the most commonly used markers to identify astrocytes, which mainly label processes and somota of astrocytes respectively. A dramatic reduction of S100β immunoreactivity was detected in the ipsilateral CA1 area at 4 h post kainate injection (Deshpande 2017). The reduction in S100β immunoreactivity was confined to the ipsilateral CA1 area underneath the injection site. As explained by Tushar Deshpande (Deshpande 2017) the apparent disappearance of S100β immunoreactivity did not indicate the absence of astrocytes. Release of S100β could be a plausible explanation for loss of immunoreactivity, indicating that S100β might not be the optimal markers for labelling astrocytes during epileptogenesis.

Therefore, for the quantification of astrocytes, a combination of GFAP and the nuclear marker Hoechst labeling was used. The ipsilateral number of GFAP positive astrocytes was reduced by 19.28 % in the CA1 SR as compared with the sham condition (Fig. 16). It is still uncertain whether astrocytes underwent certain types of death. We further quantified total cell numbers with Hoechst staining in CA1 SR. As expected, there was a 10.28 % reduction in the number of nuclei, indicating the occurrence of cell death. Moreover, non-GFAP+ cells did not change significantly, which indicating that the reduced astrocytes number mainly contributes to the reduced total cell number (Hoechst+). In addition, *gfap* expression remained similar between control and kainate-injected mice (4 h post injection). These basically rule out the possibility of altered or reduced expression of GFAP in astrocytes, which would resulted in underestimating the number of astrocytes. At 3 days post kainate injection, we observed a repopulation of GFAP positive astrocytes in the CA1 SR, indicating that the previous loss of astrocytes was transient, potentially due to the proliferation of astrocytes occurring within 3 days. Subsequently, we performed Ki67 immunostaining to confirm the

proliferation of astrocytes. A few Ki67 positive astrocytes were observed in the CA1 SR of kainate-injected mice, at 3 days post injection, while no Ki67 positive astrocytes were found in CA1 SR in controls (sham injection with saline). The newly proliferating (Ki67+) astrocytes might explain the repopulation of astrocytes. Indeed, proliferation partially contributed to the repopulation of astrocytes in mouse hilus after SE-induced degeneration (Borges et al. 2006), which is consistent with our results.

Taken together, these data highly indicate the occurrence of astrocytic death during early epileptogenesis. Cell death mechanisms can be classically divided into 3 types (details see section 1.4). The mechanism(s) underlying astrocytic death following epilepsy induction remain(s) largely unexplored. It has been showed that astrocytes in the DG area undergo apoptosis after induction of SE (Ko et al. 2016; Kim et al. 2014; Kim et al. 2010). Autophagic astroglial death was observed in the CA1 area at 6 weeks after SE induction (Ryu, Kim, Yeo, Kim, et al. 2011). Our preliminary results indicated the number of astrocytes transiently decrease at 4 h post kainate injection, indicating astrocytic death might happen early after SE induction. Nevertheless, information about astrocytic death during the development of epilepsy is inconsistent. Therefore, following steps were performed to investigate potential mechanisms of astrocytic death during early epileptogenesis.

4.2 Autophagic astrocytes are detected at 4 h post kainate injection

Autophagy is an adaptive process that occurs in response to energy shortage (Dikic and Elazar 2018), e.g. SE-induced energy deprivation. Autophagy is crucial for maintaining intracellular homeostasis and cell health, while aberrant or impaired autophagy results in diseases (Gan et al. 2015). Recently, it has been shown that autophagy can selectively eliminate potentially harmful cytosolic material, such as damaged organelles or harmful protein aggregates. This process is called selective autophagy. Selective autophagy requires labelling of cargo with ‘eat-me’ signals recognized by autophagy receptors that link the cargo to membrane via their LC3-interacting region. Well-studied targets of selective autophagy are mitochondria, which can be impaired via different mechanisms depending on the physiological context. LC3 is selectively capable of recognizing externalized cardiolipin on the surface of damaged mitochondria in neurons (Dikic and Elazar 2018). Autophagosomes can be identified

by the presence of LC3 using antibodies staining. LC3 is upregulated in astrocytes in kainate-injected mice, which was confirmed by immunostaining and *lc3* gene expression analysis. In present study, we detected a low rate (7.5 %) of LC3B+ astrocytes. HMGB1 has been recently identified as a mediator of autophagy. HMGB1, a nuclear binding-protein, translocates from the nucleus to the cytoplasm during early epileptogenesis (Maroso et al. 2010b). It is the cytoplasmic HMGB1 which binds to Beclin 1 and regulates autophagy (Tang et al. 2010b; Zhu et al. 2015; Kang et al. 2010). However, how Beclin 1 promotes autophagy remains largely unknown. Increased TNF-α following SE is also a potential trigger of autophagic astrocytic death via NF-κB p65/RelA-Ser529 phosphorylation (Ryu, Kim, Yeo, and Kang 2011). This might contribute to the increased number of L3C+ astrocytes. For future studies, transgenic mice, e.g. GFP-LC3 and mCherry-LC3 mice, are necessary for monitoring autophagy in vivo. When GFP-LC3 is expressed on the completed autophagosomes, punctate signals are observed by fluorescence microscopy as ring-shaped structures or dots (Mizushima et al. 2001; Kabeya et al. 2003), which can be used to quantify the autophagosomes in cells and tissues.

4.3 Necroptosis is activated in hippocampal astrocytes at 4 h post kainate injection

A combination of early and late apoptotic measurements (CC3 and TUNEL) were performed, which showed no apoptotic astrocytes at 4 h post kainate injection. Moreover, our previous study found that no TUNEL positive astrocytes in CA1 SR, 1, 4 or 5 days post kainate injection (Bedner et al. 2015). However, a proportion of necrotic astrocytes was found. In the next step, necroptosis, a common form of regulated cell death, was checked further. Our results showed that compared to the control, a significant increase in the number of necroptotic astrocytes and necroptosis gene expression (*ripk3* and *mlkl*) occurred in kainate-injected mice during early epileptogenesis. More interestingly, the increase of RIPK3- and MLKL- positive astrocytes were also observed in CA1 SLM , CA3 and Hilus regions. As confirmed by phosphorylation specific antibody targeting murine S345, MLKL was phosphorylated and colocalized with RIPK3 in kainate-injected mice. The formation of RIPK1/RIPK3-associated necrosome formation, as a core machinery, is necessary and sufficient to execute necroptosis (Zhang, Yang, et al. 2016). MLKL was identified as an

indispensable mediator of RIPK1/RIPK3-initiated necroptosis. Phosphorylation of MLKL by RIPK3 is a key event, and is used as a biomarker of necroptosis activation (Wang et al. 2014). Once phosphorylated, MLKL aggregates to form homodimers and eventually translocates to the plasma membrane, leading to membrane disruption and final cell death (Chen et al. 2014a; Linkermann and Green 2014a). It should be noted that phosphorylation and dimerization of MLKL are sufficient and necessary for necroptosis (Dondelinger et al. 2014; Su et al. 2014; Wang et al. 2014), which is consistent with our results. In the present study, we used laser-scanning confocal microscopy and antibody staining for analyzing necroptosis. Triple immunostaining of GFAP, RIPK3 and pMLKL precisely showed that GFAP positive astrocytes underwent necroptosis during epileptogenesis. Interestingly, we also found that pMLKL translocated into the nucleus ipsilaterally in kainate-injected mice as revealed by colocalization analysis. It has been reported that MLKL translocation to the nucleus is induced by its phosphorylation, which might facilitate necroptosis (Yoon et al. 2016). Of note, in the present study the increased level of pMLKL positive astrocytes is not paralleled by the number of PI positive astrocytes. This phenomenon was first reported by (Yoon et al. 2016) and has subsequently been proved that intrinsic ESCRT-III mechanisms could limit MLKL activation (Gong et al. 2017), which might be a phenomenon accompanying necroptosis. pMLKL translocating to membrane furtherly confirmed that cellular membrane was damaged by necrosomes, indicating the occurrence of necroptosis.

Recently, it has been shown that HSP90 is up-regulated in hippocampal astrocytes during early and chronic phases of epilepsy (Sha et al. 2017). Inhibition of HSP90 by 17AAG has been shown as an effective treatment for epilepsy via preventing the degradation of GLT-1 (Sha et al. 2017). 17AAG also exhibits an anticonvulsant effect on acute seizures. Interestingly, 17AAG is considered as a candidate inhibitor of necroptosis (see section 1.4.3.1). In addition, pharmacological inhibition of HSP90 by 17AAG disrupts the association of RIPK3 with MLKL and the formation of MLKL oligomers. It is still unknown whether 17AAG also contributes to the inhibition of necroptosis of astrocytes and/or other types of cells.

How astrocytic necroptosis is initiated during early epileptogenesis remains to be unraveled. Early increase of cytokines (e.g. TNFα) might be potential reason for triggering necroptosis in our model of TLE. TNFR1 activation by TNFα is a well described necroptosis pathway. Activation of TLR4 is also a trigger for inducing necroptosis. TLR4 could be activated by early released HMGB1 during epileptogenesis. Other possible pathways might include TLR3 activation, etc. (see section 1.4.3). Whether and how necroptotic astrocytes may contribute the development of epilepsy is completely unclear in our model of epilepsy. In order to answer this question, pharmacological inhibition and RIPK3/MLKL knockout mice should be used in the future.

4.4 Necroptosis is activated in hippocampal microglia at 4 h post kainate injection

Microglia is activated very early after seizure induction (Maroso et al. 2010b). Early IL-1β release during seizures and its receptor blockade could exhibit an anticonvulsant effectS (Vezzani et al. 2000). Necroptosis-induced cell death triggers an inflammatory reaction (Galluzzi, Kepp, et al. 2017b), which might contribute to epileptogenesis. Whether microglia undergo necroptosis is uncertain in TLE. Thus, we investigated whether microglia would undergo necroptosis during early epileptogenesis. We found that pMLKL immunoreactivity was present in microglia in kainate- and saline-injected (control) mice but not in hippocampi of normal mice. We found that pMLKL located in the cytoplasm of microglia in saline-injected mice, while in kainate-injected mice, pMLKL located not only in the cytoplasm but also in the nuclei. In order to decide whether necrosomes form in microglia in saline-injected mice, we co-labeled microglia with RIPK1/RIPK3 and pMLKL. Weakly expressed pMLKL without colocalization with RIPK1/RIPK3 in microglia in control mice might be responsible for a rapid increase of cytokines after sham-injection (Müller 2018). Colocalization of pMLKL and RIPK1 in microglia in kainate conditioned mice could indicate active necroptosis (Gunther et al. 2016b).

Morphological changes of microglia seem to be early events during epileptogenesis. Recent work showed that morphological changes of microglia (called reactive-like microglia) play an important role in epilepsy. These reactive-like microglia could drive

epileptogenesis independent of inflammatory responses (Zhao et al. 2018). Thus, we further checked if there was any morphological change of microglia early after induction of seizures. We found a few microglia with activated morphology at 4 h post kainate injection. Interestingly, a relatively high ratio of these morphologically altered microglia was also pMLKL positive. However, the potential link between the morphological changes and pMLKL expression is not clear yet. We noted that pMLKL in these morphologically altered microglia was not only located in nuclei but also in the cytoplasm, which was different to saline-injected mice. This distinct distribution of pMLKL is helpful for identifying necroptotic microglia.

4.5 Necroptosis in pyramidal neurons at 4 h post kainate injection

Death of pyramidal neurons could be induced by SE, which is proposed to be a part of acquired epileptogenesis (Dingledine, Varvel, and Dudek 2014). New pathways of neuronal death, beyond the traditional death of apoptosis and necrosis, include necroptosis, autophagy and pyroptosis. (Dingledine, Varvel, and Dudek 2014; Fricker et al. 2018b). Our previous data showed that a considerable number of pyramidal neurons underwent apoptosis during early epileptogenesis, which was confirmed by the TUNEL method (Bedner et al. 2015). MLKL expression significantly increased in the CA1 area at 24 h or 72 h after SE induced by lithium chloride (Wang, Li, et al. 2017; Wang, Liu, et al. 2017), while whether pMLKL increased in the pyramidal layer is unknown yet. We detected only a few of RIPK1/3 and pMLKL positive neurons, indicating necroptosis is not the main pathway how pyramidal neurons die at 4 h after KA injection.

TNF-α was thought to trigger neuronal apoptosis and necroptosis (Fricker et al. 2018b). TNF-α and Fas ligands can induce apoptosis of neurons during inflammation (Haase et al. 2008). The extrinsic apoptosis pathway is triggered by the ligation of TNF receptor at the cell surface, which may play a causal role in neuronal death in seizure models via caspase-8 activation (Henshall et al. 2001). The specific deletion of caspase-8 in neurons rendered neurons resistant to apoptosis induced by TNF-receptor ligation in vitro and resulted in increased neuronal survival associated with reduced activation of caspase-3 following seizure-induced brain injury (Henshall et al. 2001). Inhibition of caspase-8 stimulates necroptosis, suppressing the formation of

necroptotic complexes, which are composed of RIPK1/3 and MLKL (Feoktistova et al. 2016). Caspase-8-deficient cells are sensitized to necroptosis induced by TNF (Holler et al. 2000). TNF-α significantly increased at 4 h post kainate injection (Müller 2018). Although the increased level of TNF-α was significantly diminished at 1 day after kainate injection (Müller 2018), a considerable proportion of TUNEL positive neurons were detected in the pyramidal layer, even 5 days post kainate injection (Bedner et al. 2015). Pyramidal neurons were nearly gone in the CA1 area of animals with pure kainate injection, post 3 months; in contrast, blockade of TNF-α by Xpro largely preserved pyramidal neurons in CA1 area of animals (Müller 2018). This indicates that early increasing TNF-α might play an important role in loss of pyramidal neurons in chronic phase of TLE.

4.6 Other potential cell death during early epileptogensis

Necrosis comprises of several different subtypes (see section 1.4), which are classified by different regulated mechanisms and triggers. In the present study, we only checked necroptosis. Other types of necrosis, e.g. pyroptosis and parthanatos, were not investigated, which might limit the conclusions from our present study. First, pyroptosis is characterized as a feature of inflammasome release and caspase 1 or 11-dependence. The cleavage of gasdermin-D at Asp276 by caspase-1 in a necrotic cell may be the best unique marker of pyroptosis in mouse. Currently only an antibody for western blotting is available, targeting mouse cleaved-gasdermin D (Asp 276), but not for immunostaining, which makes it difficult to detect pyroptosis in astrocytes (Cell signaling Technology, #50928). Although caspase-1 (or caspase-11) activation is a key for indcuing pyroptotic cell death, it is not an exclusive marker of pyroptotic death among necrotic cells. The formation of MLKL oligomers and plasma membrane permeabilization result in NLRP3 inflammasome formation and associated caspase-1 activation (Conos et al. 2017; Lawlor et al. 2015). Therefore, caspase-1 activation in necrotic cells might be associated with either pyroptosis or necroptosis. Confirmation of MLKL phosphorylation or oligomerization at the plasma membrane could be helpful for distinguishing between necroptosis and pyroptosis. Pyroptosis can also be typified by TUNEL staining because of cellular DNA damaged by caspase-1 (Dingledine, Varvel, and Dudek 2014; Jorgensen and Miao 2015). Second, parthanatos, another form of regulated necrosis, is triggered by DNA damage/degradation, which results in

TUNEL positive signals (Soriano et al. 2017). Our negative TUNEL results ruled out the possibility of this type of regulated necrosis. Third, due to lack of markers, ferroptosis, lysosomal and mitopore death are currently difficult to investigate in our model of TLE (see section 1.4). Last but not least, oncosis, one form of unregulated necrosis, which is typically induced by ischemia or excessive ATP consumption in brain (see section 1.4), is so far difficult to detect in vivo, Thus, promising biological tools for detecting oncosis might be needed in the future.

In conclusion, the present study has identified astrocytic death during early epileptogenesis. The potential mechanisms of astrocytic death might involve necroptosis and autophagy. Necroptosis seems not to be cell type specific, i.e. it happens not only in astrocytes but also in microglia and pyramidal neurons. Of note, our results add a new aspect to the better understanding of how astrocytic dysfunction might lead to initiation and/or progression of TLE.

5. Abstract

Epilepsy is a disorder of the brain characterised by unprovoked, recurrent seizures and affects about 1 % of the population worldwide. A deeper understanding of the cellular mechanisms leading to epilepsy are essential for the identification of novel targets for therapeutic intervention. Growing evidence suggests that dysfunctional astrocytes are crucial players in the development of temporal lobe epilepsy (TLE). In a mouse model of TLE with hippocampal sclerosis (HS) we found a transient but significant reduction in the number of GFAP-positive astrocytes in the CA1 stratum radiatum (SR) of the ipsilateral hippocampus, starting 4 hours after kainate-induced status epilepticus. The goal of the present study was to elucidate molecular mechanism responsible for the astrocytic loss. For this purpose, we used immunohistochemical staining and semiquantitative RT-PCR analysis to identify marker of different cellular death mechanism 4 hours after epilepsy induction. We did not find any cleaved-caspase 3 or TUNEL positive astrocytes in the epileptic tissue, ruling out the involvement of apoptotic death. A contribution of autophagic cell death could also be excluded, since we observed only low/negligible expression of autophagy-related genes and proteins (*lc3-a, b*; *lamp2*, *becn1,* LC3-B). However, we found a significant increase of receptor interacting protein kinase 3 (RIPK3) and mixed lineage kinase domain-like protein (MLKL) positive astrocytes as well as enhanced expression of the corresponding necroptosis-related genes (*ripk3* and *mlkl*) in the ipsilateral CA1 SR of kainate-injected mice. Moreover, using phospho-specific antibodies ipsilaterally we observed phosphorylation of MLKL (pMLKL) and the formation of necrosome complexes between RIPK3 and pMLKL in kainate-injected animals. Co-localization analysis showed translocation of pMLKL to the nucleus and the plasma membrane in astrocytes of the ipsilateral hippocampus. Taken together, the present study suggests that a considerable proportion of hippocampal astrocytes undergo necroptotic cell death during early epileptogenesis.

6. List of figures

7. List of tables

8. References

Aggarwal BB, Gupta SC, and Kim JH. Historical perspectives on tumor necrosis factor and its superfamily: 25 years later, a golden journey. Blood 2012; 119: 651-665

Alano CC, Garnier P, Ying WH, Higashi Y, Kauppinen TM, Swanson RA. NAD(+) Depletion Is Necessary and Sufficient for Poly(ADP-Ribose) Polymerase-1-Mediated Neuronal Death. J Neurosci 2010; 30: 2967-2978

Andrabi SA, Kim NS, Yu SW, Wang H, Koh DW, Sasaki M, Klaus JA, Otsuka T, Zhang Z, Koehler RC, Hurn PD, Poirier GG, Dawson VL, T. M. Dawson TM. Poly(ADP-ribose) (PAR) polymer is a death signal. Proc Natl Acad Sci U S A 2006; 103: 18308-18313

Axe EL, Walker SA, Manifava M, Chandra P, Roderick HL, Habermann A, Griffiths G, Ktistakis NT. Autophagosome formation from membrane compartments enriched in phosphatidylinositol 3-phosphate and dynamically connected to the endoplasmic reticulum. J Cell Biol 2008; 182: 685-701

Becerra-Calixto A, Cardona-Gomez GP. The Role of Astrocytes in Neuroprotection after Brain Stroke: Potential in Cell Therapy. Front Mol Neurosci 2017; 10: 88

Bedner P, Dupper A, Huttmann K, Muller J, MHerde MK, Dublin P, Deshpande T, Schramm J, Haussler U, Haas CA, Henneberger C, Theis M, Steinhauser C. Astrocyte uncoupling as a cause of human temporal lobe epilepsy. Brain 2015; 138: 1208-1222

Bento CF, Renna M, Ghislat G, Puri C, Ashkenazi A, Vicinanza M, Menzies FM, Rubinsztein DC. Mammalian Autophagy: How Does It Work? Ann Rev Biochem 2016; 85: 685-713

Bergsbaken T, Cookson BT. Macrophage activation redirects Yersinia-infected host cell death from apoptosis to caspase-1-dependent pyroptosis. Plos Pathogens 2007; 3: 1570-1582

Bergsbaken T, Fink SL, Cookson BT. Pyroptosis: host cell death and inflammation. Nat Rev Microbiol 2009; 7: 99-109

Bhattacharyya P. Poly(ADP-Ribose)Polymerase-1 causes mitochondrial damage and neuron death mediated by Bnip3. J Neurosci 2014; 34(48):15975-15987

Birbeck GL. Epilepsy Care in Developing Countries: Part II of II. Epilepsy Curr 2010; 10: 105-110

Blumcke I, Pauli E, Clusmann H, Schramm J, Becker A, Elger C, Merschhemke M, Meencke HJ, Lehmann T, von Deimling A, Scheiwe C, Zentner J, Volk B, Romstock J, Stefan H, Hildebrandt M. A new clinico-pathological classification system for mesial temporal sclerosis. Acta Neuropathol 2007; 113: 235-244

Boison D, Steinhauser C. Epilepsy and astrocyte energy metabolism. Glia 2018; 66: 1235-1243

Borges K, McDermott D, Irier H, Smith Y, Dingledine R. Degeneration and proliferation of astrocytes in the mouse dentate gyrus after pilocarpine-induced status epilepticus. Exp Neurol 2006; 201: 416-427

Bosco D, Haefliger JA, Meda P. Connexins: key mediators of endocrine function. Physiol Rev 2011; 91: 1393-1445

Brennan MA, Cookson BT. Salmonella induces macrophage death by caspase-1-dependent necrosis. Mol Microbiol 2000; 38: 31-40

Caccamo A, Branca C, Piras IS, Ferreira E, Huentelman MJ, Liang WS, Readhead B, Dudley JT, Spangenberg EE, Green KN, Belfiore R, Winslow W, Oddo S. Necroptosis activation in Alzheimer's disease. Nat Neurosci 2017; 20: 1236-1246

Cai Z, Jitkaew S, Zhao J, Chiang HC, Choksi S, Liu J, Ward Y, Wu LG, Liu ZG. 2014. Plasma membrane translocation of trimerized MLKL protein is required for TNF-induced necroptosis. Nat Cell Biol 2014; 16: 55-56

Cai ZY, Zhang AL, Choksi S, Li WH, Li T, Zhang XM, Liu ZG. Activation of cell-surface proteases promotes necroptosis, inflammation and cell migration. Cell Res 2016; 26: 886-900

Campbell SL, Hablitz JJ. Glutamate transporters regulate excitability in local networks

in rat neocortex. Neuroscience 2004; 127: 625-635

Cao Y, Klionsky DJ. Physiological functions of Atg6/Beclin 1: a unique autophagy-related protein. Cell Res 2007; 17: 839-849

Cavus I, Kasoff WS, Cassaday MP, Jacob R, Gueorguieva R, Sherwin RS, Krystal JH, Spencer DD, Abi-Saab WM. Extracellular metabolites in the cortex and hippocampus of epileptic patients. Ann Neurol 2005; 57: 226-235

Chen X, Li WJ, Ren JM, Huang DL, He WT, Song YL, Yang C, Li WY, Zheng RX, Chen PD, Han JH. Translocation of mixed lineage kinase domain-like protein to plasma membrane leads to necrotic cell death. Cell Res 2014; 24: 105-121

Cheung EC, Joza N, Steenaart NA, McClellan KA, Neuspiel M, McNamara S, MacLaurin JG, Rippstein P, Park DS, Shore GC, McBride HM, Penninger JM, Slack RS. Dissociating the dual roles of apoptosis-inducing factor in maintaining mitochondrial structure and apoptosis. EMBO J 2006; 25: 4061-4073

Chever O, Djukic B, McCarthy KD, Amzica F. Implication of Kir4.1 channel in excess potassium clearance: an in vivo study on anesthetized glial-conditional Kir4.1 knock-out mice. J Neurosci 2010; 30: 15769-15777

Cho Y, Challa S, Moquin D, Genga R, Ray TD, Guildford M, Chan FKM. Phosphorylation-Driven Assembly of the RIP1-RIP3 Complex Regulates Programmed Necrosis and Virus-Induced Inflammation. Cell 2009; 137: 1112-1123

Clarke LE, Barres BA. Emerging roles of astrocytes in neural circuit development. Nat Rev Neurosci 2013; 14: 311-321

Conos SA, Chen KW, D. NardoD, Hara H, Whitehead L, Nunez G, Masters SL, Murphy JM, Schroder K, Vaux DL, Lawlor KE, Lindqvist LM, Vince JE. Active MLKL triggers the NLRP3 inflammasome in a cell-intrinsic manner. Proc Natl Acad Sci U S A 2017; 114: E961-E969

Coulter DA, Eid T. Astrocytic regulation of glutamate homeostasis in epilepsy. Glia 2012; 60: 1215-1226

Crunelli V, Carmignoto G, Steinhauser C. Novel astrocyte targets: New Avenues for the Therapeutic Treatment of Epilepsy. Neuroscientist 2015; 21: 62-83

Culmsee C, Zhu CL, Landshamer S, Becattini B, Wagner E, Pellecchia M, Blomgren K, Plesnila N. Apoptosis-inducing factor triggered by poly(ADP-ribose) polymerase and bid mediates neuronal cell death after oxygen-glucose deprivation and focal cerebral ischemia. J Neurosci 2005; 25: 10262

Czabotar PE, Lessene G, Strasser A, Adams JM. Control of apoptosis by the BCL-2 protein family: implications for physiology and therapy. Nat Rev Mol Cell Biol 2014; 15: 49-63

Das A, Wallace GC, Holmes C, McDowell ML, Smith JA, Marshall JD, Bonilha L, Edwards JC, Glazier SS, Ray SK, Banik NL. Hippocampal Tissue of Patients with Refractory Temporal Lobe Epilepsy Is Associated with Astrocyte Activation, Inflammation, and Altered Expression of Channels and Receptors. Neuroscience 2012; 220: 237-246

de Rivero Vaccari JP, Dietrich WD, Keane RW. Activation and regulation of cellular inflammasomes: gaps in our knowledge for central nervous system injury. J Cereb Blood Flow Metab 2014; 34: 369-375

Degterev A, Hitomi J, Germscheid M, Ch'en IL, Korkina O, Teng X, Abbott D, Cuny GD, Yuan C, Wagner G, Hedrick SM, Gerber SA, Lugovskoy A, Yuan J. Identification of RIP1 kinase as a specific cellular target of necrostatins. Nat Chem Biol 2008; 4: 313-321

Degterev A, Huang Z, M. Boyce, Y. Li, P. Jagtap, N. Mizushima, G. D. Cuny, T. J. Mitchison, M. A. Moskowitz, and J. Yuan. Chemical inhibitor of nonapoptotic cell death with therapeutic potential for ischemic brain injury. Nat Chem Biol 2005; 1: 112-119

Demarque M, Villeneuve N, Manent JB, Becq H, Represa A, Ben-Ari Y, Aniksztejn L. Glutamate transporters prevent the generation of seizures in the developing rat neocortex. J Neurosci 2004; 24: 3289-3294

Deng W, Aimone JB, Gage FH. New neurons and new memories: how does adult

hippocampal neurogenesis affect learning and memory? Nat Rev Neurosci 2010; 11: 339-350

Deshpande T, Li T, Herde MK, Becker A, Vatter H, Schwarz MK, Henneberger C, Steinhauser C, Bedner P. Subcellular reorganization and altered phosphorylation of the astrocytic gap junction protein connexin43 in human and experimental temporal lobe epilepsy. Glia 2017; 65: 1809-1820

Deshpande T. Unravelling mechanisms causing astrocytic uncoupling in epilepsy. 2017 http://hss.ulb.uni-bonn.de/2017/4838/4838.pdf

Dikic I, Elazar Z. Mechanism and medical implications of mammalian autophagy Nat Rev Mol Cell Biol 2018; 19: 349-364

Dingledine R, Varvel NH, Dudek FE. When and How Do Seizures Kill Neurons, and Is Cell Death Relevant to Epileptogenesis? Issue Clin Epileptol 2014; 813: 109-122

Dixon SJ, Lemberg KM, Lamprecht MR, Skouta R, Zaitsev EM, Gleason CE, Patel DN, Bauer AJ, Cantley AM, Yang WS, Morrison B, Stockwell BR. Ferroptosis: An Iron-Dependent Form of Nonapoptotic Cell Death. Cell 2012; 149: 1060-1072

Dolma S, Lessnick SL, Hahn WC, Stockwell BR. Identification of genotype-selective antitumor agents using synthetic lethal chemical screening in engineered human tumor cells. Cancer Cell 2003; 3: 285-926

Dondelinger Y, Declercq W, Montessuit S, Roelandt R, Goncalves A, Bruggeman I, Hulpiau P, Weber K, Sehon CA, Marquis RW, Bertin J, Gough PJ, Savvides S, Martinou JC, M. Bertrand JM, Vandenabeele P. MLKL Compromises Plasma Membrane Integrity by Binding to Phosphatidylinositol Phosphates. Cell Rep 2014; 7: 971-981

Eliasson MJL, Sampei K, Mandir AS, Hurn PD, Traystman RJ, Bao J, Pieper A, Wang ZQ, Dawson TM, Snyder SH, Dawson VL. Poly (ADP-ribose) polymerase gene disruption renders mice resistant to cerebral ischemia. Stroke 1998; 29: 282-282

Fan H, Zhang K, Shan L, Kuang F, Chen K, Zhu K, Ma H, Ju G, Wang YZ. Reactive astrocytes undergo M1 microglia/macrohpages-induced necroptosis in spinal cord injury. Mol Neurodegener 2016; 11: 14

Fatokun AA, Dawson VL, Dawson TM. Parthanatos: mitochondrial-linked mechanisms and therapeutic opportunities. Br J Pharmacol 2014; 171: 2000-2016

Feoktistova M, Wallberg F, Tenev T, Geserick P, Leverkus M, Meier P. Techniques to Distinguish Apoptosis from Necroptosis. Cold Spring Harb Protoc 2016 pdb top070375

Fink SL, Cookson BT. Caspase-1-dependent pore formation during pyroptosis leads to osmotic lysis of infected host macrophages. Cell Microbiol 2006; 8: 1812-1825

Flusberg DA, Sorger PK. Surviving apoptosis: life-death signaling in single cells. Trends Cell Biol 2015; 25: 446-458

Fremeau RT, Burman J, Qureshi T, Tran CH, Proctor J, Johnson J, Zhang H, Sulzer D, Copenhagen DR, Storm-Mathisen J, Reimer RJ, Chaudhry FA, Edwards RH. The identification of vesicular glutamate transporter 3 suggests novel modes of signaling by glutamate. Proc Natl Acad Sci U S A 2002; 99: 14488-14493

Fricker M, Tolkovsky AM, Borutaite V, Coleman M, Brown GC. Neuronal Cell Death. Physiol Rev 2018; 98: 813-880

Fuchs Y, Steller H. Programmed cell death in animal development and disease. Cell 2011; 147: 742-758

Fuchs Y, Steller H. Live to die another way: modes of programmed cell death and the signals emanating from dying cells. Nat Rev Mol Cell Biol 2015; 16: 329-344

Galluzzi L, Baehrecke EH, Ballabio A, Boya P, Pedro JMBS, Cecconi F, Choi AM, Chu CT, Codogno P, Colombo MI, Cuervo AM, Debnath J, Deretic V, Dikic I, Eskelinen EL, Fimia GM, Fulda S, Gewirtz DA, Green DR, Hansen M, Harper JW, Jaattela M, Johansen T, Juhasz G, Kimmelman AC, Kraft C, Ktistakis NT, Kumar S, Levine B, Lopez-Otin C, Madeo F, Martens S, Martinez J, Melendez A, Mizushima N, Munz C, L. Murphy O, Penninger JM, Piacentini M, Reggiori F, Rubinsztein DC, Ryan KM, Santambrogio L, Scorrano L, Simon AK, Simon HU, Simonsen A, Tavernarakis N, Tooze SA, Yoshimori T, Yuan JY, Yue ZY, Zhong Q, Kroemer G. Molecular definitions of autophagy and related processes. Embo J 2017; 36: 1811-1836

Galluzzi L, Bravo-San Pedro JM, Kepp O, Kroemer G. Regulated cell death and

adaptive stress responses. Cell Mol Life Sci 2016; 73: 2405-2410

Galluzzi L, Kepp O, Chan FKM, Kroemer G. Necroptosis: Mechanisms and Relevance to Disease. Annu Rev Pathol 2017; 12: 103-130

Galluzzi L, Kepp O, Krautwald S, Kroemer G, Linkermann A. Molecular mechanisms of regulated necrosis. Semin Cell Dev Biol 2014; 35: 24-32

Galluzzi L, Kepp O, Kroemer G. Mitochondrial regulation of cell death: a phylogenetically conserved control. Microb Cell 2016; 3: 101-108

Galluzzi L, Lopez-Soto A, Kumar S, Kroemer G. Caspases Connect Cell-Death Signaling to Organismal Homeostasis. Immunity 2016; 44: 221-231

Gan J, Qu Y, Li J, Zhao FY, Mu DZ. An evaluation of the links between microRNA, autophagy, and epilepsy. Rev Neuroscience 2015; 26: 225-237

Giaume C, Koulakoff A, Roux L, Holcman D, Rouach N. Neuron-glia interactions astroglial networks: a step further in neuroglial and gliovascular interactions. Nat Rev Neurosci 2010; 11: 87-99

Gibert B, Mehlen P. Dependence Receptors and Cancer: Addiction to Trophic Ligands. Cancer Res 2015; 75: 5171-5175

Goldberg EM, Coulte DAr. Mechanisms of epileptogenesis: a convergence on neural circuit dysfunction. Nat Rev Neurosci 2013; 14: 337-349

Gong YN, Guy C, Olauson H, Becker JU, Yang M, Fitzgerald P, Linkermann A, Green DR. ESCRT-III Acts Downstream of MLKL to Regulate Necroptotic Cell Death and Its Consequences. Cell 2017; 169: 286-300

Grootjans S, Berghe TV, Vandenabeele P. Initiation and execution mechanisms of necroptosis: an overview. Cell Death Differ 2017; 24: 1184-1195

Grosche A, Grosche J, Tackenberg M, Scheller D, Gerstner G, Gumprecht A, Pannicke T, Hirrlinger PG, Wilhelmsson U, Huttmann K, Hartig W, Steinhauser C, Pekny M, Reichenbach A. Versatile and simple approach to determine astrocyte territories in mouse neocortex and hippocampus. PLoS One 2013; 8: e69143

Gunther C, He GW, Kremer AE, Murphy JM, Petrie EJ, Amann K, Vandenabeele P, Linkermann A, Poremba C, Schleicher U, Dewitz C, Krautwald S, Neurath MF, Becker C, Wirtz S. The pseudokinase MLKL mediates programmed hepatocellular necrosis independently of RIPK3 during hepatitis. J Clin Invest 2016; 126: 4346-4360

Haase G, Pettmann B, Raoul C, Henderson CE. Signaling by death receptors in the nervous system. Curr Opin Neurobiol 2008; 18: 284-291

Haj-Yasein NN, Jensen V, Vindedal GF, Gundersen GA, Klungland A, Ottersen OP, O. Hvalby, Nagelhus EA. Evidence that Compromised K+ Spatial Buffering Contributes to the Epileptogenic Effect of Mutations in the Human Kir4.1 Gene (KCNJ10). Glia 2011; 59: 1635-1642

Hanisch UK, Kettenmann H. Microglia: active sensor and versatile effector cells in the normal and pathologic brain. Nat Neurosci. 2007. 10: 1387-1394

He WT, Wan H, Hu L, Chen P, Wang X, Huang Z, Yang ZH, ZhongCQ, Han J. Gasdermin D is an executor of pyroptosis and required for interleukin-1beta secretion. Cell Res 2015; 25: 1285-1298

Henshall DC, Bonislawski DP, Skradski SL, Lan JQ, Meller R, Simon RP. Cleavage of Bid may amplify caspase-8-induced neuronal death following focally evoked limbic seizures. Neurobiol Dis 2001; 8: 568-580

Heuser K, Eid T, Lauritzen F, Thoren AE, Vindedal GF, Tauboll E, Gjerstad L, Spencer DD, Ottersen OP, Nagelhus EA, de Lanerolle NC. Loss of Perivascular Kir4.1 Potassium Channels in the Sclerotic Hippocampus of Patients With Mesial Temporal Lobe Epilepsy. J Neuropath Exp Neur 2012; 71: 814-825

Hildebrand JM, Tanzer MC, Lucet IS, Young SN, Spall SK, Sharma P, Pierotti C, Garnier JM, Dobson RCJ, Webb AI, A. Tripaydonis A, Babon JJ, Mulcair MD, Scanlon MJ, Alexander WS, Wilks AF, Czabotar PE, Lessene G, Murphy JM, Silke J. Activation of the pseudokinase MLKL unleashes the four-helix bundle domain to induce membrane localization and necroptotic cell death. Proc Natl Acad Sci U S A 2014; 111: 15072-15077

Hinterkeuser S, Schroder W, Hager G, Seifert G, Blumcke I, Elger CE, Schramm J, Steinhauser C. Astrocytes in the hippocampus of patients with temporal lobe epilepsy display changes in potassium conductances. Eur J Neurosci 2000; 12: 2087-2096

Holler N, Zaru R, Micheau O, Thome M, Attinger A, Valitutti S, Bodmer JL, P. Schneider, Seed B, Tschopp J. Fas triggers an alternative, caspase-8-independent cell death pathway using the kinase RIP as effector molecule. Nat Immunol 2000; 1: 489-495

Huang D, Zheng X, Wang ZA, Chen X, He WT, Zhang Y, Xu JG, Zhao H, Shi W, Wang X, Zhu Y, Han J. The MLKL Channel in Necroptosis Is an Octamer Formed by Tetramers in a Dyadic Process. Mol Cell Biol 2017; 37

Ichimura Y, Kirisako T, Takao T, Satomi Y, Shimonishi Y, Ishihara N, Mizushima N, Tanida I, Kominami E, Ohsumi M, Noda T, Ohsumi Y. A ubiquitin-like system mediates protein lipidation. Nature 2000; 408: 488-492

Ito Y, Ofengeim D, Najafov A, Das S, Saberi S, Li Y, Hitomi J, Zhu H, Chen H, Mayo L, Geng J, Amin P, DeWitt JP, Mookhtiar AK, Florez M, Ouchida AT, Fan JB, Pasparakis M, Kelliher MA, Ravits J, Yuan J. RIPK1 mediates axonal degeneration by promoting inflammation and necroptosis in ALS. Science 2016; 353: 603-608

Jacobsen AV, Lowes KN, Tanzer MC, Lucet IS, Hildebrand JM, Petrie EJ, van Delft MF, Liu Z, Conos SA, Zhang JG, Huang DC, Silke J, Lessene G, Murphy JM. HSP90 activity is required for MLKL oligomerisation and membrane translocation and the induction of necroptotic cell death. Cell Death Dis 2016; 7: e2051

Jorgensen I, Miao EA. Pyroptotic cell death defends against intracellular pathogens. Immunol Rev 2015; 265: 130-142

Jost PJ, Grabow S, Gray D, McKenzie MD, Nachbur U, Huang DCS, Bouillet P, Thomas HE, Borner C, Silke J, Strasser A, Kaufmann T. XIAP discriminates between type I and type II FAS-induced apoptosis. Nature 2009; 460: 1035-U128

Kabeya Y, Mizushima N, Ueno T, Yamamoto A, Kirisako T, Noda T, Kominami E, Ohsumi Y, Yoshimori T. LC3, a mammalian homolog of yeast Apg8p, is localized in autophagosome membranes after processing. Embo J 2000; 22: 4577-4577

Kaiser WJ, Sridharan H, Huang C, Mandal P, Upton JW, Gough PJ, Sehon CA, Marquis RW, Bertin J, Mocarski ES. Toll-like receptor 3-mediated necrosis via TRIF, RIP3, and MLKL. J Biol Chem 2013; 288: 31268-31279

Kang R, Livesey KM, Zeh HJ, Loze MT, Tang D. HMGB1: a novel Beclin 1-binding protein active in autophagy. Autophagy 2010; 6: 1209-1211

Kang TC, Kim DS, Kwak SE, Kim JE, Won MH, Kim DW, Choi SY, Kwon OS. Epileptogenic roles of astroglial death and regeneration in the dentate gyrus of experimental temporal lobe epilepsy. Glia 2006; 54: 258-271

Karperien A, Ahammer H, Jelinek HF. Quantitating the subtleties of microglial morphology with fractal analysis. Front Cell Neurosci 2013; 7: 3

Karperien A, Herbert J, Alastair B. Box-Counting Analysis of Microglia Form in Schizophrenia. Alzheimers Dis Affect Disord 2008

Kayagaki N, Stowe IB, Lee BL, O'Rourke K, Anderson K, Warming S, Cuellar T, Haley B, Roose-Girma M, Phung QT, Liu PS, Lill JR, Li H, Wu J, Kummerfeld S, Zhang J, Lee WP, Snipas SJ, Salvesen GS, Morris LX, Fitzgerald L, Zhang Y, Bertram EM, Goodnow CC, Dixit VM. Caspase-11 cleaves gasdermin D for non-canonical inflammasome signalling. Nature 2015; 526: 666-671

Kettenmann H, Hanisch UK, Noda M, Verkhratsky A. Physiology of microglia. Physiol Rev 2011; 91: 461-553

Kim JE, Kim YJ, Kim JY, Kang TC. PARP1 activation/expression modulates regional-specific neuronal and glial responses to seizure in a hemodynamic-independent manner. Cell Death Dis 2014; 5: e1362

Kim JE, Ryu HJ, Kim MJ, Kim DW, Kwon OS, Choi SY, Kang TC. Pyridoxal-5'-phosphate phosphatase/chronophin induces astroglial apoptosis via actin-depolymerizing factor/cofilin system in the rat brain following status epilepticus. Glia 2010; 58: 1937-1948

Kim JE, Ryu HJ, Yeo SI, Kang TC. P2X7 receptor differentially modulates astroglial apoptosis and clasmatodendrosis in the rat brain following status epilepticus.

Hippocampus 2011; 21: 1318-1333

Kim TW, Cho hm, Choi SY, Suguira Y, Hayasaka T, Setou M, Koh HC, Hwang EM, Park JY, Kang SJ, Kim HS, Kim H, Sun W. (ADP-ribose) polymerase 1 and AMP-activated protein kinase mediate progressive dopaminergic neuronal degeneration in a mouse model of Parkinson's disease. Cell Death Dis 2013; 4: e919

Ko AR, Hyun HW, Min SJ, Kim JE. The Differential DRP1 Phosphorylation and Mitochondrial Dynamics in the Regional Specific Astroglial Death Induced by Status Epilepticus. Front Cell Neurosci 2016; 10: 124

Kuida K, Lippke JA, Ku G, Harding MW, Livingston DJ, Su MS, Flavell RA. Altered cytokine export and apoptosis in mice deficient in interleukin-1 beta converting enzyme. Science 1995; 267: 2000-2003

Lamb CA, Yoshimori T, Tooze SA. The autophagosome: origins unknown, biogenesis complex. Nat Rev Mol Cell Biol 2013; 14: 759-774

Lawlor KE, Khan N, Mildenhall A, Gerlic M, Croker BA, D'Cruz AA, Hall C, Spall SK, Anderton H, Masters SL, Rashidi M, Wicks IP, Alexander WS, Mitsuuchi Y, Benetatos CA, Condon SM, Wong WW, Silke J, Vaux DL, Vince JE. RIPK3 promotes cell death and NLRP3 inflammasome activation in the absence of MLKL. Nat Commun 2015; 6: 6282

Lewis J, Devin A, Miller A, Lin Y, Rodriguez Y, Neckers L, Liu ZG. Disruption of hsp90 function results in degradation of the death domain kinase, receptor-interacting protein (RIP), and blockage of tumor necrosis factor-induced nuclear factor-kappaB activation. J Biol Chem 2000; 275: 10519-10526

Li D, Xu T, Cao Y, Wang H, Li L, Chen S, Wang X, Shen Z. A cytosolic heat shock protein 90 and cochaperone CDC37 complex is required for RIP3 activation during necroptosis. Proc Natl Acad Sci U S A 2015; 112: 5017-5022

Li HL, Yuan JY. Cleavage of BID by caspase-8 mediates the mitochondrial damage in the FAS pathway of apoptosis. Mol Biol Cell 1998; 9: 256a-256a

Li J, McQuade T, Siemer AB, Napetschnig J, Moriwaki K, Hsiao YS, Damko E,

Moquin D, Walz T, McDermott A, Chan FK, Wu H. The RIP1/RIP3 necrosome forms a functional amyloid signaling complex required for programmed necrosis. Cell 2012; 150: 339-350

Li P, Allen H, Banerjee S, Franklin S, Herzog L, Johnston C, McDowell J, Paskind M, Rodman L, Salfeld J, Towne E, Tracey D, Wardwell S, Wei FY, Wong W, Kamen R, Seshadri T. Mice deficient in IL-1 beta-converting enzyme are defective in production of mature IL-1 beta and resistant to endotoxic shock. Cell 1995; 80: 401-411

Lin J, Kumari S, Kim C, Van TM, Wachsmuth L, Polykratis A, Pasparakis M. RIPK1 counteracts ZBP1-mediated necroptosis to inhibit inflammation. Nature 2016; 540: 124-128

Linkermann A, Green DR. Necroptosis. N Engl J Med 2014; 370: 455-465

Liu S, Liu H, Johnston A, Hanna-Addams S, Reynoso E, Xiang Y, Wang Z. MLKL forms disulfide bond-dependent amyloid-like polymers to induce necroptosis. Proc Natl Acad Sci U S A 2017; 114: E7450-E7459

Luo X, Budihardjo I, Zou H, Slaughter C, Wang XD. Bid, a Bcl2 interacting protein, mediates cytochrome c release from mitochondria in response to activation of cell surface death receptors. Cell 1998; 94: 481-490

Maelfait, J., L. Liverpool, A. Bridgeman, K. B. Ragan, J. W. Upton, and J. Rehwinkel. Sensing of viral and endogenous RNA by ZBP1/DAI induces necroptosis. Embo J. 2017. 36: 2529-2543

Mandir AS, Przedborski S, Jackson-Lewis V, Wang ZQ, Simbulan-Rosenthal CM, Smulson ME, Hoffman BE, Guastella DB, V. L. Dawson, and T. M. Dawson. Poly(ADP-ribose) polymerase activation mediates 1-methyl-4-phenyl-1, 2,3,6-tetrahydropyridine (MPTP)-induced parkinsonism. Proc Natl Acad Sci U S A. 1999. 96: 5774-5779

Maroso M, Balosso S, Ravizza T, Liu J, Aronica E, Iyer AM, Rossetti C, Molteni M, Casalgrandi M, Manfredi AA, Bianchi ME, Vezzani A. Toll-like receptor 4 and high-mobility group box-1 are involved in ictogenesis and can be targeted to reduce seizures. Nat Med 2010; 16: 413-419

Martins I, Raza SQ, Voisin L, Dakhli H, Law F, Jong DD, Allouch A, Thoreau M, Brenner C, Deutsch E, Perfettini JL. Entosis: The emerging face of non-cell-autonomous type IV programmed death. Biomed J 2017; 40: 133-140

Mehlen P, Bredesen DE. Dependence receptors: from basic research to drug development. Sci Signal 2011; 4: mr2

Mehlen P, Tauszig-Delamasure S. Dependence receptors and colorectal cancer. Gut 2014; 63: 1821-1829

Minchew CL, Didenko VV. Dual Detection of Nucleolytic and Proteolytic Markers of Lysosomal Cell Death: DNase II-Type Breaks and Cathepsin D. Methods Mol Biol 2017; 1554: 229-236

Mishra A, Reynolds JP, Chen Y, Gourine AV, Rusakov DA, Attwell D. Astrocytes mediate neurovascular signaling to capillary pericytes but not to arterioles. Nat Neurosci 2016; 19: 1619-1627

Mizushima N, Yamamoto A, Hatano M, Kobayashi Y, Kabeya Y, Suzuki K, Tokuhisa T, Ohsumi Y, Yoshimori T. Dissection of autophagosome formation using Apg5-deficient mouse embryonic stem cells. J Cell Biol 2001; 152: 657-667

Mizushima N, Yoshimori T, Ohsumi Y. The role of Atg proteins in autophagosome formation. Annu Rev Cell Dev Biol 2011; 27: 107-132

Moldoveanu T, Follis AV, Kriwacki RW, Green DR. Many players in BCL-2 family affairs. Trends Biochem Sci 2014; 39: 101-111

Müller J. Preservation of astrocytic coupling prevents epileptogenesis. 2018 http://hss.ulb.uni-bonn.de/2018/5215/5215.pdf

Murphy JM, Czabotar PE, Hildebrand JM, Lucet IS, Zhang JG, Alvarez-Diaz S, Lewis R, Lalaoui N, Metcalf D, Webb AI, Young SN, Varghese LN, Tannahill GM, Hatchell EC, Majewski IJ, Okamoto T, Dobson RC, Hilton DJ, Babon JJ, Nicola NA, Strasser A, Silke J, Alexander WS. The pseudokinase MLKL mediates necroptosis via a molecular switch mechanism. Immunity 2013; 39: 443-453

Newton K, Wickliffe KE, Maltzman A, Dugger DL, Strasser A, Pham VC, Lill JR, Roose-Girma M, Warming S, Solon M, Ngu H, Webster JD, Dixit VM. RIPK1 inhibits ZBP1-driven necroptosis during development. Nature 2016; 540: 129-133

Nunez G, London L, Hockenbery D, Alexander M, McKearn JP, Korsmeyer SJ. Deregulated Bcl-2 gene expression selectively prolongs survival of growth factor-deprived hemopoietic cell lines. J Immunol 1990; 144: 3602-3610

Oberheim NA, Wang X, Goldman S, Nedergaard M. Astrocytic complexity distinguishes the human brain. Trends Neurosci 2006; 29: 547-553

Oerlemans MI, Liu J, Arslan F, den Ouden K, van Middelaar BJ, Doevendans PA, Sluijter JPG. Inhibition of RIP1-dependent necrosis prevents adverse cardiac remodeling after myocardial ischemia-reperfusion in vivo. Basic Res Cardiol 2012; 107

Ofengeim D, Ito Y, Najafov A, Zhang Y, Shan B, DeWitt JP, Ye J, Zhang X, Chang A, Vakifahmetoglu-Norberg H, Geng J, Py B, Zhou W, Amin P, Berlink Lima J, Qi C, Yu Q, Trapp B, Yuan J. Activation of necroptosis in multiple sclerosis. Cell Rep 2015; 10: 1836-1849

Ozkara C, Aronica E. Hippocampal sclerosis. Handb Clin Neurol 2012; 108: 621-639

Pallast S, Arai A, Pekcec A, Yigitkanli K, Yu Z, Wang X, Lo EH, van Leyen K. Increased nuclear apoptosis-inducing factor after transient focal ischemia: a 12/15-lipoxygenase-dependent organelle damage pathway. J Cereb Blood Flow Metab 2010; 30: 1157-1167

Pasparakis M, Vandenabeele P. Necroptosis and its role in inflammation. Nature 2015; 517: 311-320

Puyal J, Ginet V, Clarke PG. Multiple interacting cell death mechanisms in the mediation of excitotoxicity and ischemic brain damage: a challenge for neuroprotection. Prog Neurobiol 2013; 105: 24-48

Re DB, Le Verche V, Yu CH, Amoroso MW, Politi KA, Phani S, Ikiz B, Hoffmann L, Koolen M, Nagata T, Papadimitriou D, Nagy P, Mitsumoto H, Kariya S, Wichterle H, Henderson CE, Przedborski S. Necroptosis Drives Motor Neuron Death in Models of

Both Sporadic and Familial ALS. Neuron 2014; 81: 1001-1008

Rodriguez DA, Weinlich R, Brown S, Guy C, Fitzgerald P, Dillon CP, Oberst A, Quarato G, Low J, Cripps JG, Chen T, Green DR. Characterization of RIPK3-mediated phosphorylation of the activation loop of MLKL during necroptosis. Cell Death Differ 2016; 23: 76-88

Roos WP, Thomas AD, Kaina B. DNA damage and the balance between survival and death in cancer biology. Nat Rev Cancer 2016; 16: 20-33

Rubio-Villena C, Viana R, Bonet J, Garcia-Gimeno MA, Casado M, Heredia M, Sanz P. Astrocytes: new players in progressive myoclonus epilepsy of Lafora type. Hum Mol Genet 2018; 27: 1290-1300

Ryu HJ, Kim JE, Yeo SI, Kang TC. p65/RelA-Ser529 NF-kappaB subunit phosphorylation induces autophagic astroglial death (Clasmatodendrosis) following status epilepticus. Cell Mol Neurobiol 2011; 31: 1071-1078

Ryu HJ, Kim JE, Yeo SI, Kim DW, Kwon OS, Choi SY, Kang TC. F-actin depolymerization accelerates clasmatodendrosis via activation of lysosome-derived autophagic astroglial death. Brain Res Bull 2011; 85: 368-373

Samoilova M, Li J, Pelletier MR, Wentlandt K, Adamchik Y, Naus CC, Carlen PL. Epileptiform activity in hippocampal slice cultures exposed chronically to bicuculline: increased gap junctional function and expression. J Neurochem 2003; 86: 687-699

Samoilova M, Wentlandt K, Adamchik Y, Velumian AA, Carlen PL. Connexin 43 mimetic peptides inhibit spontaneous epileptiform activity in organotypic hippocampal slice cultures. Exp Neurol 2008; 210: 762-775

Schmidt D, Loscher W. Drug resistance in epilepsy: putative neurobiologic and clinical mechanisms. Epilepsia 2005; 46: 858-877

Seifert G, Carmignoto G, Steinhauser C. Astrocyte dysfunction in epilepsy. Brain Res Rev 2010; 63: 212-221

Seifert G, Huttmann K, Binder DK, Hartmann C, Wyczynski A, Neusch C, Steinhauser

C. Analysis of astroglial K+ channel expression in the developing hippocampus reveals a predominant role of the Kir4.1 subunit. J Neurosci 2009; 29: 7474-7478

Seifert G, Schilling K, Steinhauser C. Astrocyte dysfunction in neurological disorders: a molecular perspective. Nat Rev Neurosci 2006; 7: 194-206

Seiler A, Schneider M, Forster H, Roth S, Wirth EK, Culmsee C, Plesnila N, Kremmer E, Radmark O, Wurst W, Bornkamm GW, Schweizer U, Conrad M. Glutathione peroxidase 4 senses and translates oxidative stress into 12/15-lipoxygenase dependent- and AIF-mediated cell death. Cell Metab 2008; 8: 237-248

Sha LZ, Wang XQ, Li J, Shi XZ, Wu LW, Shen Y, Xu Q. Pharmacologic inhibition of Hsp90 to prevent GLT-1 degradation as an effective therapy for epilepsy. J Exp Med 2017; 214: 547-563

Manjur S, Beg T, Mahamood M, Jayentakumar Singh L, Chanu L. Microbiol Agri Hum Health 2015

Shamas-Din A, Kale J, Leber B, Andrews DW. Mechanisms of action of Bcl-2 family proteins. Cold Spring Harb Perspect Biol 2013; 5: a008714

Shi J, Zhao Y, Wang K, Shi X, Wang Y, Huang H, Zhuang Y, Cai T, Wang F, Shao F. Cleavage of GSDMD by inflammatory caspases determines pyroptotic cell death. Nature 2015; 526: 660-665

Shorvon SD. The etiologic classification of epilepsy. Epilepsia 2011; 52: 1052-1057

Soriano J, Mora-Espi I, Alea-Reyes ME, Perez-Garcia L, Barrios L, Ibanez E, Nogues C. Cell Death Mechanisms in Tumoral and Non-Tumoral Human Cell Lines Triggered by Photodynamic Treatments: Apoptosis, Necrosis and Parthanatos. Sci Rep 2017; 7

Steinhauser C. Role for Astrocyte Dysfunction in Human Epilepsy. Epilepsia 2009; 50: 30

Steinhauser C, Dupper A, Bedner P. Astrocyte Dysfunction in Temporal Lobe Epilepsy. Glia 2013; 61: S16-S17

Steinhauser C, Seifert G. Astrocyte dysfunction in temporal lobe epilepsy. Epilepsia

2010; 51: 54-54

Steinhauser C, Seifert G, Bedner P. Astrocyte dysfunction in temporal lobe epilepsy: K+ channels and gap junction coupling. Glia 2012; 60: 1192-1202

Stockwell BR. Ferroptosis: Death by lipid peroxidation. Free Radical Bio Med 2018; 120: S7

Stoica BA, Loane DJ, Zhao ZR, Kabadi SV, Hanscom M, Byrnes KR, Faden AI. PARP-1 Inhibition Attenuates Neuronal Loss, Microglia Activation and Neurological Deficits after Traumatic Brain Injury. J Neurotrauma 2014; 31: 758-772

Streit WJ, Walter SA, Pennell NA. Reactive microgliosis. Prog Neurobiol 1999; 57: 563-581

Su LJ, Quade B, Wang HY, Sun LM, Wang XD, Rizo J. A Plug Release Mechanism for Membrane Permeation by MLKL. Structure 2014; 22: 1489-1500

Sun GW, Lu J, Pervaiz S, Cao WP, Gan YH. Caspase-1 dependent macrophage death induced by Burkholderia pseudomallei. Cell Microbiol 2005; 7: 1447-1458

Sun LM, Wang HY, Wang ZG, He SD, Chen S, Liao DH, Wang L, Yan JC, Liu WL, Lei XG, Wang XD. Mixed Lineage Kinase Domain-like Protein Mediates Necrosis Signaling Downstream of RIP3 Kinase. Cell 2012; 148: 213-227

Suzuki H, Osawa T, Fujioka Y, Noda NN. Structural biology of the core autophagy machinery. Curr Opin Struct Biol 2017; 43: 10-17

Tait SW, Green DR. Mitochondria and cell death: outer membrane permeabilization and beyond. Nat Rev Mol Cell Biol 2010; 11: 621-632

Tanaka K, Watase K, Manabe T, Yamada K, Watanabe M, Takahashi K, Iwama H, Nishikawa T, Ichihara N, Kikuchi T, Okuyama S, Kawashima N, Hori S, Takimoto M, Wada K. Epilepsy and exacerbation of brain injury in mice lacking the glutamate transporter GLT-1. Science 1997; 276: 1699-1702

Tang D, Kang R, Livesey KM, Cheh CW, Farkas A, Loughran P, Hoppe G, Bianchi ME, racey KJ, Zeh HJ, Lotze MT. Endogenous HMGB1 regulates autophagy. J Cell Biol

2010; 190: 881-892

Tatum WO. Mesial temporal lobe epilepsy. J Clin Neurophysiol 2012; 29: 356-365

Thom M. Review: Hippocampal sclerosis in epilepsy: a neuropathology review. Neuropathol Appl Neurobiol 2014; 40: 520-543

Thompson JW, Graham RM, Webster KA. DNase activation by hypoxia-acidosis parallels but is independent of programmed cell death. Life Sciences 2012; 91: 223-229

Upton JW, Kaiser WJ, Mocarski ES. Virus inhibition of RIP3-dependent necrosis. Cell Host Microbe 2010; 7: 302-313

Vanden Berghe T., Linkermann A, Jouan-Lanhouet S, Walczak H, Vandenabeele P. Regulated necrosis: the expanding network of non-apoptotic cell death pathways. Nat Rev Mol Cell Biol 2014; 15: 135-147

Vandenabeele P, Declercq W, Van Herreweghe F, Vanden Berghe T. The role of the kinases RIP1 and RIP3 in TNF-induced necrosis. Sci Signal 2010; 3: re4

Vercammen D, Brouckaert G, Denecker G, Van de Craen M, Declercq W, Fiers W, Vandenabeele P. Dual signaling of the Fas receptor: Initiation of both apoptotic and necrotic cell death pathways. J Exp Med 1998; 188: 919-930

Vercammen D, Vandenabeele P, Beyaert R, Declercq W, Fiers W. Tumour necrosis factor-induced necrosis versus anti-Fas-induced apoptosis in L929 cells. Cytokine 1997; 9: 801-808

Verkhratsky A, Nedergaard M. Physiology of Astroglia. Physiol Rev 2018; 98: 239-389

Vezzani A, Moneta D, Conti M, Richichi C, Ravizza T, De Luigi A, De Simoni MG, Sperk G, Andell-Jonsson S, Lundkvist J, Iverfeldt K, Bartfai T. Powerful anticonvulsant action of IL-1 receptor antagonist on intracerebral injection and astrocytic overexpression in mice. Proc Natl Acad Sci U S A 2000; 97: 11534-11539

von Karstedt S, Montinaro A, Walczak H. Exploring the TRAILs less travelled: TRAIL in cancer biology and therapy. Nat Rev Cancer 2017; 17: 352-366

Wajant H. The Fas signaling pathway: more than a paradigm. Science 2002; 296: 1635-1636

Wallraff A, Kohling R, Heinemann U, heis M, Willecke K, Steinhauser C. The impact of astrocytic gap junctional coupling on potassium buffering in the hippocampus. J Neurosci 2006; 26: 5438-5447

Wang HY, Sun LM, Su LJ, Rizo J, Liu L, Wang LF, Wang FS, Wang XD. Mixed Lineage Kinase Domain-like Protein MLKL Causes Necrotic Membrane Disruption upon Phosphorylation by RIP3. Mol Cell 2014; 54: 133-146

Wang J, Li Y, Huang WH, Zeng XC, Li XH, Li J, Zhou J, Xiao J, Xiao B, Ouyang DS, Hu K. The Protective Effect of Aucubin from Eucommia ulmoides Against Status Epilepticus by Inducing Autophagy and Inhibiting Necroptosis. Am J Chinese Med 2017; 45: 557-573

Wang J, Liu Y, Li XH, Zeng XC, Li J, Zhou J, Xiao B, Hu K. Curcumin protects neuronal cells against status-epilepticus-induced hippocampal damage through induction of autophagy and inhibition of necroptosis. Can J Physiol Pharm 2017; 95: 501-509

Weinlich R, Oberst A, Beere HM, Green DR. Necroptosis in development, inflammation and disease. Nat Rev Mol Cell Biol 2017; 18: 127-136

Wen X, Klionsky DJ. An overview of macroautophagy in yeast. J Mol Biol 2016; 428: 1681-1699

Wieser HG, Hane A. Antiepileptic drug treatment in seizurefree mesial temporal lobe epilepsy patients with hippocampal sclerosis following selective amygdalo-hippocampectomy. Seizure 2004;13: 534-536

Xia BQ, Gao ZB. MLKL form Cation Channels. Biophys J 2017; 112: 172a-172a

Yang CK, He SD. Heat shock protein 90 regulates necroptosis by modulating multiple signaling effectors. Cell Death Dis 2016; 7

Yang WS, Kim KJ, Gaschler MM, Patel M, Shchepinov MS, Stockwell BR. Peroxidation of polyunsaturated fatty acids by lipoxygenases drives ferroptosis. Proc Natl Acad Sci

U S A 2016; 113: E4966-4975

Yang WS, SriRamaratnam R, Welsch ME, Shimada K, Skouta R, Viswanathan VS, Cheah JH, Clemons PA, Shamji AF, Clish CB, Brown LM, Girotti AW, Cornish VW, Schreiber SL, Stockwell BR. Regulation of ferroptotic cancer cell death by GPX4. Cell 2014; 156: 317-331

Yang WS, Stockwell BR. Synthetic lethal screening identifies compounds activating iron-dependent, nonapoptotic cell death in oncogenic-RAS-harboring cancer cells. Chem Bio 2008; 15: 234-245

Yin XM, Wang K, Gross A, Zhao YG, Zinkel S, Klocke B, Roth KA, Korsmeyer SJ. Bid-deficient mice are resistant to Fas-induced hepatocellular apoptosis. Nature 1999; 400: 886-891

Yoon S, Bogdanov K, Kovalenko A, Wallach D. Necroptosis is preceded by nuclear translocation of the signaling proteins that induce it. Cell Death Differ 2016; 23: 253-260

Yu SW, Wang H, Poitras MF, Coombs C, Bowers WJ, Federoff HJ, Poirier GG, Dawson TM, Dawson VL. Mediation of poly(ADP-ribose) polymerase-1-dependent cell death by apoptosis-inducing factor. Science 2002; 297: 259-263

Yu WF, Mechawar N, Krantic S, Quirion R. Evidence for the Involvement of Apoptosis-Inducing Factor-Mediated Caspase-Independent Neuronal Death in Alzheimer Disease. Am J Pathol 2010; 176: 2209-2218

Zhang J, ang Y, He WY, Sun LM. Necrosome core machinery: MLKL. Cell Mol Life Sci 2016; 73: 2153-2163

Zhang T, Zhang Y, Cui MY, Jin L, Wang YM, Lv FX, Liu YL, Zheng W, Shang HB, Zhang J, Zhang M, Wu HK, Guo JJ, Zhang XQ, Hu XL, Cao CM, Xiao RP. CaMKII is a RIP3 substrate mediating ischemia- and oxidative stress-induced myocardial necroptosis. Nat Med 2016; 22: 175-182

Zhao J, Jitkaew S, Cai Z, Choksi S, Li Q, Luo J, Liu ZG. Mixed lineage kinase domain-like is a key receptor interacting protein 3 downstream component of TNF-induced

necrosis. Proc Natl Acad Sci U S A 2012; 109: 5322-5327

Zhao XF, Liao Y, Morgan S, Mathur R, Feustel P, Mazurkiewicz J, Qian J, Chang J, Mathern GW, Adamo MA, Ritaccio AL, Gruenthal M, Zhu XJ, Huang YF. Noninflammatory Changes of Microglia Are Sufficient to Cause Epilepsy. Cell Rep 2018; 22: 2080-2093

Zhao XM, Chen Z, Zhao JB, Zhang PP, Pu YF, Jiang SH, Hou JJ, Cui YM, Jia XL, Zhang SQ. Hsp90 modulates the stability of MLKL and is required for TNF-induced necroptosis. Cell Death Dis 2016; 7: e2089

Zhu X, Messer JS, Wang Y, Lin F, Cham CM, Chang J, Billiar TR, Lotze MT, Boone DL, Chang EB. Cytosolic HMGB1 controls the cellular autophagy/apoptosis checkpoint during inflammation. J Clin Invest 2015; 125: 1098-1110

9. Acknowledgements

First, I would like to gratefully thank Prof. Dr. Christian Steinhäuser for giving me the precious chance to work on this interesting project in his lab. Of course, this project would never have been possible without his supervision and support.

I am thankful to Dr. Peter Bedner, especially for the animal models used in this study. I am also thankful to Dr. Gerald Seifert, whose expertise in RNA experiment was valuable for my thesis. I would like to thank Dr. Ronald Jabs for introducing me to the confocal microscopy.

I would like to express appreciation to Prof. Dr. Christian Henneberger for scientific advices.

I am thankful to Thomas Erdman for excellent technical support. I would like to express gratitude towards Dr. Silke Künzel for their help in administrative matters.

It gives me pleasure to thank all the members of the laboratory: Alberto, Aline, Björn, Camile, Catia, Dr.Daniel, Dimitri, Julia, Kirsten, Lukas and Tushar for excellent work environment.

Limited words are inadequate to express my gratitude towards my family and loved ones.